Convergence of adenosine and GABA signaling for synapse stabilization during development

Ferran Gomez-Castro, Stefania Zappettini, Jessica C Pressey, Carla G Silva, Marion Russeau, Nicolas Gervasi, Marta Figueiredo, Claire Montmasson, Marianne Renner, Paula M Canas, et al.

Title: Convergence of adenosine and GABA signaling for synapse stabilization during development

Authors: Ferran Gomez-Castro [1]†, Stefania Zappettini [2]†, Jessica C. Pressey [1,3]†, Carla G. Silva [2,4], Marion Russeau [1], Nicolas Gervasi [1,5], Marta Figueiredo [6], Claire Montmasson [1], Marianne Renner [1], Paula M. Canas [4], Francisco Q. Gonçalves [4], Sofia Alçada-Morais [4], Eszter Szabó [4], Ricardo J. Rodrigues [4], Paula Agostinho [4,7], Angelo R. Tomé [4,8], Ghislaine Caillol [9], Olivier Thoumine [10], Xavier Nicol [11], Christophe Leterrier [8], Rafael Lujan [12], Shiva K. Tyagarajan [6], Rodrigo A. Cunha [4,7], Monique Esclapez [2], Christophe Bernard [2*] and Sabine Lévi [1*]

Affiliations:

[1] INSERM UMR-S 1270, Sorbonne Université, Institut du Fer à Moulin, 75005, Paris, France.

[2] Aix Marseille Univ, INSERM, INS, Inst Neurosci Syst, Marseille, France.

[3] Department of Cell and Systems Biology, University of Toronto, 25 Harbord Street, Toronto, Ontario, M5S 3G5, Canada.

[4] CNC-Center for Neuroscience and Cell Biology, University of Coimbra, 3004-504 Coimbra, Portugal.

[5] Center for Interdisciplinary Research in Biology, College de France, INSERM U1050, CNRS UMR7241, Labex Memolife, Paris, France.

[6] Institute of Pharmacology and Toxicology, University of Zürich, 8057 Zurich, Switzerland.

[7] Faculty of Medicine, University of Coimbra, 3004-504 Coimbra, Portugal.

[8] Department of Life Sciences, University of Coimbra, 3000-456 Coimbra, Portugal

[9] Aix Marseille Univ., CNRS, INP UMR7051, NeuroCyto, Marseille, France.

[10] Univ. Bordeaux, CNRS, Interdisciplinary Institute for Neuroscience, UMR 5297, F-33000, Bordeaux, France.

[11] Sorbonne Université, Inserm, CNRS, Institut de la Vision, 17 rue Moreau, F-75012 Paris, France.

[12] Synaptic Structure Laboratory, Instituto de Investigación en Discapacidades Neurológicas (IDINE), Dept. Ciencias Médicas, Facultad de Medicina, Universidad Castilla-La Mancha, Campus Biosanitario, C/Almansa 14, 02008 Albacete, Spain.

† "These authors contributed equally to this work"

*Corresponding authors. Sabine Lévi Email: sabine.levi@inserm.fr, Christophe Bernard Email: christophe.bernard@univ-amu.fr.

Abstract: During development, neural circuit formation requires the stabilization of active GABAergic synapses and the elimination of inactive ones. Here we demonstrate that, while the activation of postsynaptic $GABA_A$ receptors ($GABA_ARs$) and adenosine A_{2A} receptors ($A_{2A}Rs$) stabilize GABAergic synapses, only $A_{2A}R$ activation is sufficient. Both $GABA_AR$- and $A_{2A}R$-dependent signaling pathways act synergistically to produce cAMP through recruitment of the Calcium (Ca^{2+})-Calmodulin (CaM)-Adenylyl Cyclase (AC) pathway. Protein kinase A (PKA) thus activated, phosphorylates gephyrin on Ser303, which is required for $GABA_AR$ stabilization. Finally, the stabilization of pre- and post- synaptic GABAergic elements involves the interaction between gephyrin and the synaptogenic membrane protein Slitrk3. We propose that $A_{2A}Rs$ act as detectors of active GABAergic synapses releasing GABA and ATP/adenosine, to regulate their fate towards stabilization or elimination.

One-Sentence Summary: A_{2A} receptors ~~are key controllers of~~control the stabilization and ~~/~~elimination of GABAergic synapses during synaptogenesis.

Introduction

During development, brain circuits go through different phases of synapse formation, stabilization and elimination, which involve numerous molecular mechanisms, in particular at GABAergic synapses. Synaptic cell adhesion molecules are essential for synapse formation and maturation, including neuroligins and leucine-rich repeat transmembrane proteins (LRRTMs) that interact with presynaptic neurexins, Slit- and Trk-like family proteins (Slitrks), which bind to presynaptic protein tyrosine phosphatases (PTPs), immunoglobulin superfamily proteins (IgSFs), cadherin family proteins, and transmembrane tyrosine kinase receptors (*1*–*4*). The γ-aminobutyric acid (GABA) neurotransmitter itself regulates the maturation and innervation patterns of GABAergic synapses, as well as their elimination and pruning (*4*–*8*). GABA operates via the activation of type A GABA receptors ($GABA_A$Rs) and elevation in intra-neuronal calcium Ca^{2+} level following the activation of voltage-dependent Ca^{2+} channels (*9*, *10*). In addition, the adenosine signaling pathway ~~emerges as an important actor in~~is also involved during development: extracellular adenosine builds-up with synaptic activity (*11*, *12*), and adenosine A_{2A} receptors (A_{2A}Rs) control the migration speed of GABAergic neurons (*13*), axonal elongation and dendritic branching (*14*), and synapse stabilization/elimination at the neuromuscular junction (*15*). Since GABA could be co-released with Adenosine Triphosphate (ATP)/adenosine in a synaptic -activity-dependent manner (*16*, *17*), we tested the role of adenosine signaling on GABAergic synaptogenesis in the brain.

Results

Transient expression of A_{2A}Rs at GABAergic synapses

In the adult hippocampus, there is a low density of A_{2A}Rs, which are essentially presynaptic (*18*). During the peak of synaptogenesis, between postnatal days P5 and P16, we found a transient

increased density of A_{2A}Rs in mouse hippocampi, in particular in purified synaptic contacts (fig. S1). Electron microscopy showed their post/peri-synaptic localization on symmetric, presumably GABAergic synapses (fig. S1). We also confirmed the presence of A_{2A}Rs in primary cultures of hippocampal neurons. A_{2A}Rs were clustered at synapses containing glutamic acid decarboxylase 67 kD (GAD67, a GABA synthesizing enzymes), and clustering increased during synaptogenesis between 7 and 14 days *in vitro* (DIV) (fig. S1). A_{2A}Rs were not present at all GABAergic synapses but they accumulated at a subset (39.1 ± 3.7 %, n= 34 cells, 3 independent experiments) of synapses. DNA-PAINT imaging further confirmed that A_{2A}Rs were located near the GABAergic post-synapse identified by the presence of the scaffolding molecule gephyrin at DIV 10 (fig. S1). We then asked whether such enrichment of post/peri-synaptic A_{2A}Rs at GABAergic synapses was accompanied by an increase in activity-dependent release of their ligand adenosine.

Increased release of ATP/adenosine during synaptogenesis

Adenosine can originate from its direct activity-dependent release by presynaptic terminals or neighboring glial cells, and/or from the conversion of ATP released by neurons or glial cells via the ecto-5′-nucleotidase CD73 (*11*, *12*). The evoked release of adenosine was larger from P7 than P60 (adult) hippocampal synaptosomes (fig. S2), and blocking CD73 with adenosine 5'-(α,β-methylene)diphosphate (AMPCP, 100 µM) decreased extracellular adenosine by 25% (fig. S2). Accordingly, we found a large density of CD73 in synapses during the peak of synaptogenesis (fig. S2), in keeping with the tight association of the enzyme with A_{2A}Rs (*19*). Therefore, one fraction of extracellular adenosine comes from local extracellular ATP metabolism and most of the adenosine is likely released as such through non-concentrative nucleoside transporters upon its intracellular formation as a by-product of metabolic activity sustaining synaptic activity (*11*, *12*, *20*). The activity-dependent secretion of ATP and adenosine was also ~~more important~~larger at P7

than at P60 (fig. S2). Thus, the activation of synaptic terminals at early stage of synaptogenesis bolsters the release of adenosine (via yet unclear mechanisms) and of vesicular ATP, which is efficiently converted into extracellular adenosine by CD73. Given the presence of A_{2A}Rs at inhibitory synapses and the activity-dependent production of its ligand adenosine during the period of synaptogenesis, we hypothesized a role for this pathway in GABAergic synapse formation/elimination. Since GABA controls the number of GABAergic synapses during development (*4–8*), we tested the relative contribution of $GABA_A$R and A_{2A}R pathways.

A_{2A}Rs and $GABA_A$Rs control GABAergic synapse fate

Incubating neurons with tetanus toxin (TeNT, 1-40 nM) *in vitro*, which abolishes vesicular release of neurotransmitters (*21*), resulted in the disappearance of 43% of GABAergic synaptic terminals labeled for the vesicular GABA Transporter (VGAT) and of 62% of post-synaptic $GABA_A$R γ2 subunit clusters, indicating synapse dismantling (fig. S3). Synaptic loss was fully prevented by the activation of A_{2A}Rs with CGS21680 (30 nM) or $GABA_A$Rs with muscimol (10 µM) for 30 min (fig. S3). The rescue of GABAergic synapses occurred within 30 min of A_{2A}R or $GABA_A$R activation ruling out *de novo* synapse formation, which requires hours (*22*). Together, these results show that in the absence of synaptic transmission, the activation of either A_{2A}Rs or $GABA_A$Rs by their respective ligands is sufficient to maintain GABAergic synapses, which would have disappeared otherwise. This led us to hypothesize that both adenosine and GABA signaling pathways play a role in activity-dependent synapse stabilization, and that when presynaptic sites are inactive, such synapses are eliminated. Since the activation of either receptor could rescue GABAergic synapses to an extent similar to that observed when both receptors were simultaneously activated (fig. S3), we further hypothesized a convergence of both A_{2A}R and $GABA_A$R signaling pathways.

A_{2A}Rs are sufficient to stabilize GABAergic synapses

To test the interdependence of the two A_{2A}R and $GABA_A$R pathways, we blocked one while activating the other, and we investigated the fate of GABAergic synapses *in vitro*. We knocked-down with specific shRNAs the $GABA_A$R γ2 subunit, which leads to synaptic loss (*23*), or A_{2A}Rs (*24*) and we activated A_{2A}Rs or $GABA_A$Rs with their selective agonists CGS21680 (30 nM) or muscimol (10 μM), respectively. Neurons transfected at DIV 6-7 with shRNAs against $GABA_A$Rγ2 (shγ2) or A_{2A}Rs (shA_{2A}R) showed respectively a 51 % and 43 % reduction of GABAergic synapses (Fig. 1 A and B). Since <10 out of 100,000 cells were transfected and since we did not find any evidence of synapse destabilization in the non-transfected cells surrounding the transfected ones, we conclude that the destabilization of GABAergic synapses occurs due to the loss of postsynaptic $GABA_A$Rs or A_{2A}Rs. The activation of A_{2A}Rs with CGS21680 rescued GABAergic synapses in neurons lacking $GABA_A$Rγ2 (Fig. 1A). In contrast, activation of $GABA_A$Rs by muscimol failed to rescue GABAergic synapses in shA_{2A}R-expressing neurons (Fig. 1B). Thus, A_{2A}R activation appears to be necessary and sufficient for GABAergic synapse stabilization, whereas $GABA_A$R activation is not necessary as long as A_{2A}Rs remain activated. According to this scheme, blocking A_{2A}Rs should result in synapse loss.

A_{2A}R blockade triggers GABAergic synapse loss

A 30 min application of the selective A_{2A}R antagonist SCH58261 (100 nM) *in vitro* decreased the number of clusters of the presynaptic protein VGAT as well as of postsynaptic $GABA_A$Rγ2 and scaffolding protein gephyrin (fig. S4), demonstrating a destabilization of GABAergic synapses at both pre- and post-synaptic sites. Acute treatment with SCH58261 induced a loss of GABAergic synapses expressing the $GABA_A$R γ2 subunit but also of synapses containing the α1 or α2 subunits

(fig. S4), suggesting that several types of GABAergic synapses are controlled by A_{2A}Rs. Not all synapses disappeared as ~30% of GABAergic synapses were destabilized (fig. S4), in keeping with the finding that not all GABAergic synapses are equipped with A_{2A}Rs at any given developmental time (fig. S1). The fact that the loss of GABAergic synapses induced by A_{2A}R blockade was similar to that found in shA_{2A}R-expressing neurons (Fig. 1A) suggests that synaptic loss was not due to an indirect effect on network activity. In keeping with the reduced synaptic clustering of $GABA_A$Rγ2, quantum-dot based single-particle tracking of $GABA_A$Rγ2 in DIV 8 hippocampal neurons revealed that the membrane diffusion of $GABA_A$Rs increased within 10 min after bath application of SCH58261 (100 nM) (fig. S5). Finally, this adenosine-dependent mechanism seems specific to A_{2A}Rs since blocking adenosine A_1 receptors had no effect on the density of GABAergic synapses (fig. S6). We then set to confirm these results *ex vivo*.

Immunohistochemistry revealed that blocking A_{2A}Rs for 30 min with SCH58261 (100 nM) in P6 hippocampal slices triggered a 47% loss of VGAT-containing synaptic terminals (Fig. 1C). Single-cell recordings of miniature inhibitory postsynaptic currents (mIPSCs) in hippocampal CA1 pyramidal cells at P6 showed that a 30 min application of SCH58261 (100 nM) decreased the frequency of mIPSCs by ~40% (Fig. 1D). The amplitude of mIPSCs was decreased by ~30% (Fig. 1D). We found the same effect on mIPSCs recorded in CA1 interneurons (fig. S7) and in layer V pyramidal cells of V1 visual cortex (fig. S7). Since the effects of SCH58261 on GABAergic currents could be an indirect consequence of the modulation of glutamatergic neurotransmission by A_{2A}Rs, we verified that the effect was still present in the presence of glutamate receptor blockers (fig. S8). Together, these results show that A_{2A}Rs control the stability of GABAergic synapses in different cell types and brain regions at early stages of development. We then assessed whether this role of A_{2A}Rs was developmentally regulated and studied the minimum time of A_{2A}R inactivity necessary to trigger synapse removal.

Time-course of $A_{2A}R$-mediated stabilization of GABAergic synapses

In keeping with the transient increased density of A_{2A}Rs during the first two postnatal weeks (fig. S1), we found that the control of GABAergic synapses by A_{2A}Rs *ex vivo* was restricted to the period of synaptogenesis (between P4 and P12), with a maximum effect at P6 (fig. S9). A morphological analysis performed in cultures confirmed that the action of A_{2A}Rs was also developmentally regulated (fig. S10).

We then assessed whether there is a specific ~~critical specific~~ time window beyond which A_{2A}R inactivity triggers an irreversible synapse destabilization. Varying the time of application of SCH58261, we found that the effect on mIPSCs was reversible if A_{2A}R blockade did not exceed 10 min (fig. S9). Beyond 20 min, the effect was irreversible (fig. S9). Similarly, there was no loss of GABAergic synapses 10 min following A_{2A}R blockade in cultures, while it occurred after 30 min treatment (fig. S11). Thus, the A_{2A}R-dependent control of GABAergic synapse density is developmentally regulated and a period of at least 20 min of inactivity of A_{2A}Rs is sufficient to trigger the removal of GABAergic synapses.

Together, our results show that A_{2A}Rs satisfy the three requirements of a system able to control the fate of synapses towards stabilization or elimination during development. It is time-dependent, its activation maintains synapses and absence of activation results in synapse elimination. We then investigated the molecular mechanisms upstream and downstream of A_{2A}R activation.

Adenosine is required for synapse stabilization

Application of the CD73 inhibitor AMPCP (100 µM) together with adenosine deaminase (ADA, 4-20 U/mL), which hydrolyses adenosine into inosine, decreased mIPSC amplitude (30%) and frequency (74%) *ex vivo* (Fig. 2A). The same treatment reduced the time $GABA_AR\gamma2$ spent at

inhibitory synapses *in vitro*, an effect that was prevented by the direct activation of A_{2A}Rs with their agonist CGS21680 (fig. S6). This increased escape of $GABA_AR\gamma2$ from inhibitory synapses upon removal of ambient adenosine was accompanied by a rapid disappearance of active inhibitory synaptic boutons (labelled by pre-loading of a VGAT-Oyster^{550} antibody into synaptic vesicles during multiple vesicular exocytosis/endocytosis cycles), and increased trafficking of vesicle packets *(22)* into axons (fig. S11), probably resulting from destabilization of presynaptic active zones. This rapid ~~and dynamic~~ dismantling of GABAergic pre- and post- synaptic compartments induced by the withdrawal of ambient adenosine with ADA ~~+~~ and- AMPCP resulted in a net loss of the number of GABAergic synapses that could be prevented by A_{2A}R activation *in vitro* (Fig. 2B).

To test whether glial cells are necessary to produce adenosine required to activate A_{2A}Rs, we pretreated cultures with the gliotoxin cytosine arabinoside (araC), resulting in the complete loss of Glial Fibrillary Acidic Protein (GFAP)~~GFAP~~-stained glial cells (fig. S12) and application of ADA ~~+~~ and- AMPCP still induced synapse loss, which was prevented by CGS21680 (fig. S12). This indicates that glial cells are not the main source of adenosine and that neurons can produce adenosine (directly or indirectly as a byproduct of its phosphorylated forms) in the absence of glial cells in a sufficient quantity to activate A_{2A}Rs.

Altogether, these results show that direct adenosine activation of A_{2A}Rs is necessary and sufficient to maintain synapse integrity. We then looked at the downstream effects of A_{2A}R activation, starting with the possible cooperativity between GABAergic and A_{2A}R signaling pathways as suggested above (fig. S3).

Convergence of A_{2A}R and $GABA_AR$ signaling pathways

Involvement of the AC/cAMP pathway

A_{2A}Rs are G protein-coupled receptors and their prime transducing system is the activation of adenylyl cyclases (ACs), which generate cyclic adenosine monophosphate (cAMP). If synapse stabilization is G protein-dependent, blocking G protein activity should destabilize synapses. Recording CA1 pyramidal cells with an intracellular solution containing guanosine diphosphate-β-S to block G protein activity directly led to a decrease of mIPSC frequency and amplitude *ex vivo* (~20% and 15% respectively; fig. S13), reproducing the effect of A_{2A}R blockade. This result is consistent with a postsynaptic action.

Then, we tested the involvement of the AC/cAMP signaling cascade, which is downstream of A_{2A}R activation. Bath application of 3-Isobutyl-1-methylxanthine (IBMX 100 µM, a non-selective inhibitor of phosphodiesterases that metabolize cAMP) and forskolin (10 µM, an activator of ACs) prevented the SCH58261-induced decrease of mIPSC frequency and amplitude in CA1 pyramidal cells *ex vivo* (fig. S13). Similarly, IBMX and forskolin prevented the loss of GABAergic synapses induced by SCH58261 in hippocampal neuron cultures (fig. S13). Therefore, the A_{2A}R-dependent control of GABAergic synapses occurs via the activation of the AC/cAMP signaling cascade.

A_{2A}Rs and $GABA_A$Rs elevate intracellular cAMP levels

At what level do the A_{2A}R and $GABA_A$R signaling pathways converge to regulate synaptogenesis? A_{2A}Rs and $GABA_A$Rs are linked to AC/cAMP and Ca^{2+} signaling, respectively. During development, the activation of $GABA_A$Rs leads to a rise in intracellular Ca^{2+} concentration ($[Ca^{2+}]_i$) (*9, 10*). Since hippocampal neurons express type 1 and type 8 Ca^{2+}-CaM activated ACs (*25*), we hypothesized that GABA signaling converge on A_{2A}R signaling by tuning CaM-stimulated ACs and their downstream effectors.

Acute activation of $GABA_A$Rs with 10 µM muscimol significantly increased $[Ca^{2+}]_i$ in DIV8 hippocampal neurons, while decreasing it in DIV14 neurons (fig. S14), in keeping with the

developmentally regulated effect of $GABA_AR$s on $[Ca^{2+}]_i$. In contrast, an acute application of CGS21680 did not change $[Ca^{2+}]_i$ in DIV8 or DIV14 neurons (fig. S14). Buffering intracellular Ca^{2+} with BAPTA-AM (20 µM) lead to the destabilization of inhibitory synapses, an effect that could be prevented by $A_{2A}R$ activation with CGS21680 (Fig. 3A). Thus, activation of $A_{2A}R$s is sufficient to maintain synapse integrity in the absence of intracellular Ca^{2+} signaling.

Since GABA but not adenosine signaling can elevate $[Ca^{2+}]_i$ and since $A_{2A}R$-mediated activation of ACs can be boosted by CaM (*10*), we tested the convergence of the $GABA_AR$ and $A_{2A}R$ pathways on cAMP. To address this question, we performed cAMP imaging in DIV8 hippocampal neurons infected with recombinant Sindbis virus encoding EPAC-SH150, a sensor with increased sensitivity for cAMP (*26*). As expected, $A_{2A}R$ activation with CGS21680 increased intracellular cAMP levels (fig. S15). $GABA_AR$ activation with muscimol also increased cAMP levels within a similar range as CGS21680 (fig. S15). Application of both CGS21680 and muscimol strongly elevated intracellular cAMP levels (fig. S15), demonstrating that the activation of $GABA_AR$s and $A_{2A}R$s converge with additive effects on cAMP production.

Stabilization of GABAergic synapses requires cAMP production

We then tested the implication of intracellular Ca^{2+} and CaM in GABAergic synapse stabilization. The loss of GABAergic synapses induced by expressing shRNA against $GABA_AR$ γ2 subunit (shγ2) in DIV10 neurons was prevented by the activation of CaM with the cell-permeable activator CALP3 (100 µM) during 30 min (Fig. 3B). Thus, CaM is involved in the stabilization of GABAergic synapses. Application of the AC inhibitor SQ22536 (20 µM) prevented the CALP3-mediated rescue of GABAergic synapses (Fig. 3B), demonstrating that CaM stabilizes synapses through activation of ACs.

Hippocampal neurons express Ca^{2+} dependent and independent ACs targeted respectively to lipid raft and non-raft plasma membranes (*27*). To investigate the involvement of Ca^{2+} dependent and independent ACs, we used genetically encoded 'cAMP sponges' targeted to (Lyn-cAMP sponge) or outside (Kras-cAMP sponge) lipid rafts, enabling local perturbation of cAMP downstream signaling (*28*). A variant of Lyn-cAMP sponge (Lyn-mut-cAMP sponge) unable to bind and buffer cAMP was used as a control. In basal conditions, none of cAMP sponges altered the density of GABAergic synapses (fig. S16). However, buffering cAMP near lipid rafts blocked the CALP3-mediated rescue of GABAergic synapses in neurons expressing shγ2 (Fig. 3C). This effect was specific of sponges targeted to lipid rafts since the density of synapses in neurons expressing Lyn-mut-cAMP or Kras-cAMP sponges were not distinguishable from CALP3-treated neurons lacking $GABA_AR\gamma2$ (Fig. 3C). Thus, the convergence of $GABA_AR$ and $A_{2A}R$ pathways on the stabilization of GABAergic synapses relies on cAMP production by Ca^{2+}-dependent CaM-activated ACs. We then investigated the mechanism downstream of cAMP production.

Adenosine stabilizes synapses through PKA-phospho-regulation of gephyrin

Protein kinase A (PKA) is a downstream effector of cAMP following $A_{2A}R$ activation. As expected, intracellular inhibition of PKA with the protein kinase inhibitor peptide (PKI) decreased mIPSC amplitude and frequency *ex vivo* (26% and 50%, respectively; fig. S17), to the same extent as that found with SCH58261 (100 nM). Since PKA-mediated phosphorylation of gephyrin is required for its postsynaptic stabilization and the anchoring of $GABA_ARs$ at synapses (*29*), we hypothesized that PKA activation via the $A_{2A}R$-AC/cAMP cascade insures the phosphorylation of gephyrin required to maintain $GABA_ARs$ at the synapse.

Gephyrin is a direct substrate of PKA, hence we tested whether gephyrin phosphorylation at the Ser303 PKA-sensitive site was increased after $A_{2A}R$ activation by CGS21680. For this, we used

HEK293 cells and measured gephyrin phosphorylation using S303 site specific gephyrin phospho-antibody (*30*). Removal of ambient adenosine with ADA~~+~~ and~~–~~ AMPCP and simultaneous activation of A_{2A}Rs with CGS21680 significantly increased gephyrin phosphorylation at the Ser303 site (Fig. 4A). These effects of ADA~~+~~ and~~–~~ AMPCP or ADA~~+~~ and~~–~~ AMPCP~~+~~ and CGS21680 were not observed in cells that expressed a gephyrin phospho-null mutant (gephyrin-S303A) (Fig. 4A). This demonstrates that gephyrin can be phosphorylated on its unique PKA site upon A_{2A}R activation.

We then directly tested the contribution of PKA-dependent phosphorylation of gephyrin in synapse stabilization *in vitro* by expressing constructs harboring mutations of the PKA Ser303 site to aspartate (S303D) to mimic the gephyrin phosphorylated state (*30*). Decreasing extracellular adenosine with AMPCP~~+~~ and~~–~~ ADA led to synapse destabilization in neurons expressing wild type gephyrin (Fig. 4B), whereas the expression of the gephyrin-S303D mutant prevented synapse loss upon removal of extracellular adenosine (Fig. 4B). Thus, the PKA Ser303 phospho-site of gephyrin is required for the A_{2A}R-mediated synapse stabilization. This effect was specific of this phospho-site since decreasing extracellular adenosine led to synapse destabilization in neurons expressing the glycogen synthase kinase 3β (GSK3β) phospho-null gephyrin mutant (gephyrin-S270A) (fig. S18). We conclude that activation of A_{2A}Rs leads to GABAergic synapse stabilization through CaM-AC-cAMP-PKA-mediated phosphorylation of gephyrin at position Ser303. This mechanism accounts for the disappearance of the postsynaptic site when A_{2A}Rs are not activated by adenosine for more than 10 min (fig. S11).

Gephyrin phosphorylated on Ser303 interacts with Slitrk3

How can we explain the concurrent loss of the presynaptic element? Overexpression of the PKA-phosphorylation site gephyrin-~~-~~S303D mutant ~~S303D~~ was sufficient to rescue the loss of VGAT-

containing terminals on neurons transfected with shγ2 (Fig. 4C). This demonstrates that gephyrin is sufficient to stabilize synapses. We thus hypothesized that gephyrin phosphorylated at Ser303 interacts with the post-synaptic Neuroligin-2 (*31*, *32*) or Slitrk3 (*33*) transmembrane proteins that bind in the synaptic cleft to presynaptic Neurexins or PTPδ~~σ~~ to organize inhibitory synapses. The knock-down of post-synaptic Neuroligin-2 with a specific shRNA or the antibody-induced blockade of pre-synaptic Neurexin led, as expected (*34*–*36*), to a loss of GABAergic synapses, which could be rescued upon $A_{2A}R$ activation with CGS21680 (fig. S19). Thus, $A_{2A}R$-dependent synapse stabilization does not depend upon the Neurexin-Neuroligin-2 trans-synaptic complex. In contrast, $GABA_AR$ activation did not rescue the synapse loss induced by the expression of a shRNA against Neuroligin-2 (fig. S19).

Commenté [CB1]: Delta, non?

$A_{2A}R$ or $GABA_AR$ activation did not prevent synaptic loss induced by a shRNA against post-synaptic Slitrk3 (*33*) (Fig. 5A), supporting the involvement of Slitrk3 in $A_{2A}R$- and $GABA_AR$-dependent synapse stabilization. We then overexpressed the ~~Myc-~~Slitrk3-Y969A mutant, since this site is ~~critical for~~involved in the formation of GABAergic synapses (*37*) (Fig. 5B). $A_{2A}R$ activation was not able to restore synapses in cells overexpressing ~~Myc-~~Slitrk3-Y969A (Fig. 5B). Therefore, deletion of Slitrk3 or a single amino acid mutation of Slitrk3 was enough to prevent $A_{2A}R$-dependent stabilization of GABAergic synapses. Finally, using co-immunoprecipitation experiments, we found that gephyrin-WT and gephyrin-S303D interact directly with Slitrk3 (Fig. 5C). These results suggest that $A_{2A}R$ signaling stabilizes the pre- and post-synaptic GABAergic elements via PKA-dependent gephyrin phosphorylation and Slitrk3 recruitment.

Transient blockade of $A_{2A}R$s induces cognitive deficits

All previous experiments were performed *in vitro* and *ex vivo* to unravel the molecular mechanism. We next tested whether the role of $A_{2A}R$s could also be evidenced *in vivo* during the postnatal

synaptogenesis period. We could not use $A_{2A}R$ knockout animals, because a delayed migration of GABAergic neurons occurs in these animals (*13*), which would result in a decreased number of GABAergic synapses. This would prevent us to distinguish between effects due to a delayed migration from a direct effect on the stability of GABAergic synapses. We thus injected shRNAs against $A_{2A}Rs$ *in vivo* in the hippocampus at P3. This led to the loss of GABAergic synapses evaluated at P16 (fig. S20), confirming the physiological role of $A_{2A}Rs$ in the stabilization of GABAergic synapses. Additionally, we treated pups during the peak of synaptogenesis between P3 and P16 with SCH58261 (0.1 mg/kg). Although we cannot rule out non-specific effects, the treatment produced a loss of GABAergic synapses at P16 in the hippocampus (fig S20) similar to that found *in vitro* (fig. S4) and *ex vivo* (Fig. 1C). Given such synaptic loss, we predicted detrimental functional consequences, in particular for hippocampus-dependent spatial memory. We thus tested P70 animals, which had been treated between P3 and P16 with SCH58261. As predicted, we found deficits in the novel object location task (fig. S20). In contrast, open field, anxiety and novel object recognition tests were not modified (fig. S20). These results indicate that interfering with $A_{2A}Rs$ *in vivo* during synaptogenesis has long-term deleterious effects on cognitive function.

Discussion

This $A_{2A}R$-dependent mechanism adds to other molecules and signaling pathways known to control hippocampal GABAergic synapse during development (*1*, *4*, *38*), including GABA (*4*–*8*) and $GABA_AR$-induced elevation of intra-neuronal Ca^{2+} level following the activation of voltage-dependent Ca^{2+} channels (*9*, *10*). We propose that this in turn activates Ca^{2+}-CaM-sensitive ACs leading to a rise in intracellular cAMP in neurons. Thus, one ~~key~~ outcome of $GABA_AR$ activation in immature neurons is to elevate intracellular cAMP levels. A hypothesis is that adenosine/ATP

is co-released with GABA (*16*, *17*) during development, which would provide A_{2A}Rs with a direct information that the presynaptic terminal is active. Once activated, Gs-coupled A_{2A}Rs will trigger a rise in intracellular cAMP levels, leading in turn to PKA activation and stabilization of GABAergic synapses (fig. S21). Such A_{2A}R-mediated control of synapse selection seems to be autonomous, since it does not require BDNF-TrkB receptor signaling (fig. S22).

We found additive effects of GABA and adenosine pathways on cAMP levels. ~~Interestingly,~~ ACs can act as coincidence detectors, promoting cellular responses only when convergent regulatory signals occur close in time and space (*39*). Our results show that the $GABA_AR$ and A_{2A}R systems are spatially close and operate within a similar time frame to control the fate of some GABAergic synapses. This effect of GABA/adenosine co-signaling at GABAergic synapses would occur only during a ~~critical~~ specific period of development because of the transient expression of A_{2A}Rs and because of the transient depolarizing action of $GABA_A$Rs and their ability to activate CaM-sensitive ACs.

This described A_{2A}R mechanism therefore provides a conceptual framework to understand how some synapses are stabilized or removed during development. During neural development, inactive synapses are eliminated~~The common view is tha~~.~~t inactive synapses are eliminated~~ . ~~-~~This requires the existence of a machinery that includes a detector of activity from the presynaptic terminal and a mechanism that removes the synapse when the detector is not activated. The adenosine-operated A_{2A}R can subserve all these functions, in addition to the involvement of GABA itself. The post/peri-synaptic localization of A_{2A}Rs can detect the activity-dependent release of adenosine/ATP (*20*, *40*, *41*), which mostly involves a direct release of adenosine as a signal proportional to the metabolic support of synaptic activity as well as a CD73-mediated extracellular formation of vesicular ATP-derived adenosine (*11*, *12*, *20*). The non-activation of A_{2A}Rs will prevent the continuous phosphorylation of gephyrin, which is essential for synapse

stabilization. ~~Importantly, s~~Synapse removal requires a certain period of $A_{2A}R$ inactivity (20 min), which permits persistence of somewhat quiet but not silent ~~which may guarantee unwanted disappearance of~~ synapses. ~~Notably, this $A_{2A}R$-mediated control of synapse selection seems to be autonomous, since it does not strictly require BDNF-TrkB receptor signaling (fig. S22).~~

Caffeine, the most commonly psychoactive drug consumed in the world, including during pregnancy, is a natural antagonist of $A_{2A}Rs$ ~~(PMID 28603504)~~. Exposure to caffeine during the peak of synaptogenesis may trigger the removal of some synapses, with deleterious effects.

Commenté [S2]:

Methods

Electrophysiology: mIPSCs were recorded in coronal CA1 hippocampal slices (350 µm) from male GIN-mice as in (*42*).

Stereotaxic hippocampal injection of $shA_{2A}R$ was done at P3 with 0.15 µL of AAV2.1-U6-shNT-GFP or AAV2.1-U6-shA2AR-GFP (70 nL/min).

Immunohistochemistry: For acute SCH58261 treatment, P6 slices were fixed with 4% paraformaldehyde (PFA), cryoprotected in 20% sucrose, frozen on dry ice, and incubated in rabbit anti-VGAT antibody (1:1000, SYSY). Images were acquired with a Zeiss LSM 510 microscope. For chronic SCH58261 treatment or $shA_{2A}R$ expression, P16 brains were post-fixed in 4% PFA, cryoprotected (30% sucrose) and cut in parasagittal free-floating sections (30 µm) (*43*) that were incubated in rabbit anti-VGAT (1:1000, from B. Gasnier). Z-stacks were acquired with a Leica SP5 confocal microscope and quantified using Imaris. For $A_{2A}R$ detection, P3-12 coronal free-floating sections (100 µm) were incubated in goat anti-$A_{2A}R$ antibody (1:200, Santa Cruz). Images were acquired with a Zeiss Z2 microscope. Ultrastructural analysis of $A_{2A}R$ was performed using

the pre-embedding immunogold method (*44*) with guinea pig anti-$A_{2A}R$ (Frontier Institute, Japan). Images were acquired with Jeol-1010 microscope.

$A_{2A}R$ binding (*18*) was with 2 nM of ^{3}H-SCH58261 using 140-210 μg of protein. Release of ATP and adenosine (*20*) from hippocampal synaptosomes was assessed using the luciferin-luciferase assay (ATP) and HPLC (adenosine) upon K^{+}-induced depolarization (*20*).

Western blotting: $A_{2A}R$ density (*18*, *24*) was studied with goat (Santa Cruz) or mouse (Millipore) anti-$A_{2A}R$ antibodies. Validation of shA_{2A}Rs was done with rabbit anti-$A_{2A}R$ (1:500, Alomone) antibodies in N2a cells infected with AAV2.1-U6-shNT-GFP/AAV2.1-U6-shA2AR-GFP. Gephyrin-Slitrk3 interaction was assessed with rabbit anti-Slitrk3 (1:1000, Sigma) antibodies in HEK293T cells transfected with pCMV3-Myc-Slitrk3 or eGFP-gephyrin-WT (*45*) or eGFP-gephyrin-S303D (*30*). Gephyrin phosphorylation was analyzed with rabbit custom made anti-phospho-gephyrin and mouse anti-gephyrin (3B11, 1:1000, SYSY) antibodies in HEK293T cells transfected with eGFP-gephyrin-WT or eGFP-gephyrin-S303A.

Behavioral testing: Open-field, NOL, NOR, elevated plus maze was done as in (*46*) at P70 on wild-type males treated with saline or SCH58261 (0.1 mg/kg) between P3-P16.

Cultures of hippocampal neurons were prepared as described (*47*).

Immunocytochemistry was done using rabbit anti-VGAT (1:500, from B. Gasnier), mouse anti-gephyrin (mAb7a, 1:500, SYSY) and guinea pig anti-$GABA_AR\gamma2$ (1:2000, from J.M. Fristchy), or mouse anti-VGAT (1:500, SYSY) and rabbit anti-$GABA_AR\alpha1$ or $GABA_AR\alpha2$ (1:500, SYSY), or mouse anti-GAD 67 (1:500, Chemicon) and rabbit anti-$A_{2A}R$ (1:100, Alomone). Image acquisition and cluster analysis was as in (*47*).

Single particle tracking of $GABA_AR\gamma2$ was as described (47, *48*).

DNA-PAINT was performed with rabbit anti-$A_{2A}R$ (1:100, Alomone) and mouse anti-gephyrin (mAb7a, 1:500, SYSY) on an inverted Nikon Eclipse Ti microscope using 561 and 647 nm lasers.

Calcium imaging of AAV-GCaMP6-ruby infected neurons was done on a Leica DMI4000 microscope (Yokogawa CS20 spinning Nipkow disk) with a 491 nm laser. Time lapse (0.33 Hz for 600 seconds) of stacks (~21 sections, step 0.3 µm) were acquired.

cAMP imaging of EPAC-sh150 (*26*) was done on a two-photon Leica TCS/MP5 microscope with a Ti:sapphire laser (Coherent). Z-stacks (8-10 sections, step 1-2 µm) were acquired every 15 seconds.

Videomicroscopy of presynaptic terminals (*22*) stained with rabbit anti-VGAT-Oyster^{550} (1:200, SYSY) was done using an Olympus IX71 microscope. Time-lapse (1 image every 5 min) were acquired.

A detailed "Materials and Methods" can be found in the Supplementary Material.

References

1. D. Krueger-Burg, T. Papadopoulos, N. Brose, Organizers of inhibitory synapses come of age. *Curr. Opin. Neurobiol.* **45**, 66-77 (2017). doi: 10.1016/j.conb.2017.04.003; pmid: 28460365

2. A. M. Craig, Y. Kang, Neurexin-neuroligin signaling in synapse development. *Curr. Opin. Neurobiol.* **17**, 43-52 (2007). doi: 10.1016/j.conb.2007.01.011; pmid: 17275284

3. T. C. Südhof, Towards an understanding of synapse formation. *Neuron.* **100**, 276-293 (2018). doi: 10.1016/j.neuron.2018.09.040; pmid: 30359597

4. Z. J. Huang, P. Scheiffele, GABA and neuroligin signaling: linking synaptic activity and adhesion in inhibitory synapse development. *Curr. Opin. Neurobiol.* **18**, 77-83 (2008). doi: 10.1016/j.conb.2008.05.008; pmid: 18513949

5. Z. J. Huang, G. Di Cristo, F. Ango, Development of GABA innervation in the cerebral and

cerebellar cortices. *Nat. Rev. Neurosci.* **8**, 673-686 (2007). doi: 10.1038/nrn2188; pmid: 17704810

6. W. C. Oh, S. Lutzu, P. E. Castillo, H. B. Kwon, De novo synaptogenesis induced by GABA in the developing mouse cortex. *Science* **353**, 1037-1040 (2016). doi: 10.1126/science.aaf5206; pmid: 27516412

7. B. Chattopadhyaya, G. Di Cristo, C. Z. Wu, G. Knott, S. Kuhlman, Y. Fu, *et al.*, GAD67-Mediated GABA synthesis and signaling regulate inhibitory synaptic innervation in the visual cortex. *Neuron* **54**, 889-903 (2007). doi: 10.1016/j.neuron.2007.05.015; pmid: 17582330

8. X. Wu, Y. Fu, G. Knott, J. Lu, G. Di Cristo, Z. Josh Huang, GABA signaling promotes synapse elimination and axon pruning in developing cortical inhibitory interneurons. *J. Neurosci.* **32**, 331-43 (2012). doi: 10.1523/JNEUROSCI.3189-11.2012; pmid: 22219294

9. X. Leinekugel, V. Tseeb, Y. Ben-Ari, P. Bregestovski, Synaptic $GABA_A$ activation induces Ca^{2+} rise in pyramidal cells and interneurons from rat neonatal hippocampal slices. *J. Physiol.* **487**, 319-29 (1995). doi: 10.1113/jphysiol.1995.sp020882; pmid: 8558466

10. T. S. Perrot-Sinal, A. P. Auger, M. M. McCarthy, Excitatory actions of GABA in developing brain are mediated by L-type Ca^{2+} channels and dependent on age, sex, and brain region. *Neuroscience* **116**, 995-1003 (2003). doi: 10.1016/S0306-4522(02)00794-7; pmid: 12617940

11. B. P. Klyuch, N. Dale, M. J. Wall, Deletion of ecto-5'-nucleotidase (CD73) reveals direct action potential-dependent adenosine release. *J. Neurosci.* **32**, 3842-3847 (2012). doi: 10.1523/JNEUROSCI.6052-11.2012; pmid: 22423104

12. M. J. Wall, N. Dale, Neuronal transporter and astrocytic ATP exocytosis underlie activity-dependent adenosine release in the hippocampus. *J. Physiol.* **591**, 3853-71 (2013). doi:10.1113/jphysiol.2013.253450; pmid: 23713028

13. C. G. Silva, C. Métin, W. Fazeli, N. J. Machado, S. Darmopil, P.-S. Launay, *et al.*, Adenosine receptor antagonists including caffeine alter fetal brain development in mice. *Sci. Transl. Med.* **5**, 197ra104-197ra104 (2013). doi: 10.1126/scitranslmed.3006258; pmid: 23926202

14. S. Alçada-Morais, N. Gonçalves, V. Moreno-Juan, B. Andres, S. Ferreira, J. M. Marques, *et al.*, Adenosine A_{2A} receptors contribute to the radial migration of cortical projection neurons through the regulation of neuronal polarization and axon formation. *Cereb Cortex* **bhab188** (2021). doi: 10.1093/cercor/bhab188; pmid: 34184030

15. L. Nadal, N. Garcia, E. Hurtado, A. Simó, M. Tomàs, M. A. Lanuza, *et al.*, Presynaptic muscarinic acetylcholine autoreceptors (M1, M2 and M4 subtypes), adenosine receptors (A_1 and A_{2A}) and tropomyosin-related kinase B receptor (TrkB) modulate the developmental synapse elimination process at the neuromuscular junction. *Mol. Brain* **9**, 67 (2016). doi: 10.1186/s13041-016-0248-9; pmid: 27339059

16. Y. H. Jo, R. Schlichter, Synaptic corelease of ATP and GABA in cultured spinal neurons. *Nat. Neurosci.* **2**, 241–245 (1999). doi: 10.1038/6344; pmid: 10195216

17. Y. H. Jo, L. W. Role, Coordinate release of ATP and GABA at in vitro synapses of lateral hypothalamic neurons. *J. Neurosci.* **22**, 4794–4804 (2002). doi: 10.1523/JNEUROSCI.22-12-04794.2002; pmid: 12077176

18. N. Rebola, P. M. Canas, C. R. Oliveira, R. A. Cunha, Different synaptic and subsynaptic localization of adenosine A_{2A} receptors in the hippocampus and striatum of the rat.

Neuroscience **132**, 893-903 (2005). doi: 10.1016/j.neuroscience.2005.01.014; pmid: 15857695

19. E. Augusto, M. Matos, J. Sévigny, A. El-Tayeb, M. S. Bynoe, C. E. Müller, *et al.*, Ecto-5′-nucleotidase (CD73)-mediated formation of adenosine is critical for the striatal adenosine A_{2A} receptor functions. *J. Neurosci.* **33**, 11390-11399 (2013). doi: 10.1523/JNEUROSCI.5817-12.2013; pmid: 23843511

20. R. A. Cunha, E. S. Vizi, J. A. Ribeiro, A. M. Sebastião, Preferential release of ATP and its extracellular catabolism as a source of adenosine upon high- but not low-frequency stimulation of rat hippocampal slices. *J. Neurochem.* **67**, 2180-7 (1996). doi: 10.1046/j.1471-4159.1996.67052180.x; pmid: 8863529

21. E. Link, L. Edelmann, J. H. Chou, T. Binz, S. Yamasaki, U. Eisel, *et al.*, Tetanus toxin action: Inhibition of neurotransmitter release linked to synaptobrevin proteolysis. *Biochem. Biophys. Res. Commun.* **189**, 1017-1023 (1992). doi: 10.1016/0006-291X(92)92305-H; pmid: 1361727

22. F. A. Dobie, A. M. Craig, Inhibitory Synapse Dynamics: Coordinated Presynaptic and Postsynaptic Mobility and the Major Contribution of Recycled Vesicles to New Synapse Formation. *J. Neurosci.* **31**, 10481–10493 (2011). doi: 10.1523/JNEUROSCI.6023-10.2011; pmid: 21775594

23. R. W. Li, W. Yu, S. Christie, C. P. Miralles, J. Bai, J. J. LoTurco, A. L. De Blas, Disruption of postsynaptic $GABA_A$ receptor clusters leads to decreased GABAergic innervation of pyramidal neurons. *J. Neurochem.* **95**, 756–770 (2005). doi: 10.1111/j.1471-4159.2005.03426.x; pmid: 16248887

24. A. P. Simões, N. J. Machado, N. Gonçalves, M. P. Kaster, A. T. Simões, A. Nunes, *et al.*,

Adenosine A_{2A} receptors in the amygdala control synaptic plasticity and contextual fear memory. *Neuropsychopharmacology* **41**, 2862-2871 (2016). doi: 10.1038/npp.2016.98; pmid: 27312408

25. A. C. Conti, J. W. Maas, L. M. Muglia, B. A. Dave, S. K. Vogt, T. T. Tran, *et al.*, Distinct regional and subcellular localization of adenylyl cyclases type 1 and 8 in mouse brain. *Neuroscience* **146**, 713-729 (2007). doi: 10.1016/j.neuroscience.2007.01.045; pmid: 17335981

26. M. Polito, J. Klarenbeek, K. Jalink, D. Paupardin-Tritsch, P. Vincent, L. R. V Castro, The NO/cGMP pathway inhibits transient cAMP signals through the activation of PDE2 in striatal neurons. *Front. Cell. Neurosci.* **7**, 211 (2013). doi: 10.3389/fncel.2013.00211; pmid: 24302895

27. D. M. F. Cooper, V. G. Tabbasum, Adenylate cyclase-centred microdomains. *Biochem. J.* **462**, 199-213 (2014). doi: 10.1042/BJ20140560; pmid: 25102028

28. S. Averaimo, A. Assali, O. Ros, S. Couvet, Y. Zagar, I. Genescu, *et al.*, A plasma membrane microdomain compartmentalizes ephrin-generated cAMP signals to prune developing retinal axon arbors. *Nat. Commun.* **7**, 12896 (2016). doi: 10.1038/ncomms12896; pmid: 27694812

29. P. Zacchi, R. Antonelli, E. Cherubini, Gephyrin phosphorylation in the functional organization and plasticity of GABAergic synapses. *Front. Cell. Neurosci.* **8**, 103 (2014). doi: 10.3389/fncel.2014.00103; pmid: 24782709

30. C. E. Flores, I. Nikonenko, P. Mendez, J.-M. Fritschy, S. K. Tyagarajan, D. Muller, Activity-dependent inhibitory synapse remodeling through gephyrin phosphorylation. *Proc. Natl. Acad. Sci. U. S. A.* **112**, E65-72 (2015). doi: 10.1073/pnas.1411170112; pmid:

25535349

31. S. K. Tyagarajan, J.-M. Fritschy, Gephyrin: a master regulator of neuronal function? *Nat. Rev. Neurosci.* **15**, 141–56 (2014). doi: 10.1038/nrn3670; pmid: 24552784

32. V. Tretter, J. Mukherjee, H. M. Maric, H. Schindelin, W. Sieghart, S. J. Moss, Gephyrin, the enigmatic organizer at GABAergic synapses. *Front. Cell. Neurosci.* **6**, 23 (2012). doi: 10.3389/fncel.2012.00023; pmid: 22615685

33. H. Takahashi, K. I. Katayama, K. Sohya, H. Miyamoto, T. Prasad, Y. Matsumoto, *et al.*, Selective control of inhibitory synapse development by Slitrk3-PTPδ trans-synaptic interaction. *Nat. Neurosci.* **15**, 389-98, S1-2. (2012). doi: 10.1038/nn.3040; pmid: 22286174

34. B. Chih, H. Engelman, P. Scheiffele, Control of excitatory and inhibitory synapse formation by neuroligins. *Science* **307**, 1324-1328 (2005). doi: 10.1126/science.1107470; pmid: 15681343

35. M. Mondin, B. Tessier, O. Thoumine, Assembly of synapses: Biomimetic assays to control neurexin/neuroligin interactions at the neuronal surface. *Curr. Protoc. Neurosci.* Chapter **2**:Unit 2.19 (2013). doi: 10.1002/0471142301.ns0219s64; pmid: 23853109

36. A. A. Chubykin, D. Atasoy, M. R. Etherton, N. Brose, E. T. Kavalali, J. R. Gibson, *et al.*, Activity-dependent validation of excitatory versus inhibitory synapses by neuroligin-1 versus neuroligin-2. *Neuron* **54**, 919-931 (2007). doi: 10.1016/j.neuron.2007.05.029; pmid: 17582332

37. J. Li, W. Han, K. Wu, Y. D. Li, Q. Liu, W. Lu, A conserved tyrosine residue in Slitrk3 carboxyl-terminus is critical for GABAergic synapse development. *Front. Mol. Neurosci.* **12**, 213 (2019). doi: 10.3389/fnmol.2019.00213; pmid: 31551708

38. J. Ko, G. Choii, J. W. Um, The balancing act of GABAergic synapse organizers. *Trends Mol. Med.* **21**, 256-268 (2015). doi: 10.1016/j.molmed.2015.01.004; pmid: 25824541

39. A. G. Nair, O. Gutierrez-Arenas, O. Eriksson, P. Vincent, J. H. Kotaleski, Sensing positive versus negative reward signals through adenylyl cyclase-coupled GPCRs in direct and indirect pathway striatal medium spiny neurons. *J. Neurosci.* **35**, 14017-14030 (2015). doi: 10.1523/JNEUROSCI.0730-15.2015; pmid: 26468202

40. J. B. Mitchell, C. R. Lupica, T. V. Dunwiddie, Activity-dependent release of endogenous adenosine modulates synaptic responses in the rat hippocampus. *J. Neurosci.* **13**, 3439-3447 (1993). doi: 10.1523/jneurosci.13-08-03439.1993; pmid: 8393482

41. A. Wieraszko, G. Goldsmith, T. N. Seyfried, Stimulation-dependent release of adenosine triphosphate from hippocampal slices. *Brain Res.* **485**, 244-50 (1989). doi: 10.1016/0006-8993(89)90567-2; pmid: 2566360

42. R. Cossart, C. Dinocourt, J. C. Hirsch, A. Merchan-Perez, J. De Felipe, Y. Ben-Ari, *et al.*, Dendritic but not somatic GABAergic inhibition is decreased in experimental epilepsy. *Nat. Neurosci.* **4**, 52–62 (2001). doi: 10.1038/82900; pmid: 11135645

43. T. Notter, P. Panzanelli, S. Pfister, D. Mircsof, J. M. Fritschy, A protocol for concurrent high-quality immunohistochemical and biochemical analyses in adult mouse central nervous system. *Eur. J. Neurosci.* **39**, 165-75 (2014). doi: 10.1111/ejn.12447; pmid: 24325300

44. R. Luján, Z. Nusser, J. D. B. Roberts, R. Shigemoto, P. Somogyi, Perisynaptic location of metabotropic glutamate receptors mGluR1 and mGluR5 on dendrites and dendritic spines in the rat hippocampus. *Eur. J. Neurosci.* 8, 1488-1500 (1996). doi: 10.1111/j.1460-9568.1996.tb01611.x; pmid: 8758956

45. S. K. Tyagarajan, H. Ghosh, G. E. Yévenes, I. Nikonenko, C. Ebeling, C. Schwerdel, *et al.*, Regulation of GABAergic synapse formation and plasticity by GSK3beta-dependent phosphorylation of gephyrin. *Proc. Natl. Acad. Sci. U. S. A.* **108**, 379–84 (2011). doi: 10.1073/pnas.1011824108; pmid: 21173228

46. M. P. Kaster, N. J. Machado, H. B. Silva, A. Nunes, A. Paula, M. Santana, Caffeine acts through neuronal adenosine A_{2A} receptors to prevent mood and memory dysfunction triggered by chronic stress. *Proc. Natl. Acad. Sci. U. S. A.* **112**, 7833–7838 (2015). doi: 10.1073/pnas.1423088112; pmid: 26056314

47. S. Battaglia, M. Renner, M. Russeau, E. Côme, S. K. Tyagarajan, S. Lévi, Activity-dependent inhibitory synapse scaling is determined by gephyrin phosphorylation and subsequent regulation of $GABA_A$ receptor diffusion. *Eneuro* **5**, ENEURO.0203-17.2017 (2018). doi: 10.1523/ENEURO.0203-17.2017; pmid: 29379879

48. H. Bannai, S. Lévi, C. Schweizer, M. Dahan, A. Triller, Imaging the lateral diffusion of membrane molecules with quantum dots. *Nat. Protoc.* **1**, 2628–2634 (2006). doi: 10.1038/nprot.2006.429; pmid: 17406518

Acknowledgments:

We warmly thank Antoine Triller for providing gephyrin-mRFP construct, Ann Marie Craig for shRNA against Slitrk3 coupled to CFP, Quingjun Tian and Wei Lu for Slitrk3-Y969A mutant, Peter Scheiffele for shRNA against Neuroligin-2. We are also grateful to the Animal Facility & Cell and Tissue Imaging Facility of Institut du Fer à Moulin (IFM).

Funding:

Inserm (SL, CB)

Sorbonne Université-UPMC (SL)

Agence Nationale de la Recherche ADONIS ANR-14-CE13-0032 (SL, CB)

DIM NeRF from Région Ile-de-France (SL)

Fondation pour la Recherche sur le Cerveau FRC/Rotary 'Espoir en tête' (SL)

La Caixa Foundation LCF/PR/HP17/52190001 (RAC)

Centro 2020 CENTRO-01-0145-FEDER-000008: BrainHealth 2020 and CENTRO-01-0246-FEDER-000010 (RAC)

FCT POCI-01-0145-FEDER-03127 and UIDB/04539/2020 (RAC)

Spanish Ministerio de Economía y Competitividad (RTI2018-095812-B-I00) (RL)

Junta de Comunidades de Castilla-La Mancha (SBPLY/17/180501/000229) (RL)

CNRS ATIP AO2016 (CL)

Author contributions:

Conceptualization: SL, CB and RAC

Immunofluorescence experiments in hippocampal cultures: FGC, MRu and CM, performed most (FGC) and some (MRu and CM) immunofluorescence experiments in hippocampal cultures, and analyzed the data.

MRu performed hippocampal cultures and molecular biology.

SZ, CGS and CB performed electrophysiological experiments, and ME performed post hoc morphology.

JCP performed calcium imaging, characterized the shA_{2A}R by western blot, performed the stereotaxic injection of AAVshA_{2A}R in the hippocampus in vivo, chronically treated animals with SCH, performed immunohistochemistry in chronically treated and shA_{2A}R expressing animals and quantified the data.

SZ and ME performed and analyzed the immunofluorescence in acute hippocampal slices treated with A_{2A}R antagonists.

RL performed the electron microscopy of A_{2A}R.

SL and MRu performed the single particle tracking experiments and analyzed the data.

GC and CL performed DNA-PAINT experiments and MRe analyzed the data.

NG performed cAMP imaging and analyzed the data.

PMC, FQG, SAM, ES, RJR, PA, ART performed and analyzed the biochemical experiments exploring ATP and adenosine release as well as A_{2A}R density during the synaptogenesis period of development in vivo.

ST designed the biochemical experiments testing gephyrin phosphorylation and gephyrin-Slitrk3 interaction; MF performed the experiments and analyzed the data.

OT produced Neurexin blocking antibody.

XN produced the cAMP sponges.

FGC, SZ, CB, SL prepared the figures.

Funding acquisition: SL, CB and RAC.

Project administration: SL, CB and RAC.

Supervision of the work: SL, CB and RAC.

Writing – original draft: SL, CB and RAC.

Writing – revised manuscript: SL & CB.

Writing – review & editing: SL, CB, RAC, FGC, CL, XN, OT, MRe.

Competing interests: Authors declare that they have no competing interests.

Data and materials availability: All data are available in the main text or the supplementary materials.

Supplementary Materials

Materials and Methods

Figs. S1 to S22

Figure Legends

Fig. 1. $A_{2A}R$ activation stabilizes GABAergic synapses. (**A**) VGAT staining (left) and quantification (right) in DIV 10-11 neurons transfected with non-target (shNT) or on-target $GABA_AR\gamma2$ (shγ2) shRNAs exposed or not to CGS21680 (30 nM) for 30 min. shNT n=60, shγ2 n=52, shγ2 ~~+~~ and CGS21680 n=54, 4 cultures. The loss of GABAergic synapses upon suppression of $GABA_AR\gamma2$ was rescued by activation of $A_{2A}Rs$. (**B**) VGAT staining (left) and quantification (right) in DIV 10-11 neurons transfected with non-target (shNT) or on-target $A_{2A}R$ ($shA_{2A}R$) shRNAs exposed or not to muscimol (mus, 10 µM) for 30 min. shNT n=44, $shA_{2A}R$ n=47, $shA_{2A}R$ ~~+~~ and muscimol n=36, 4 cultures. The loss of GABAergic synapses upon suppression of $A_{2A}R$

was not rescued by $GABA_AR$ activation. Scale bar, 5 µm. Arrowheads show examples of inhibitory synapses labeled for VGAT. (**C**) Acute application of SCH58261 (100 nM) during 30 min in hippocampal slices decreased by 47% the density of VGAT-immunoreactive terminals (8 slices, 3 P6 pups) as compared to controls (6 slices, 3 P6 pups). (**D**) Application of SCH58261 (100 nM) during 30 min reduced the amplitude and frequency of $GABA_AR$-mediated mIPSCs in CA1 pyramidal cells (8 cells, 8 slices, 6 P6 pups). Top: Left, examples of mIPSCs recorded before and after application of SCH58261. Insets: IPSC amplitude or interevent interval. Values were normalized to the control values (A, B); histograms represent means and s.e.m.; Mann-Whitney test (A, B, C); Kolmogorov-Smirnov test (D): ns - not significant; *p≤0.05; **p<0.01; ***p<0.001.

Fig. 2. Synapse stabilization requires extracellular adenosine production. (**A**) Decreasing extracellular adenosine levels with a 30 min treatment of ADA (4-20 U/mL), AMPCP (100 µM) or ADA ~~+~~and AMPCP led to a decrease of mIPSCs amplitude and frequency in CA1 pyramidal cells. N= 12 cells, 12 slices, 6 pups. (**B**) Immunostaining and quantification of VGAT and $GABA_AR\gamma2$ in DIV 10 neurons in the absence or presence of the indicated drugs for 30 min. Arrowheads show examples of inhibitory synapses labeled for VGAT and $GABA_AR\gamma2$. Scale bar, 5 µm. Decreasing extracellular adenosine levels leads to synapse destabilization, an effect prevented by the direct activation of $A_{2A}Rs$ with 30 nM CGS21680. N= 26-41 cells, 3 cultures. Histograms represent means and s.e.m.; Kolmogorov-Smirnov test (A), Mann-Whitney test (B): ns - not significant; *p≤0.05; **p<0.01; ***p<0.001.

Fig. 3. GABAergic synapse stabilization by calmodulin-activated calcium-sensitive ACs. (**A**) Immunostaining and quantification of VGAT in DIV 10 neurons in the absence or presence of the indicated drugs for 30 min. Scale bar, 5 µm. Decreasing intracellular calcium levels with BAPTA-

AM (20 µM) in the absence or presence of ADA (4-20 U/mL) and AMPCP (100 µM) leads to synapse destabilization, an effect prevented by the direct activation of A_{2A}Rs with CGS21680 (30 nM). N= 35-38 cells, 3 cultures. (**B**) Calp3 (100 µM) activation of calmodulin for 30 min rescued the loss of GABAergic synapses in DIV 10-11 neurons expressing $GABA_AR\gamma2$ shRNA (shγ2). The effect of calmodulin was blocked by an adenylyl cyclase inhibitor SQ22536 (20 µM). Scale bar, 5 µm. shNT n=38, shγ2 n=42, shγ2 +and CALP3 n=43, shγ2 +and CALP3 +and SQ22536 n=30, 3 cultures. (**C**) VGAT staining and quantification of DIV 10-11 neurons transfected with non-target (shNT) or on-target $GABA_AR\gamma2$ (shγ2) and/or the different sponges constructs (lyn-cAMP, lyn-mutated cAMP, K-Ras cAMP) exposed to CALP3 for 30 min. Scale bar, 5 µm. shNT n=40, shγ2 n=37, shγ2 +and CALP3 n=40, shγ2 +and CALP3 +and lyn-cAMP sponge n=23, shγ2 +and CALP3 +and lyn-mutated sponge n=27, shγ2 +and CALP3 +and K-Ras n=31, 4 cultures. Arrowheads show examples of inhibitory synapses labeled for VGAT. In all graphs, histograms represent means and s.e.m.; Values normalized to their respective controls; Mann-Whitney test: ns - not significant; *p≤0.05; **p<0.01; ***p<0.001.

Fig. 4. GABAergic synapse stabilization requires phosphorylation of gephyrin on Ser303. (**A**) Western blot and quantification of the gephyrin S303 phosphorylation in control and after 30 min exposure to ADA (4-20 U/mL) +and AMPCP (100 µM) without or with CGS21680 (30 nM)– in HEK293 cells transfected with gephyrin-WT or gephyrin-S303A constructs. Note the significant increased phosphorylation of P-S303 of gephyrin-WT but not gephyrin-S303A upon acute A_{2A}R activation with CGS21680. (**B**) Immunostaining (left) and quantification (right) of $GABA_AR\gamma2$ and VGAT in the absence or presence of ADA +and AMPCP in DIV 10 neurons transfected with 3'UTR gephyrin shRNA and egfp-gephyrin- WT, S303A or S303D constructs. Scale bar, 5 µm. Arrowheads show examples of inhibitory synapses triple-stained for VGAT, $GABA_AR\gamma2$ and gephyrin. WT n=53, WT+ and ADA+ and AMPCP n=49, S303A n=48, S303A+ and ADA+ and

AMPCP n=53, S303D n=45, S303D + and ADA + and AMPCP n=47, 4 cultures. Gephyrin-S303A or S303D block the ADA + and AMPCP effect. (**C**) VGAT staining (left) and quantification (right) of DIV 10-11 neurons transfected with non-target (shNT) or on-target $GABA_AR\gamma2$ (shγ2) shRNAs with egfp-gephyrin-WT or egfp-gephyrin-S303D. Scale bar, 5 µm. Arrowheads show examples of inhibitory synapses labeled for VGAT. shNT n=35, shγ2 n=49, shγ2 + and- geph-S303D n=60, 3 cultures. The loss of GABAergic synapses upon suppression of $GABA_AR\gamma2$ can be rescued upon overexpression of gephyrin-S303D. In all graphs, histograms represent means and s.e.m.; values were normalized to corresponding controls (B, C); ANOVA test (A); Mann-Whitney test (B, C): ns - not significant; **p<0.01; ***p<0.001.

Fig. 5. A_{2A}Rs stabilize GABAergic synapses via the synaptogenic organizer Slitrk3. (**A**) The loss of GABAergic synapses following Slitrk3 suppression cannot be rescued by $A_{2A}R$ or $GABA_AR$ activation. VGAT staining (left) and quantification (right) of DIV 10-11 neurons transfected with shMock or shSlitrk3 exposed or not to muscimol (Mus, 10 µM) or CGS21680 (CGS, 30 nM) for 30 min. Scale bar, 5 µm. (Muscimol) shMock n=42, shSlitrk3 n=34, shSlitrk3 + and- muscimol n=41, 3 cultures. (CGS) shNT n=41, shSlitrk3 n=37, shSlitrk3 + and- CGS n=36, 3 cultures. (**B**) The loss of GABAergic synapses following overexpression of the Slitrk3-Y969A mutant cannot be rescued by the activation of A_{2A}Rs. VGAT staining (left) and quantification (right) of DIV 10-11 neurons transfected with Slitrk3-WT or Slitrk3-Y969A exposed or not to CGS21680 for 30 min. Scale bar, 5 µm. (Muscimol) eGFP n=35, Slitrk3-WT n=38, Slitrk3-Y969A n=39, Slitrk3-Y969A + and- CGS n=41, 2 cultures. (**C**) Pull down of gephyrin-WT using the GFP tag followed by a blot for Slitrk3 showing gephyrin-Slitrk3 interaction in HEK293 cells. In all images, arrowheads show examples of inhibitory synapses labeled for VGAT. In all graphs, histograms represent means and s.e.m.; values were normalized to corresponding controls; Mann-Whitney test (A, B): ns - not significant; *p<0.05; ***p<0.001.

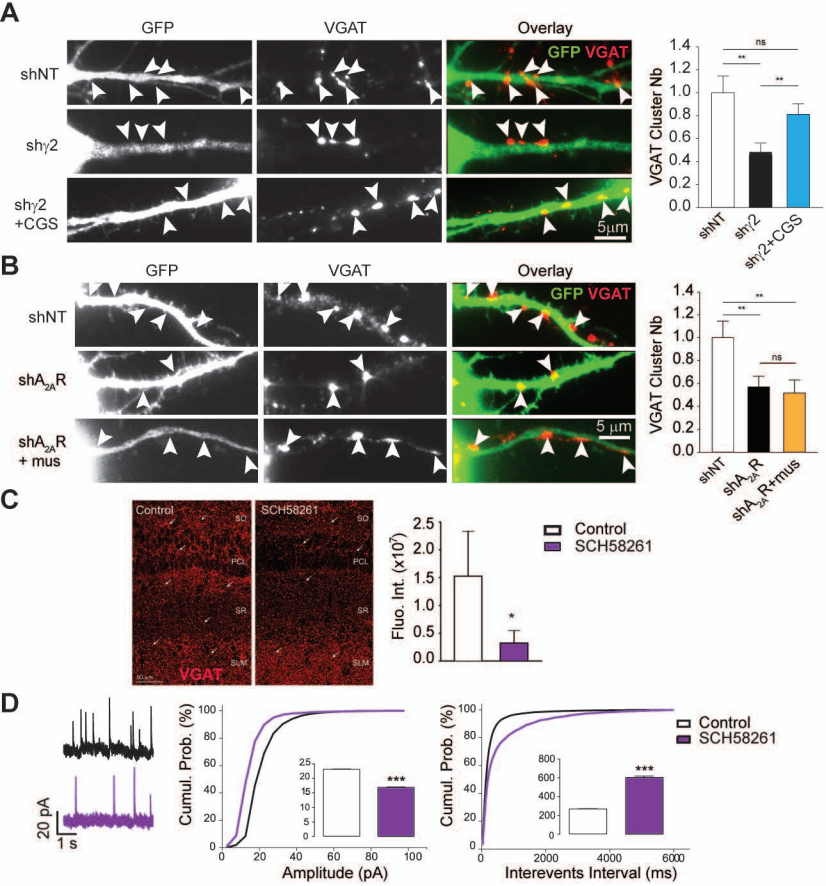
A
GFP
VGAT
Overlay
GFP VGAT
shNT
shγ2
shγ2 +CGS
5μm
VGAT Cluster Nb
ns
**
**
shNT
shγ2
shγ2+CGS
B
GFP
VGAT
Overlay
GFP VGAT
shNT
shA2AR
shA2AR + mus
5 μm
VGAT Cluster Nb
**
**
ns
shNT
shA2AR
shA2AR+mus
C
Control
SCH58261
SO
PCL
SR
SLM
VGAT
Fluo. Int. (x10^7)
Control
SCH58261
*
D
20 pA
1 s
Cumul. Prob. (%)
***
Amplitude (pA)
Cumul. Prob. (%)
Control
SCH58261
***
Interevents Interval (ms)

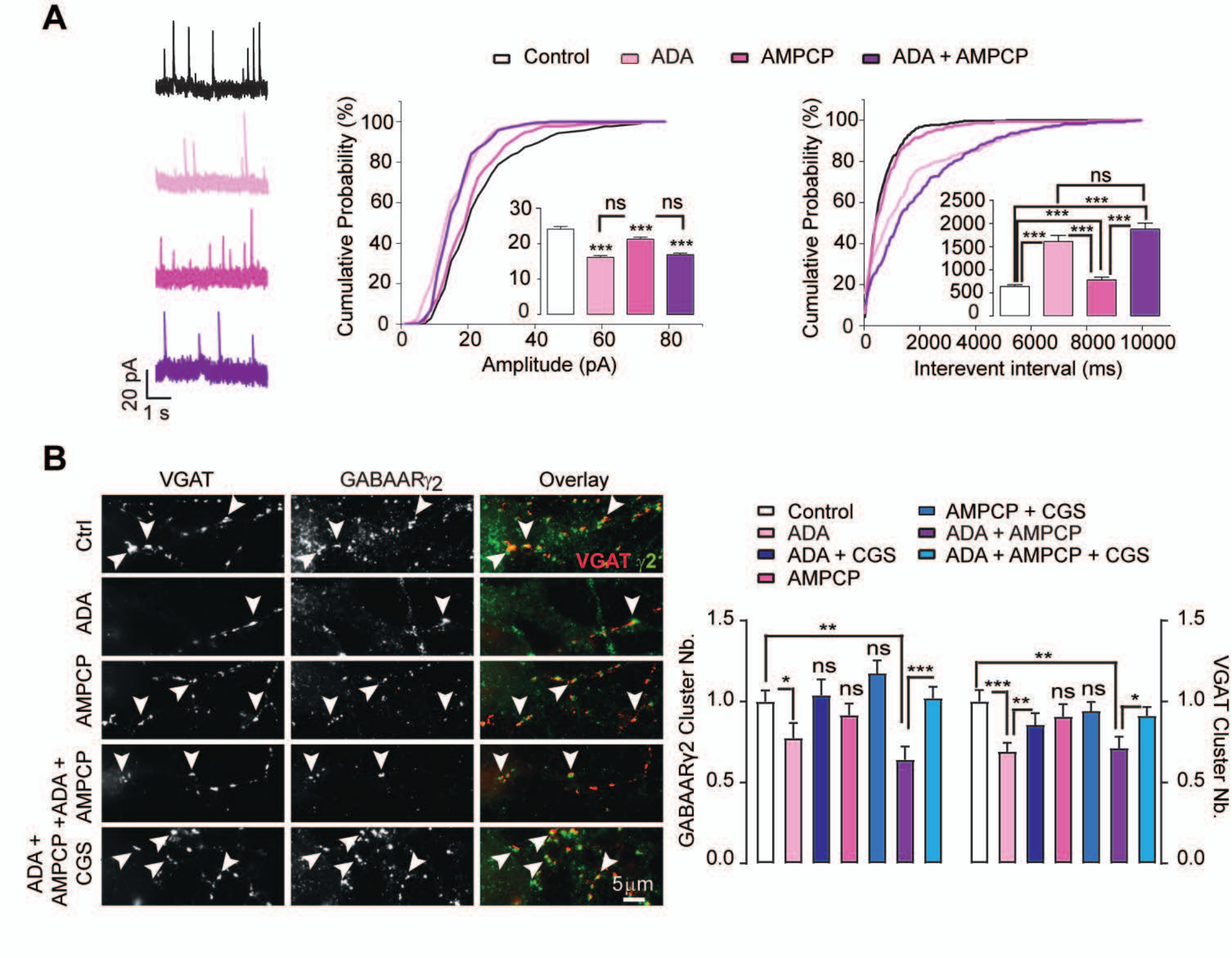
A
Control
ADA
AMPCP
ADA + AMPCP
20 pA
1 s
Cumulative Probability (%)
Amplitude (pA)
Interevent interval (ms)
ns
***
B
VGAT
GABAARγ2
Overlay
Ctrl
ADA
AMPCP
ADA + AMPCP + CGS
ADA + CGS
VGAT γ2
5µm
GABAARγ2 Cluster Nb.
VGAT Cluster Nb.

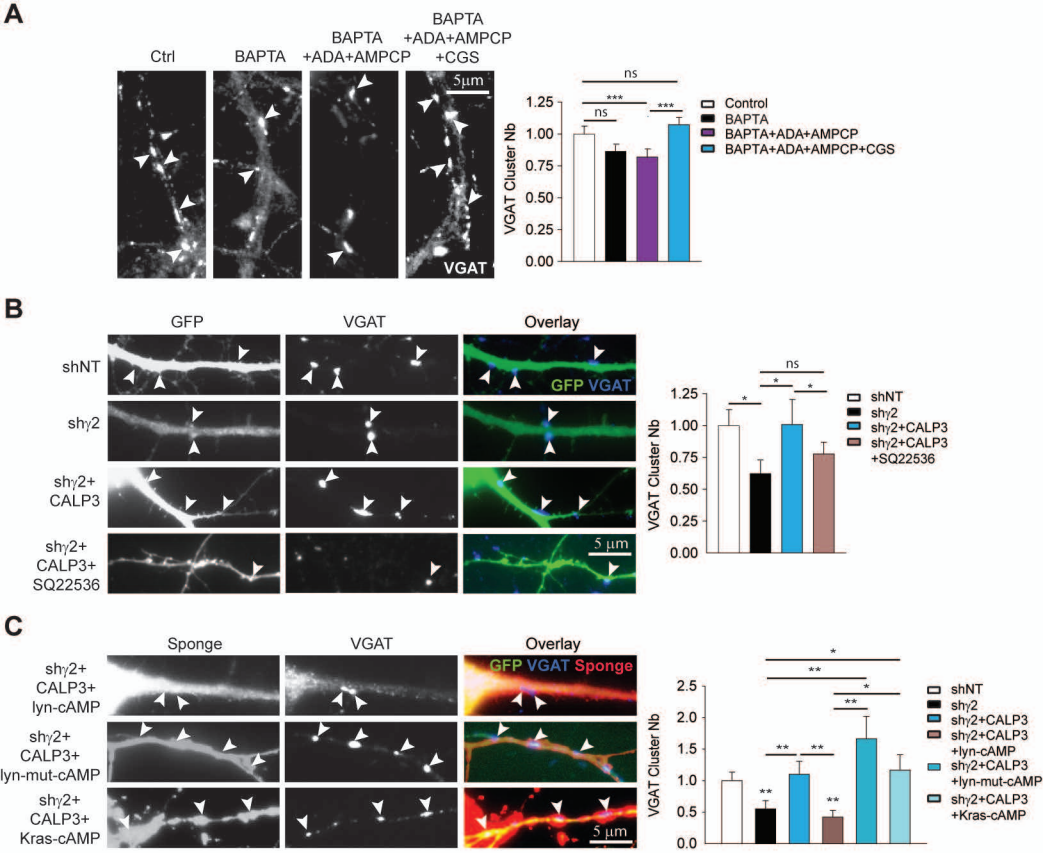
A
Ctrl
BAPTA
BAPTA +ADA+AMPCP
BAPTA +ADA+AMPCP +CGS
5µm
VGAT
ns
***
ns
***
VGAT Cluster Nb
1.25
1.00
0.75
0.50
0.25
0.00
Control
BAPTA
BAPTA+ADA+AMPCP
BAPTA+ADA+AMPCP+CGS
B
GFP
VGAT
Overlay
shNT
shγ2
shγ2+ CALP3
shγ2+ CALP3+ SQ22536
GFP VGAT
5 µm
ns
*
*
*
VGAT Cluster Nb
1.25
1.00
0.75
0.50
0.25
0.00
shNT
shγ2
shγ2+CALP3
shγ2+CALP3 +SQ22536
C
Sponge
VGAT
Overlay
shγ2+ CALP3+ lyn-cAMP
shγ2+ CALP3+ lyn-mut-cAMP
shγ2+ CALP3+ Kras-cAMP
GFP VGAT Sponge
5 µm
*
**
*
**
**
**
**
**
VGAT Cluster Nb
2.5
2.0
1.5
1.0
0.5
0.0
shNT
shγ2
shγ2+CALP3
shγ2+CALP3 +lyn-cAMP
shγ2+CALP3 +lyn-mut-cAMP
shγ2+CALP3 +Kras-cAMP

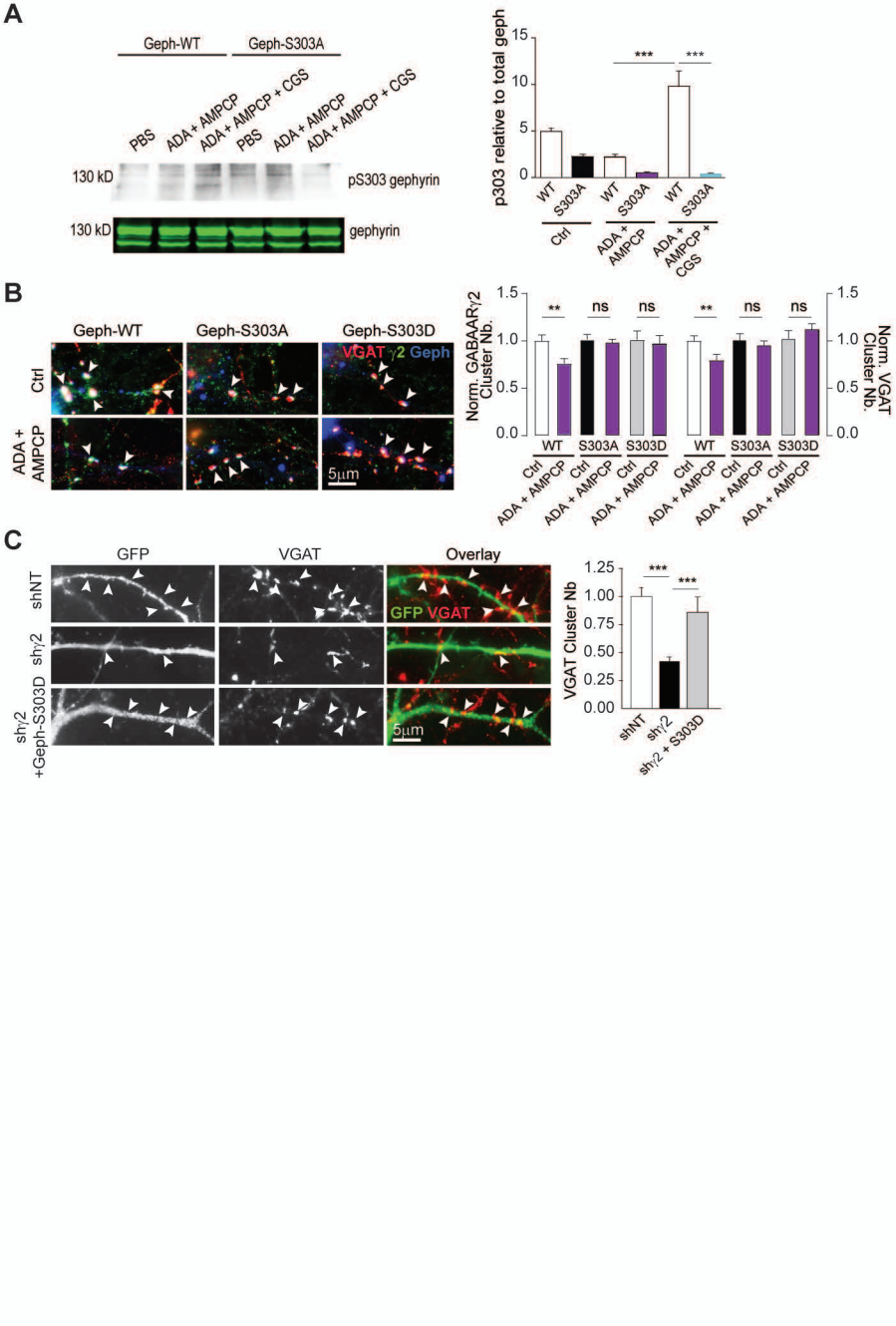
A
Geph-WT
Geph-S303A
PBS
ADA + AMPCP
ADA + AMPCP + CGS
PBS
ADA + AMPCP
ADA + AMPCP + CGS
130 kD
pS303 gephyrin
130 kD
gephyrin
p303 relative to total geph
***
***
WT
S303A
WT
S303A
WT
S303A
Ctrl
ADA + AMPCP
ADA + AMPCP + CGS
B
Geph-WT
Geph-S303A
Geph-S303D
Ctrl
ADA + AMPCP
VGAT γ2 Geph
5µm
Norm. GABAARγ2 Cluster Nb.
Norm. VGAT Cluster Nb.
**
ns
ns
**
ns
ns
WT
S303A
S303D
WT
S303A
S303D
Ctrl
ADA + AMPCP
C
GFP
VGAT
Overlay
shNT
shγ2
shγ2 +Geph-S303D
GFP VGAT
5µm
VGAT Cluster Nb
***
***
shNT
shγ2
shγ2 + S303D

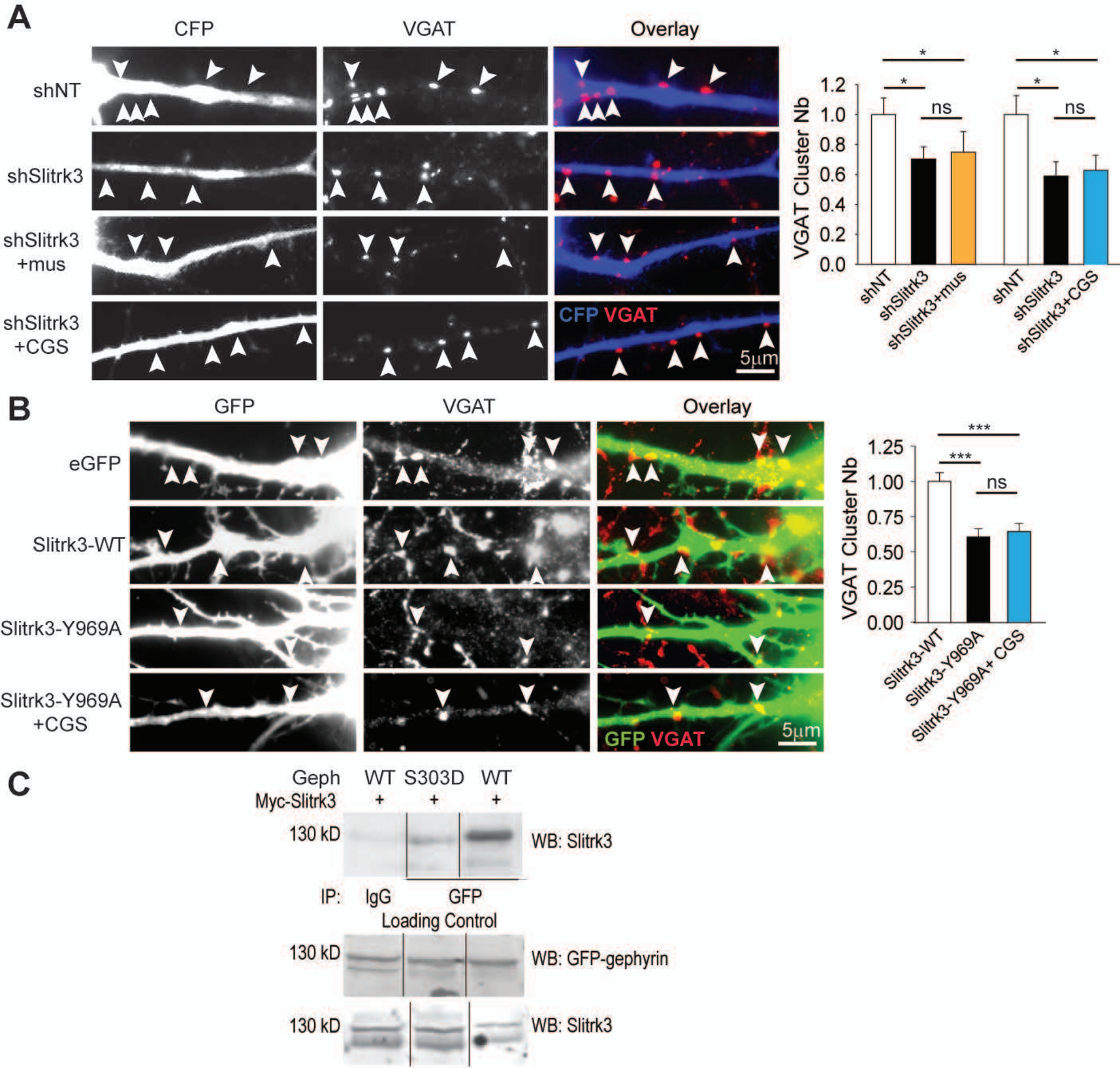
A
CFP
VGAT
Overlay
shNT
shSlitrk3
shSlitrk3 +mus
shSlitrk3 +CGS
CFP VGAT
5µm
VGAT Cluster Nb
1.2
1.0
0.8
0.6
0.4
0.2
0.0
*
*
ns
*
*
ns
shNT
shSlitrk3
shSlitrk3+mus
shNT
shSlitrk3
shSlitrk3+CGS
B
GFP
VGAT
Overlay
eGFP
Slitrk3-WT
Slitrk3-Y969A
Slitrk3-Y969A +CGS
GFP VGAT
5µm
VGAT Cluster Nb
1.25
1.00
0.75
0.50
0.25
0.00
***
***
ns
Slitrk3-WT
Slitrk3-Y969A
Slitrk3-Y969A+ CGS
C
Geph
WT
S303D
WT
Myc-Slitrk3
+
+
+
130 kD
WB: Slitrk3
IP:
IgG
GFP
Loading Control
130 kD
WB: GFP-gephyrin
130 kD
WB: Slitrk3

Science
AAAS

Supplementary Materials for

Convergence of adenosine and GABA signaling for synapse stabilization during development

Authors: Ferran Gomez-Castro [1]†, Stefania Zappettini [2]†, Jessica C. Pressey [1,3]†, Carla G. Silva [2,4], Marion Russeau [1], Nicolas Gervasi [1,5], Marta Figueiredo [6], Claire Montmasson [1], Marianne Renner [1], Paula M. Canas [4], Francisco Q. Gonçalves [4], Sofia Alçada-Morais [4], Eszter Szabó [4], Ricardo J. Rodrigues [4], Paula Agostinho [4,7], Angelo R. Tomé [4,8], Ghislaine Caillol [9], Olivier Thoumine [10], Xavier Nicol [11], Christophe Leterrier [8], Rafael Lujan [12], Shiva K. Tyagarajan [6], Rodrigo A. Cunha [4,7], Monique Esclapez [2], Christophe Bernard [2*] and Sabine Lévi [1*]

Correspondence to: sabine.levi@inserm.fr, christophe.bernard@univ-amu.fr

This PDF file includes:

Materials and Methods

Animals

For all biochemical experiments, adult C57Bl6 mice (up to 6 weeks old) were purchased from Charles River (Lyon, France) and maintained at CNC animal house facilities under controlled environment (23 ± 2°C; 12 hours light/dark cycle and *ad libitum* access to food and water) (both genders pooled). Mice were handled according to European Union guidelines (2010/63) after approval by the Animal's Ethics Committee of the Center for Neuroscience and Cell Biology (Orbea 78-201) and the Portuguese Veterinarian Office. All efforts were made to reduce the number of animals used and to minimize their stress and discomfort, following ARRIVE guidelines.

For all electrophysiological and morphological experiments performed on tissue sections, GIN male mice (P3-P13) (FVB-Tg(GadGFP)45704Swn/J, Jackson Laboratories) were used. Mice were housed in standard mouse cages under conventional laboratory conditions (12 hours/12 hours dark-light cycle, constant temperature, constant humidity, and food and water *ad libitum*). Animal care and experimental procedures were conducted in accordance with institutional guidelines and with the European Union guidelines and were approved by the Aix-Marseille University Chancellor's Animal Research Committee, Marseille (France).

For *in vivo* shA_{2A}R stereotaxic injection and chronic SCH58261 treatment, C57Bl6 mice (P1) were purchased from Janvier (France) and maintained at IFM animal house facilities under controlled environment (23 ± 2°C; 12 hours light/dark cycle and *ad libitum* access to food and water) (both genders pooled). Mice were handled according to European Union guidelines (2010/63) after approval by the Animal's Ethics Committee (APAFIS#20170222104585v4).

For electron microscopy of A_{2A}R, three P7 and P30 mice, obtained from the Animal House Facility (School of Medicine, University of Castilla-La Mancha), were used in this study for pre-embedding immunohistochemical analyses. The care and handling of animals prior to and during the experimental procedures were in accordance with Spanish (RD 1201/2005) and European Union (86/609/EC) regulations, and the protocols were approved by the University's Animal Care and Use Committee. For each developmental stage, the animals used were from different litters.

For all experiments performed on primary cultures of hippocampal neurons, animal procedures were carried out according to the European Community Council directive of 24 November 1986 (86/609/EEC), the guidelines of the French Ministry of Agriculture and the Direction Départementale de la Protection des Populations de Paris (Institut du Fer à Moulin, Animalerie des Rongeurs, license C 72-05-22). All efforts were made to minimize animal suffering and to reduce the number of animals used.

Electrophysiology in CA1 hippocampal slices

Coronal hippocampal slices (350 µm) were prepared from male GIN-mice with a vibroslicer Leica VT 1200S in a cold (lower than 4 ºC) cutting solution containing (mM) 140.0 potassium gluconate, 10.0 HEPES, 15.0 sodium gluconate, 0.2 EGTA, 4.0 NaCl, pH 7.2. After recovery for at least one hour in aCSF containing (mM) 126.0 NaCl, 25.0 $NaHCO_3$, 10.0 D-glucose, 3.5 KCl, 2.0 $CaCl_2$, 1.3 $MgCl_2$ and 1.2 NaH_2PO_4 equilibrated with 5% CO_2 in 95% O_2 at room temperature (RT), slices were transferred to a chamber containing the same aCSF and kept at a temperature between 33-35 ºC. Cells were patched under visual control (Nikon FN1 microscope – Scientifica Patch Star manipulators). Currents were recorded with an Axopatch700B amplifier and Digidata 1322 interface (Axon Instruments) using an internal pipette solution containing (mM) 120.0 Cs-gluconate, 20.0 CsCl, 1.1 EGTA, 0.1 $CaCl_2$, 10.0 HEPES, 2.0 Mg-

ATP, 0.4 Na-GTP, 2 $MgCl_2$, using CsOH to adjust pH (pH 7.3, 280 mOsM). Miniature inhibitory postsynaptic currents (mIPSCs) were recorded at a holding potential of +10mV, the reversal potential for glutamatergic events (*42*), (in presence of 1 µM TTX). Average series resistance (RS) in pyramidal cells from P6 were 23.3 ± 1.5 MΩ. When the RS changed during the recording by more than 20%, the recording was terminated. All recorded cells were filled with biocytin for *post-hoc* morphological identification. All cells presented in this study were identified *post hoc*.

Immunohistochemical detection of VGAT upon acute SCH58261 treatment

After 30 minutes of incubation with 100 nM SCH58261 (n=8) or ACSF (n= 6) in slices from P6 mice (n=3) were processed in parallel for detection of VGAT-containing axon terminals as follows. Slices were fixed overnight at 4°C in a solution containing 4% paraformaldehyde (PFA) in 0.12 M sodium phosphate buffer (pH 7.4 - PB). Then they were rinsed in PB, cryoprotected in 20% sucrose and quickly frozen on dry ice. After several rinses in 0.02 M potassium phosphate-buffered saline (KPBS, pH 7.2-7.4), slices were incubated in a solution containing normal donkey serum (NDS, 1:30; Vector Laboratory) diluted in KPBS with 0.3% Triton-X100, for 2 hours at RT. They were incubated in a solution containing rabbit anti-VGAT (1:1000, 131002, Synaptic Systems) diluted in KPBS containing 0.3% Triton-X100 and NDS (1/100), overnight at RT. After several rinses in KPBS, slices were incubated for 2 hours in Cy3-donkey anti-rabbit IgG (1:100) diluted in KPBS with 0.3% Triton-X100. All slices were mounted on slides and coverslipped with Fluoromount (Electron microscopy).

Quantification was performed as followed: for each slice, a single optical image was acquired with a Zeiss LSM 510 laser-scanning microscope and 20X objective. All images were acquired from the CA1 hippocampal region, using identical parameters. The number of VGAT-labeled axon terminals in this region of interest (ROI) which area corresponds to the size of the confocal slice (450 µm x 450 µm) were estimated by determining the level of fluorescence using Image J software. The level of fluorescence was determined by the corrected total fluorescence (CTCF) in each CA1 region for each slice. CTCF = mean gray value x Area) - (Area x Mean fluorescence background). The average CTFC ± s.e.m. was calculated for each group of SCH58261 and control slices and the two populations compared using non parametric Wilcoxon Rank Sum test.

Stereotaxic injection of shA_{2A}R

Neonatal mice (P3) were anesthetized on ice for 3 minutes, and then maintained with isoflurane (4%) for the duration of the surgery. Mice were immobilized and placed on the stereotaxic apparatus, and the skull was leveled. The skull of the pup was sterilized using 70% ethanol and a small incision was made above the injection site targeting the hippocampus (RC: 2.2; L/M: 1.5; D/V: 1.7). Using a glass pipette, 0.15 µL of virus (AAV2.1-U6-shNT-GFP or AAV2.1-U6-shA2AR-GFP) was injected bilaterally into the hippocampus at a rate of 70 nL/minute followed by a 2-minute wait period before the pipette was slowly removed. The mice were rapidly warmed on a heating pad until their skin color returned to normal and they began moving, and they were subsequently returned to their biological mother. Following surgery, animals remained housed with their mothers until animals were collected for immunohistochemistry at post-natal day 16 (P16).

Immunohistochemical detection of VGAT upon chronic SCH58261 treatment or shA_{2A}R expression during synaptogenesis in vivo

Mice (P16) were perfused transcardially with ice-cold aCSF (containing in mM: NaCl 125, KCl 2.5, $CaCl_2$ 2.5, $MgCl_2$ 2, $NaHCO_3$ 26, NaH_2PO_4 1.25, glucose 25 at pH 7.4 (*43*), and then post-fixed in 4% PFA at 4ºC for 75 minutes. The fixed brains were cryoprotected in 30% sucrose and parasagittal free-floating sections were made using a cryotome at a thickness of 30 µm. Standard immunohistochemistry was performed on free-floating sections. Slices were permeabilized in 0.5% Triton X-100 and blocked using 5% goat serum for 3 hours at room temperature and subsequently incubated in rabbit anti-VGAT (1:1000, gift from B. Gasnier, Univ. Paris Descartes, Paris) for 24 hours at 4ºC. Slices were rinsed 3x in 0.1M phosphate buffer (PB) and incubated in goat-anti rabbit Alexa 555- conjugated secondary antibody. Images were acquired with a Leica SP5 confocal system using standard Leica imaging software. Images were obtained using either a 10x or 63x oil objective, and z-stacks were acquired using a z spacing of 0.3 µm. Using Imaris 8.1.2, VGAT immunostaining was quantified in the *stratum pyramidale, lucidum and radiatum* of the CA3 region of the hippocampus. A total of 9 control and SCH58261 treated animals (2-3 slices per animal) were included for analysis. A total of 3 shNT- and 3 shA_{2A}R-injected animals were included, with 2-3 slices per animal included for analysis.

Immunohistochemical detection of A_{2A}R during development

Mice were deeply anesthetized on cold ice (postnatal day 3, P3, P6, P9, n=6) or with chloral hydrate (P12, adults, n=6) and perfused intracardially with a fixative solution containing 4% PFA in 0.12 M sodium PB (pH 7.4). After perfusion, the brains were removed from the skull, post-fixed in the same fixative solution for 2 hours at RT (P12 up to P60) or overnight at 4°C (P3 to P9), cryoprotected in a solution of 30% sucrose in PB overnight at 4 ºC, quickly frozen on dry ice and sectioned coronally with a thickness of 100 µm (pups up to P9) or 40 µm (P12 up to P60) with a cryostat (Leica CM3050S, Heidelberg, Germany). The sections were rinsed in PB, collected sequentially in tubes containing an ethylene glycol-based cryoprotective solution and stored at -20°C until histological processing. One every eight (P3 to P9) or ten (P12 up to P60) sections was stained with cresyl violet to determine the general histological characteristics of the tissue. Selected adjacent sections were processed for immunohistochemical detection of A_{2A}R as follows: sections were pre-treated for 30 minutes in 1 % H_2O_2, rinsed in PB and in 0.02 M potassium KPBS (pH 7.2-7.4), pre-incubated for 1 hour in 3 % normal horse serum (NHS, Vector Laboratories) diluted in KPBS containing 0.3 % Triton X-100 and incubated overnight at RT in goat anti-A_{2A}R polyclonal antibody (1:200, sc-7504, Santa Cruz Biotechnology) diluted in KPBS containing1 % NHS and 0.3 % Triton X-100. After several rinses in KPBS, sections were incubated for 1 hour at RT in biotinylated horse anti-goat immunoglobulin G (IgG; Vector Laboratories) diluted 1:200 in KPBS containing 3 % NGS and then for 1 hour at RT in an avidin-biotin-peroxidase complex solution prepared in KPBS according to the manufacturer's recommendations (Vectastain ABC kit, Vector Laboratories). Sections from P3 to P60 mice were processed in parallel and for the same period of time (15 minutes) in 3,3'-diaminobenzidine tetrahydrochloride (DAB, Sigma fast tablets; Sigma), rinsed in KPBS, mounted onto Superfrost Plus slides, dehydrated and coverslipped with Permount. Sections were examined under a Zeiss Imager Z2 microscope equipped with AxioCam HR color digital cameras and using the AxioVision 4.7 software (Carl Zeiss, Taper, Sintra, Portugal).

EM immunohistochemical detection of A_{2A}R

For immunohistochemistry, animals were anaesthetized by intraperitoneal injection of ketamine/xylazine 1:1 (0.1 mL/kg body weight) and transcardially perfused with ice-cold fixative

containing 4% paraformaldehyde, with 0.05% glutaraldehyde and 15% (v/v) saturated picric acid made up in 0.1 M PB (pH 7.4). After perfusion, brains were removed and immersed in the same fixative for 2 hours or overnight at 4ºC. Tissue blocks were washed thoroughly in 0.1 M PB. Coronal 60 µm thick sections were cut on a Vibratome (Leica V1000). The following primary antibodies were used: polyclonal guinea pig anti-$A_{2A}R$ (AB_2571656; Frontier Institute co., Japan). The secondary antibodies used were goat anti-guinea pig IgG coupled to 1.4 nm gold (1:100; Nanoprobes Inc., Stony Brook, NY, USA).

Immunohistochemical reactions for electron microscopy were carried out using the pre-embedding immunogold method described previously (*44*). Briefly, free-floating sections were incubated in 10% (v⁄v) NGS diluted in TBS. Sections were then incubated in anti-$A_{2A}R$ antibodies [3-5 µg⁄mL diluted in TBS containing 1% (v⁄v) NGS], followed by incubation in goat anti-guinea pig IgG coupled to 1.4 nm gold (Nanoprobes Inc., Stony Brook, NY, USA), respectively. Sections were postfixed in 1% (v⁄v) glutaraldehyde and washed in double-distilled water, followed by silver enhancement of the gold particles with an HQ Silver kit (Nanoprobes Inc.). Sections were then treated with osmium tetraoxide (1% in 0.1 M phosphate buffer), block-stained with uranyl acetate, dehydrated in graded series of ethanol and flat-embedded on glass slides in Durcupan (Fluka) resin. ROI were cut at 70-90 nm on an ultramicrotome (Reichert Ultracut E, Leica, Austria) and collected on single slot pioloform-coated copper grids. Staining was performed on drops of 1% aqueous uranyl acetate followed by Reynolds's lead citrate. Ultrastructural analyses were performed in a Jeol-1010 electron microscope.

Preparation of total membranes and synaptosomes

Total membranes and membranes from nerve terminals were prepared as previously described (*18*). After deep anesthesia under halothane atmosphere, mice were killed by decapitation. The hippocampi were quickly removed into ice-cold sucrose (0.32 M) solution containing 1 mM EDTA, 10 mM HEPES, 1 mg/mL bovine serum albumin (BSA), pH 7.4 at 4°C, supplemented with a protease inhibitor, phenylmethylsulfonyl fluoride (PMSF 0.1 mM), a cocktail of inhibitors of proteases (CLAP 1%, Sigma) and the antioxidant dithiothreitol (1 mM) and homogenized with a teflon potter elvehjem. The homogenates were centrifuged at 3,000 *g* for 10 minutes at 4°C and the resulting supernatant was divided to prepare total membranes and synaptosomes. To prepare total membranes, the supernatant was further centrifuged at 30,000 *g* for 60 minutes at 4°C; the supernatants were discarded and the pellet, corresponding to total membranes from different brain cell types, was resuspended in appropriate solutions for Western blot or binding assays. To prepare synaptic membranes (membranes from synaptosomes, i.e. purified synapses, the supernatant was first centrifuged at 14,000 *g* for 12 minutes at 4°C; the resulting pellet (P2 fraction) was resuspended in 1 mL of a 45% (v/v) Percoll solution in HEPES buffer (140 mM NaCl, 5 mM KCl, 25 mM HEPES, 1 mM EDTA, 10 mM glucose; pH 7.4). After centrifugation at 14,000 *g* for 2 minutes at 4°C, the white top layer was collected (synaptosomal fraction), resuspended in 1 mL Krebs-HEPES buffer (140 mM NaCl, 5 mM KCl, 5 mM $NaHCO_3$, 1.2 mM NaH_2PO_4, 1 mM $MgSO_2$, 2 mM $CaCl_2$, 10 mM glucose, and 10 mM HEPES, pH 7.4). Western blot characterization showed that these hippocampal synaptosomes are enriched in presynaptic markers (synaptophysin, SNAP-25, syntaxin-I) with <2% of astrocytic markers (GFAP, GLT-I) and virtually no markers of oligodendrocytes or of microglia, as gauged by the lack of CD11b immunoreactivity (unpublished data). After homogenization with a micro potter elvehjem, the mixture was centrifuged at 30,000 *g* for 60 minutes, the supernatant was discarded and the pellet was resuspended in appropriate solutions for Western blot or binding assays.

Western blot analysis of $A_{2A}R$ density during development

The amount of protein in total membranes, synaptosomal, presynaptic, postsynaptic and non-active zone fractions, was determined using the bicinchoninic acid method (Pierce) to carefully dilute all extracts to a final concentration of 2 μg protein/μL in SDS-PAGE buffer. Western blotting was performed as previously described (*18*). Electrophoresis was carried out using a 7.5% SDS-PAGE gel after loading 60 μg of different fractions. The composition of the resolving gel was 7.5% acrylamide, 0.5 M Tris pH 8.8, 0.2% SDS, 0.2% APS, 6 μL TEMED, water up to 8.7 mL. The composition of stacking gel was 4% acrylamide, 0.125M Tris pH 6.8, 0.1% SDS, 0.05% APS, 10 μL TEMED, water up to 10mL. Proteins were then transferred to polyvinylidene difluoride (PVDF) membranes (GE Healthcare, Carnaxide, Portugal). Membranes were blocked for 1 hour at RT with 5% low-fat milk in Tris-buffered saline or 3% BSA (depending on the antibodies used), pH 7.6, and containing 0.1% Tween 20 (TBS-T). Membranes were then incubated overnight at 4 ºC with primary antibodies. We used goat anti-$A_{2A}R$ antibody (1:500, sc-7504, Santa Cruz Biotechnology) or mouse anti-$A_{2A}R$ antibody (1:1,000, 05-717, Millipore), which selectivity was confirmed in tissue from $A_{2A}R$ knockout mice (*18*), diluted in Tris-buffered saline (137 mM NaCl and 20 mM Tris–HCl, pH 7.6) with 0.1% TBS-T and 5% BSA (fatty acid free). To validate the effectiveness of the subsynaptic separation, we also used other primary antibodies, namely SNAP-25 (1:10000; S5187, Sigma), PSD95 (1:10000; MAB1596, Millipore), synaptophysin (1:10000; ab14692, Abcam) or syntaxin-I (1:20000; S0664, Sigma). After washing twice with TBS-T, the membranes were incubated with appropriate secondary antibody conjugated with alkaline phosphatase (Amersham, Buckinghamshire, UK) for 2 hours at RT. After washing, the membranes were revealed using an ECF kit (Amersham) and visualized with an imaging system (VersaDoc 3000, Bio-Rad, Amadora, Portugal) and quantified with the Quantity One software (Bio-Rad). The membranes were then re-probed and tested for β-tubulin immunoreactivity using a mouse anti-β-tubulin-III antibody (1:1000; ab18207 from Abcam), to confirm that similar amounts of protein were applied to the gels (*18*).

A_{2A} Receptor binding

The binding assays were performed as previously described (*18*). Briefly, the total membranes or synaptosomal membranes were suspended in a preincubation solution (containing 50 mM Tris, 1 mM EDTA, 2 mM EGTA, pH7.4) and a sample was collected to determine the protein concentration using the BCA assay (Pierce). Adenosine deaminase (ADA, 2 U/mL, Roche, Amadora, Portugal) was added and the membranes were incubated for 30 minutes at 37 ºC to remove endogenous adenosine. The mixtures were centrifuged at 25,000 *g* for 20 minutes at 4°C, and the pelleted membranes were resuspended in Tris-Mg solution (containing 50 mM Tris and 10 mM $MgCl_2$, pH 7.4) with 4 U/mL of ADA. Binding with 2 nM of the selective $A_{2A}R$ antagonist, ^{3}H-SCH58261 (specific activity of 77 Ci/mmol; prepared by GE Healthcare and offered by Dr. E.Ongini, Shering-Plough, Milan, Italy) was performed for 1 hour at RT with 140-210 μg of protein, with constant swirling. The binding reactions were stopped by addition of 4 mL of ice-cold Tris-Mg solution and filtration through Whatman GF/C glass microfiber filters (GE Healthcare) in a filtration system (Millipore). The radioactivity was measured after adding 2 mL of scintillation liquid (AquaSafe 500 Plus, Zinsser Analytic, Frankfurt, Germany). The specific binding was expressed as fmol/mg protein and was estimated by subtraction of the non-specific binding, which was measured in the presence of 2 μM of xanthine amine congener (Sigma), a mixed $A_1R/A_{2A}R$ antagonist. All binding assays were performed in duplicate.

Western blot validation of shRNAs against A_{2A}Rs in N2a cell cultures

N2a cells were grown in DMEM (Invitrogen) supplemented with 10% fetal bovine serum (FBS) and were grown to 60% confluency. The N2a cells were infected with AAV2.1-U6-shNT-GFP or AAV2.1-U6-shA2AR-GFP and left to express the viruses for 72 hours prior to harvesting. Cells were homogenized in RIPA buffer (50 mM Tris·HCl, pH 7.4, 150 mM NaCl, 1 mM EDTA, 1% Nonidet P-40, 0.1% SDS, 0.5% DOC) containing phosphatase and protease inhibitors (Roche). The samples were solubilized for 72 hours at 4^{o}C and centrifuged at 20,000 g for 30 minutes at 4^{o}C. Supernatants were collected and subjected to Western blotting analysis. Protein samples (20µg) were loaded onto pre-cast 10% SDS polyacrylamide gels (Invitrogen) and separated using electrophoresis. The separated proteins were transferred onto a nitrocellulose membrane (GE Healthcare) and probed with rabbit anti-A_{2A}R (1:500, AAR-002, Alomone) and mouse anti-TUJ1 (1:1000, MAB1195, R&D Systems) antibodies. The primary antibodies were visualized using fluorescent secondary antibodies (1:1000 DyLight 700 or 800, Rockland) using an Odyssey infrared imaging system (LI-COR Bioscience). These experiments were performed on 3 independent biological replicates.

Validation of the interaction between gephyrin and slitrk3

HEK293T cells were grown in DMEM supplemented with 10% FBS to 60% confluency prior to transfection with 2 µg pCMV3-Myc-SLITRK3 (Sino Biologicals; Cat. number: HG15976-NM) or eGFP-gephyrin-WT (*45*) or eGFP-gephyrin-S303D (*30*). For immunoprecipitation 500 µL of lysate (eGFP-gephyrin or eGFP-gephyrin S303D) was incubated with 1 µL of mouse anti-GFP antibody (NB600-597, Novus Biologicals) for 90 minutes. The lysate was then incubated with 25 µL of Pierce™ Protein A/G UltraLink™ Resin from ThermoFisher Scientific (Cat: 53132) for 45 minutes in a rotator wheel at 4°C. The supernatant was discarded and protein complexes immobilized in the beads were incubated with 500 µL lysate containing Myc-Slitrk3 for 1 hour at 4°C. The beads were washed once in EBC-based high-salt buffer (50 mM Tris-HCl pH 8.0, 500 mM NaCl and 1% Nonidet P-40 (Sigma-Aldrich) and twice in EBC buffer. After boiling the samples in 2x SDS sample buffer containing 15% 2-mercaptoethanol (Bio-Rad) for 3 minutes at 90°C the supernatant was loaded onto SDS-polyacrylamide gels and electrophoresis was run at RT. After electro-transferring the protein bands onto PVDF membranes in Tris-glycine transfer buffer, Western blotting was performed by blocking the membranes with 5% Western blocking reagent (Roche Diagnostic) in Tris-buffered saline with Tween 20 (TBST) for 30 minutes at RT and later incubating with the primary antibody rabbit anti-Slitrk3 (1:1000, ABN356, Sigma) overnight at 4°C. Secondary antibodies coupled to horseradish peroxidase or IRDye (LI-COR) were used to visualize the protein bands.

Western blot for gephyrin phosphorylation

HEK293T cells were grown in DMEM supplemented with 10% FBS to 60% confluency prior to transfection with 2 µg eGFP-gephyrin wild type (WT) or eGFP-gephyrin S303A mutant. The cells were treated with phosphate buffer saline (PBS) or ADA+AMPCP (ADA 20 U/mL and AMPCP 100 µM) or ADA+ADP+CGS21680 (30 nM). Whole cell lysate was prepared after 30 minutes treatment using EBC buffer (see above). Gephyrin phosphorylation was detected using a rabbit anti-gephyrin antibody (1:500; PO4 S303, custom made Genescript). Total gephyrin protein was detected using a mouse anti-gephyrin antibody 3B11 (1:1000, 14711, Synaptic Systems).

Release of ATP

The release of ATP was measured on-line using the luciferin-luciferase assay (*20*). Briefly, one aliquot of the synaptosomal suspension (35 μL with circa 40 μg of protein) and 15 μL of ATP assay mix (containing luciferin and luciferase; from Sigma) were added to 150 μL of Krebs-HEPES solution. This suspension was equilibrated at 25ºC from 3 minutes (for stimulus dependent evoked release of ATP) up to 10 minutes (when testing the impact of most drugs) to ensure the functional recovery of the synaptosomes. The suspension was then transferred to a well of a white 96-well plate, which was maintained for 1 minutes at 25ºC inside a luminometer (Perkin Elmer Victor3) before initiating the recording of the electrical signal generated by the photomultiplier. We first measured the basal outflow of ATP during 60 seconds, before triggering the evoked release of ATP with a chemical stimulus consisting of a Krebs-HEPES solution with an isomolar substitution of NaCl by 32 mM of KCl. After this chemical stimulation, the light levels were recorded for an additional 200 seconds. The evoked release of ATP was calculated by integration of the area of the peak upon subtraction of the estimated basal ATP outflow and always discounting the (minor) variation of luminescence caused by possible mechanic or osmolarity alterations, which was evaluated in a parallel assay in the same batch of nerve terminals by adding medium with an amount of Krebs-HEPES solution equal to the amount of K^+-rich solution used in the test situation. The levels of ATP were estimated using a calibration curve for ATP, which were linear between $2x10^{-12}$ and $8x10^{-5}$ M (*20*). To test the impact of drugs on ATP release, these drugs were added to the synaptosomes during the 10 minutes equilibration period at 25°C and were present throughout the assays. None of the tested drugs modified the light emission by the luciferin-luciferase assay when testing different concentrations of ATP standards.

Release of adenosine

Adenosine release from hippocampal synaptosomes was carried out as essentially previously described (*20*). Hippocampal synaptosomes (0.6-0.9 mg protein) were layered over GF-B filters (Whatman, Sigma, Sintra, Portugal), placed in swinney filter holders with 90 μL of volume. They were superfused in a closed-loop manner with 2 mL of Krebs solution containing the adenosine deaminase inhibitor erythro-9-(2-hydroxy-3-nonyl)adenine (EHNA, 10 μM, from Sigma) and the nucleoside transporter inhibitor nitrobenzylthioinosine (NBTI, 1 μM; from Sigma). This solution was maintained at 37°C. After 15 minutes, a sample of 250 μL was collected for HPLC analysis of the basal concentration of adenosine. We immediately added to the remaining superfusion solution 250 μL of Krebs without sodium and with EHNA and NBTI and 240 mM KCl, to obtain a final concentration of 30 mM K^+ to depolarize the synaptosomes and trigger adenosine release. After 2 minutes of superfusion in a closed-loop manner, a sample of 250 μL was collected for HPLC analysis of adenosine release. When we tested the effect of the inhibitor of ecto-5'-nucleotidase α,β-methylene ADP (AMPCP, 100 μM, from Sigma), it was present in all solutions used for superfusion of the synaptosomes. The separation and quantification of adenosine was carried out by High Pressure Liquid Chromatography (HPLC), as previously described (*20*), employing a LiChroCart-RT 125-4 C-18 reverse-phase column (particle size, 5 μm), combined with an UV detector set to 254 nm. The mobile phase consisted of KH_2PO_4 (100 mM; from BDH Aristar, VWR, Carnaxide, Portugal) and methanol (85/15% v/v) at pH 6.50, with a flow rate of 1 mL/min, and a loop volume of 100 μL. The quantification of adenosine was achieved by calculating the peak areas then converted to concentration values by calibration with known

standards ranging from 0.1 to 10 μM. The evoked release was quantified as the total amount of adenosine present after addition of K^+ minus the basal amount of adenosine.

Behavioral Testing

Behavioral experiments were performed on wild-type littermates that had received chronic saline or SCH58261 (0.1 mg/kg) intraperitoneal injections between P3-P16. Behavioral testing was performed on male mice between 9:00 am - 3:00 pm. Automatic animal tracking was completed using a ceiling mounted Panasonic camera (WV BP332) and the ViewPoint analysis software.

Animals were placed in the center of the open-field arena (50 cm x 50 cm) made of white plexiglass and allowed to freely explore for 20 minutes for 3 consecutive days. Total distance was measured as an indication of habituation to the open-field. Once animals were habituated to the open-field arena, animals completed the acquisition phase by being placed in the center of the open-field, containing two identical objects and one visual cue, and allowed to explore for 10 minutes. 24 hours later one of the objects was moved to a new location and animals were again allowed to freely explore the objects for 10 minutes. The final day, one of the objects was replaced with a novel object and animals were allowed to freely explore the objects. Discrimination index was calculated as (time new location-time old location)/time exploring new location.

The elevated plus maze consisted of two opposing arms (30 cm x 8 cm, no walls), perpendicular to two enclosed arms (30 cm x 8 cm, 15 cm high walls), elevated 50 cm above the floor. The maze was dimly lit and animals were placed in the center of the maze and allowed to freely explore for 5 minutes.

Neuronal cultures

Primary cultures of hippocampal neurons were prepared as previously described (*47*) with some modifications of the protocol. Briefly, hippocampi were dissected from embryonic day 18 or 19 Sprague-Dawley rats of either sex. Tissue was then trypsinized (0.25% v/v), and mechanically dissociated in 1x HBSS (Invitrogen, Cergy Pontoise, France) containing 10 mM HEPES (Invitrogen). Neurons were plated at a density of 60 or 120 × 10^3 cells/mL onto 18-mm diameter glass coverslips (Assistent, Winigor, Germany) pre-coated with 50 μg/mL poly-D,L-ornithine (Sigma-Aldrich, Lyon, France) in a plating medium composed of Minimum Essential Medium (MEM, Sigma) supplemented with horse serum (10% v/v, Invitrogen), L-glutamine (2 mM) and Na^+ pyruvate (1 mM) (Invitrogen). After attachment for 3-4 hours, cells were incubated in culture medium that consists of Neurobasal medium supplemented with B27 (1x), L-glutamine (2 mM), and antibiotics (penicillin 200 U/mL, streptomycin, 200 μg/mL) (Invitrogen), and kept for up to 4 weeks at 37ºC in a 5% CO_2 humidified incubator. Each week, one fifth of the culture medium volume was renewed.

Neuronal transfection

The following constructs were used: *GEPHN* 3'-UTR shRNA and control shRNA-3m (*45*) , eGFP-gephyrin P1 variant (45), eGFP-gephyrin S303A, S303D and S270A mutants (*45*, *30*), shRNA against $A_{2A}R$ (*24*), non-target shRNA coupled to GFP (*47*), gephyrin-mRFP (*47*), pCMV3-Myc-Slitrk3 (Sino Biologicals plasmid #HG15976-NM), shRNA against $GABA_AR$ γ2 subunit (*23*), shRNA against Slitrk3 coupled to CFP (kindly provided by Ann Marie Craig) (*33*), Slitrk3-Y969A mutant (kindly provided by Quingjun Tian and Wei Lu) (*37*), shRNA against Neuroligin 2 (kindly provided by Peter Scheiffele, Addgene plasmid # 59358) (*34*) and a scrambled shRNA

sequence "shMock" (kindly provided by Ann Marie Craig, Vancouver, Canada), pcX-LynLyn-cAMP Sponge-mCherry, pcX-cAMP Sponge-mRFPKras, pcX-LynLyn-cAMP Sponge mutated (all sponges were provided by Xavier Nicol, Paris, France, (*28*)). All the constructs were sequence-verified by Beckman Coulter Genomics.

Transfections were carried out at DIV 6-7 for neurons undergoing synaptogenesis, DIV 14 mature neurons were transfected using Lipofectamine 2000 (Invitrogen) or Transfectin (BioRad, Hercules, USA), according to the manufacturers' instructions (DNA:transfectin ratio 1 µg:3 µL), with 1 µg of plasmid DNA per 20 mm well. The following ratios of plasmid DNA were used in co-transfection experiments: 1 µg for ShNT-eGFP/ $shA_{2A}R$-eGFP, 0.5:0.5 µg for $ShGABA_AR\gamma2$: pcX-LynLyn-cAMP Sponge-mCherry/pcX-LynLyn-cAMP Sponge mutated, 0.5:0.25 µg for $ShGABA_AR\gamma2$: pcX-cAMP Sponge-mRFPKras, 0.5:0.5 µg for eGFP-gephyrin-WT/eGFP-gephyrin-S303D/eGFP-gephyrin-S270A: *GEPHN* 3' UTR shRNA, 0.8:0.5 µg for $GABA_AR$ γ2-GFP: gephyrin-mRFP, 0.5:0.2 µg for ShNT/$ShGABA_AR\gamma2$: eGFP, 0.5:0.5 µg for $ShGABA_AR\gamma2$: eGFP-gephyrin-S303D, 1 µg for ShNT-eGFP/shNL2-eGFP, 1 µg for ShMocK/ShSlitrk3, 0.1:0.2 µg for Slitrk3-WT/ Slitrk3-Y969A mutant : eGFP. Experiments were performed 2-5 days post-transfection.

Pharmacological manipulations

For immunocytochemical experiments, muscimol (10 µM, HelloBio), SCH58261 (100 nM, Abcam), CGS21680 (30 nM, Abcam), ADA (4-20 U/mL, Roche), AMPCP (100 µM, Sigma), DPCPX (100 nM, Merck), 3-isobutyl-1-methylxanthine (IBMX, 100 µM, Tocris), Forskolin (FSK, 10 µM, Tocris), BAPTA-AM (20 µM, Tocris), CALP3 (100 µM, Tocris), SQ22536 (20 µM, Sigma) were directly added to the culture medium and the neurons were returned to a 5% CO_2 humidified incubator for 10 minutes to 1 hour before use. Recombinant neurexin1β-Fc (Nrx1β-Fc) was produced in HEK293T cells, collected and purified as described (*35*). For experiments using arabinosylcytosine C (araC, 5 µM, Sigma), cells were treated at DIV1 and then the appropriate drugs were added for 30 minutes at DIV8-9. For experiments using tetanus toxin (1-40 nM, Alomone Labs) or Nrx1β-Fc protein (60 µg/mL), cells were treated for 2 days (from DIV7 to 9) and then the appropriate drugs were added for 30 minutes to the toxin or the protein solution. For experiments using K252a (200 nM, Sigma), cells were treated for for 30 minutes or 2 hours in absence or presence of CGS21680 (CGS, 30 nM). For single particle tracking experiments, neurons were labeled at 37°C in imaging medium (see below for composition), transferred to a recording chamber and recorded within 45 minutes at 31°C in imaging medium in presence of the appropriate drugs. The imaging medium consisted of phenol red-free minimal essential medium supplemented with glucose (33 mM; Sigma) and HEPES (20 mM), glutamine (2 mM), Na^+-pyruvate (1 mM), and B27 (1X) from Invitrogen. For electrophysiological experiments, SCH58261 (100 nM, Abcam), ADA (4-20 U/mL, Roche), AMPCP (100 µM, Sigma), NBQX (10 µM, Tocris), D-AP5 (1 µM, Tocris), MCPG (500 µM, Tocris) were directly added to the aCSF medium in presence of tetrodotoxin (TTX, 1 µM, Abcam), equilibrated with 5% CO_2 in 95% O_2 and bath applied with a peristaltic system to the hippocampal slices for 30 minutes at 30-32ºC. GDPβS (10 µM, Tocris), IBMX + FSK (10 µM, Tocris), PKI (10 µM, Tocris) were added in the Cs-gluconate solution in the patch pipette. After the recordings the slices were fixed with PFA (4% w/v; Sigma) overnight, rinsed 3 times in 0.12 M PB, cryoprotected in a 20% sucrose solution overnight at 4°C and quickly frozen on dry ice.

For chronic neonatal treatment with SCH58261, C57bl6 wild-type littermates received chronic saline or SCH58261 (0.1 mg/kg) intraperitoneal injections between P3-P16. Animals

remained with their mother in their home cage between injections and were either collected for experimentation at P16 or left to adulthood where they were used for behavioral assessment (P70).

Immunocytochemistry

To label and quantify the density of inhibitory synapses, pre-treated neurons were fixed for 15 minutes at RT in 4% PFA and sucrose (14% w/v; Sigma) solution in 1x PBS. Cells were then washed and permeabilized with a solution containing Triton X-100 (0.25% w/v, Carl Roth GmbH) diluted in PBS 1x. Cells were then incubated for 1 hour at RT in goat serum (GS; 10% v/v; Invitrogen) and Triton X-100 (0.1% w/v) in PBS to block nonspecific staining. Neurons were then incubated for 1 hour at RT with a primary antibody mix consisting of rabbit anti-VGAT (1:500, provided by B. Gasnier, Univ. Paris Descartes, Paris), mouse anti-gephyrin (mAb7a, 1:500, 147011, Synaptic Systems) and guinea pig ani-$GABA_AR\gamma2$ subunit (1:2000, provided by J.M. Fristchy, Univ. Zurich) in PBS supplemented with GS (10% v/v, Invitrogen) and Triton X-100 (0.1% w/v). After washes, cells were incubated for 45 minutes at RT with a secondary antibody mix containing donkey anti-guinea pig-cy3 (1:400, Jackson Immunoresearch), goat anti-rabbit-FITC (1:300, Jackson Immunoresearch) and donkey anti-mouse-cy5 antibodies (1:300, Jackson Immunoresearch) in PBS-GS-Triton X-100 solution, washed, and finally mounted on glass slides using Mowiol 4-88 (48 mg/mL, Sigma). Sets of neurons compared for quantification were labeled simultaneously.

For immunocytochemical detection of $GABA_AR$ α1 or α2 subunits, neurons were fixed and permeabilized as above and then incubated for 1 hour at RT with a primary antibody mix consisting of mouse anti-VGAT (1:500, Synaptic Systems) and rabbit anti-$GABA_AR$ α1 or α2 subunits (1:500, 224203 & 224103, Synaptic Systems) in PBS-GS-Triton X-100 solution. After washes, cells were incubated for 45 minutes at RT with a secondary antibody mix containing goat anti-rabbit-cy3 (1:400, Jackson Immunoresearch) and goat anti-mouse-FITC (1:400, Jackson Immunoresearch) in PBS-GS solution, washed, and finally mounted on glass slides using Mowiol 4-88 (48 mg/mL, Sigma).

For $A_{2A}R$ detection over time in culture, cells were fixed for 15 minutes at RT in PFA solution (as above), washed in PBS, and permeabilized with Triton X-100 as above. After washes, cells were incubated for 1 hour at RT in PBS-GS-Triton X-100 blocking solution and incubated for 1 hour with a mouse antibody against GAD 67 (1:500, MAB5406, Chemicon) and a rabbit antibody against $A_{2A}R$ (1:100, AAR-002, Alomone labs) in PBS-GS-Triton X-100 staining solution. After washes, cells were incubated for 45 minutes at RT with goat anti-rabbit-cy3 (1:500, Jackson Immunoresearch) and goat anti-mouse-FITC (1:300, Jackson Immunoresearch) antibodies in PBS-GS-Triton X-100solution, washed, and mounted on glass slides using Mowiol 4-88 (48 mg/mL, Sigma). Sets of neurons compared for quantification were labeled simultaneously.

Fluorescence image acquisition and analysis

Image acquisition was performed using a 63x objective (NA 1.40) on a Leica (Nussloch, Germany) DM6000 upright epifluorescence microscope with a 12-bit cooled CCD camera (Micromax, Roper Scientific) run by MetaMorph software (Roper Scientific, Evry, France). Image exposure time was determined on bright cells to obtain optimal fluorescence to noise ratio and to avoid pixel saturation. All images from a given culture were acquired with the same exposure time and acquisition parameters.

A blind analysis of VGAT, gephyrin, or $GABA_AR$ clusters was performed using MetaMorph software as routinely done (*47*). Image folders were randomized before analysis. For each neuron, a well-focused dendrite was chosen and a ROI surrounding the dendrite was manually selected. Only primary dendrites were considered for cluster analysis. Systematically, the region of interest was started after the cell body and, when possible, the entire length of the dendrite (~20-130 µm) was considered so that no cluster was excluded from the analysis. Images were then flattened, background filtered (kernel size, 3 X 3 X 2) to enhance cluster outlines, and a user defined intensity threshold was applied to select clusters and avoid their coalescence. A VGAT cluster was considered only if it exceeded a size of 3 pixels. This excluded most mobile VGAT packets not yet integrated into synapses or background noise. Clusters were then outlined and the corresponding regions were transferred onto raw images to determine the mean cluster number, area and fluorescence intensity. For quantification of gephyrin or $GABA_AR$ synaptic clusters, gephyrin or receptor clusters comprising at least 3 pixels and colocalized on at least 1 pixel with VGAT clusters were considered. Then, the dendritic length of the ROI was measured to determine the number of clusters per 10 µm. For each culture, we analyzed ~10 cells per experimental condition and ~20 clusters per cell. Due to the variability in synapse density between cultures, the number of clusters per 10 µm in each culture was normalized to the respective control values, allowing for comparisons between cultures.

Single particle tracking and analysis

Neurons were stained as previously described (*47*, *48*). Briefly, cells were incubated for 3-5 minutes at 37 °C with primary antibodies against extracellular epitopes of $GABA_AR$-γ2 subunit (guinea pig, 1:750/1:1000 provided by J.M. Fritschy), washed, and incubated for 3-5 minutes at 37ºC with biotinylated Fab secondary antibodies (goat anti-guinea pig, 4-12 µg/mL; Jackson Immunoresearch, West Grove, USA) in imaging medium. The imaging medium consisted of phenol red–free MEM supplemented with glucose (33 mM; Sigma-Aldrich) and Hepes (20 mM), glutamine (2 mM), Na^+-pyruvate (1 mM), and B27 (1X) from Invitrogen.

After washes, cells were incubated for 1 minute with streptavidin-coated quantum dots (QDs) emitting at 605 nm (1 nM; Invitrogen) in borate buffer (50 mM) supplemented with sucrose (200 mM) or in PBS (1 M; Invitrogen) supplemented with 10% (v/v) casein (Sigma). Washing and incubation steps were all done in imaging medium.

Cells were imaged using an Olympus IX71 inverted microscope equipped with a 60x objective (NA 1.42; Olympus) and a Lambda DG-4 monochromator (Sutter Instrument). Quantum Dot (QD) real time recordings (integration time of 75 milliseconds over 800 consecutive frames) were acquired with Hamamatsu ImagEM EMCCD camera and MetaView software (Meta Imaging 7.7). Cells were imaged within 45 minutes following labeling.

QD tracking and trajectory reconstruction were performed with homemade software (Matlab; The Mathworks, Natick, MA) as described previously (*47*, *48*). One to two sub-regions of dendrites were quantified per cell. In cases of QD crossing, the trajectories were discarded from analysis. Values of the mean square displacement (MSD) plot versus time were calculated for each trajectory by applying the relation:

$$MSD(n\tau) = \frac{1}{N-n}\sum_{i=1}^{N-n}\left[\left(x((i+n)\tau) - x(i\tau)\right)^2 + \left(y((i+n)\tau) - y(i\tau)\right)^2\right]$$

(*48*), where τ is the acquisition time, N is the total number of frames, n and i are positive integers with n determining the time increment. Diffusion coefficients (D) were calculated by fitting the first four points without origin of the MSD *versus* time curves with the equation:

$MSD(n\tau) = 4Dn\tau + b$ where b is a constant reflecting the spot localization accuracy. Synaptic dwell time was defined as the duration of detection of QDs at synapses on a recording divided by the number of exits as detailed previously (*48*). Dwell times < 5 frames were not retained.

DNA-PAINT imaging

For 2-color PAINT imaging of $A_{2A}R$ and gephyrin at inhibitory synapses, rat hippocampal neurons in culture were fixed for 10 minutes at RT in PFA solution (as above), washed in PBS, and permeabilized with Triton X-100 as above. After washes, cells were incubated for 1 hour at RT in PBS-GS-Triton X-100 blocking solution and incubated overnight at 4°C with a rabbit antibody against $A_{2A}R$ (1:100, Alomone Labs) and mouse anti-gephyrin (mAb7a, 1:500, Synaptic Systems) in PBS-GS-Triton X-100 staining solution. After washes, cells were incubated for 45 minutes at RT with DNA-coupled anti-rabbit and anti-mouse secondary antibodies (Ultivue).

DNA-PAINT imaging was carried out on an inverted N-STORM Nikon Eclipse Ti microscope with a 100x oil-immersion objective (N.A. 1.49) and an Andor iXon Ultra EMCCD camera (image pixel size, 160 nm), using specific lasers for PAINT imagers (561 and 647 nm). Coverslips were imaged in imaging buffer with DNA-PAINT Imager-650 and Imager-560 at 0.5 nM (Ultivue). The sample was alternatively illuminated at 647 and 561 nm (full laser power), and 20,000-30,000 images of each channel were acquired at 25–33 Hz. The z position was maintained during acquisition by a Nikon perfect focus system. Acquired sequences were processed using the N-STORM software (Nikon). After drift correction and localization merging, 3D stacks of synapses were reconstructed using ThunderSTORM.

The centroid of each cluster of gephyrin detections was found using the *kmeans* function in Matlab (The Mathworks). This position was then used to calculate the distance of each $A_{2A}R$ detection, in 3D, to the centroid of the post-synaptic side of the synapse. For each synapse, a mean value of distances was calculated.

Calcium Imaging

GCaMP6-ruby AAV viruses were used to infect hippocampal neurons at DIV3 by addition of 0.3 µL of viral solution in the culture medium. At 5 days post infection, cells were imaged at 37°C in an open chamber mounted on an inverted spinning-disc microscope (Leica DMI4000, Yokogawa CS20 spinning Nipkow disk, 40x/0.6 N.A. objective) in an extracellular solution containing the following in mM: 2 $CaCl_2$, 2 KCl, 3 $MgCl_2$, 10 HEPES, 20 glucose, 120 NaCl, pH7.4. Cells were selected using expression of the reporter protein ruby, and intracellular Ca^{2+} was imaged using 491 nm light from a laser. Emitted light was collected using a 525-39 (± 25) nm emission filter. Time lapse (0.33 Hz for 600 seconds) of confocal stacks (of ~21 images acquired with an interval of 0.3 µm) were acquired with a cooled EM-CCD camera (512 x 512, 16 µm pixel size) using Metamorph. The analysis was performed on a section of the stack where the soma was in focus at different time points. Fluorescence intensities collected in the soma or dendrites before (F0) and following (F) bath addition of the drugs, were background-subtracted before being displayed as F/F0 values. Data were analyzed using Metamorph. Normalization of fluorescence intensity was performed for each cell by dividing the mean fluorescence intensity by the average of fluorescence intensities of the 4 time points before drug application. Statistics (paired t test) were run on the last time point before drug application (120 seconds) compared to the latest time point after drug application (600 seconds).

cAMP Imaging

Recombinant Sindbis virus encoding EPAC-sh150 (*26*) were used to infect hippocampal neurons at DIV8 by addition of 1 µL of viral solution in the culture medium (~5×10^5 particles per slice). 12 hours after infection, hippocampal neurons were transferred onto the microscope stage and were continuous superfused at 0.5 mL/min with a solution containing the following (in mM): 2 $CaCl_2$, 2 KCl, 3 $MgCl_2$, 10 HEPES, 20 glucose, 120 NaCl, pH 7.4 at 32°C. Two-photon imaging was performed using an upright Leica TCS MP5 microscope with resonant scanning (8 kHz), a Leica 25x/0.95 HCX IRAPO immersion objective and a tunable Ti:sapphire laser (Coherent Chameleon Vision II) with dispersion correction set to 860 nm for CFP excitation. The emission path consisted of an initial 700 nm low-pass filter to remove excess excitation light (E700 SP, Chroma Technologies), 506 nm dichroic mirror for orthogonal separation of emitted signal, 479/40 CFP emission filter, 542/50 YFP emission filter (FF506-Di01-25 × 36; FF01-479/40; FF01-542/50; Brightline Filters; Semrock) and two-channel Leica HyD detector for simultaneous acquisition. Due to the high quantum efficiency and low dark noise of the HyD photodetectors, detector gain was typically set at 10–15% with laser power at 1–5%. Z-stack images (12-bit; 512 × 512) were typically acquired every 15 seconds. The z-step size was 1–2 µm and total stack size was typically 8–10 sections. Images were processed in ImageJ by using maximum z-projections followed by translation registration correction to reduce x/y movement. However, z-projections were occasionally complicated by movement in the z-axis and were therefore corrected with a custom Matlab script before measurement in ImageJ. After correcting movement in the x/y/z directions, ROIs were selected for measurement if they could only be measured for the whole experimental time course.

Videomicroscopy of presynaptic terminals

Inhibitory synapses were stained by incubating live neurons for 48 hours at 37°C in a 5% CO_2 humidified incubator with a primary VGAT antibody directly coupled to Oyster550 (*22*) (1:200, Synaptic Systems) diluted in conditioned culture medium. Cells were washed and imaged in recording medium in the presence of the appropriate drugs.

Cells were imaged using an Olympus IX71 inverted microscope equipped with a 60x objective (NA 1.42; Olympus) and a Lambda DG-4 monochromator (Sutter Instrument). Time lapse imaging of VGAT-Oyster550 (1 image every 5 minutes) were acquired with Hamamatsu ImagEM EMCCD camera and MetaView software (Meta Imaging 7.7). Cells were imaged for 40 minutes following labeling.

Statistics

Sample size selection for experiments was based on published experiments, pilot studies as well as in-house expertise. All results were used for analysis except in few cases. Cells with signs of suffering (apparition of blobs, fragmented neurites) were discarded from the analysis.

For all quantifications, values were expressed as means ± s.e.m. and differences were considered significant for p-values less than 5% *(*$p \leq 0.05$; **$p < 0.01$; ***$p < 0.001$).* SigmaPlot 12.5 software (Systat Software) was used to compare immunohistochemical and immunocytochemistry data using the non-parametric Mann-Whitney test. For diffusion coefficient values having non-normal distributions, a non-parametric Kolmogorov-Smirnov test was run under Matlab (The Mathworks, Natick, MA). Clampfit 10.2 and Minianalysis software (Synaptosoft) were used to analyze synaptic events collected from electrophysiological recordings. Cumulative distributions of frequency and amplitude were examined using the same number of events (50) per cell per condition. The statistical analysis was done using a 50 milliseconds binning

for the interevent interval and 2.5 pA for the amplitude). Data collected from electrophysiological recordings, having non-normal distributions, we used a non-parametric two tailed Kolmogorov-Smirnov test with OriginLab 7.5 (OriginLab Corporation). For Western blot and receptor binding, means were compared using the one- or two-way ANOVA followed by Dunnett's or Bonferroni post hoc test (Western blots) and paired t-test independent means (receptor binding assay) using GraphPad Prim software.

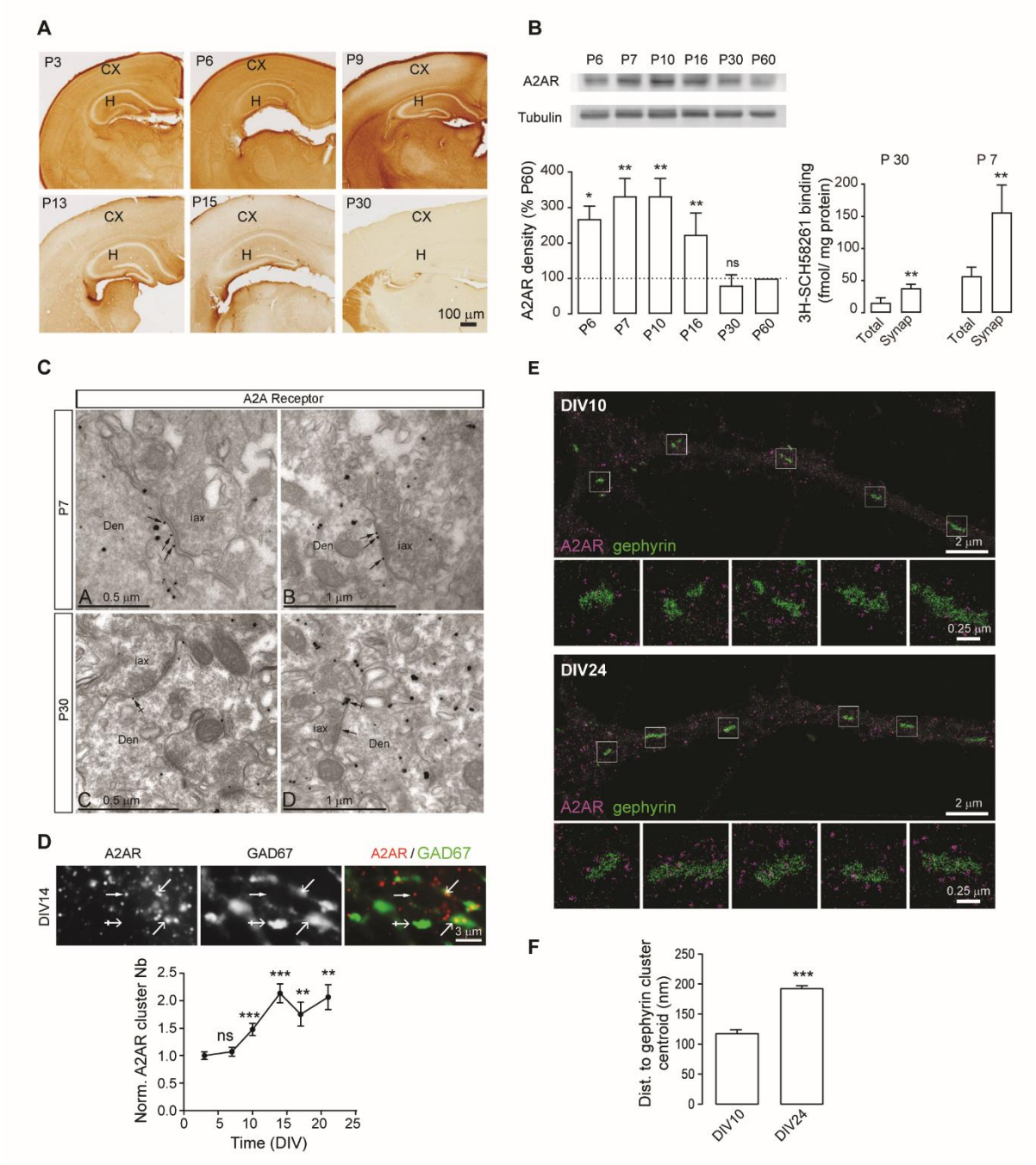

Fig. S1. Increased density of postsynaptic A_{2A}Rs during the peak of synaptogenesis.

(**A**) Immunohistochemical detection of A_{2A}Rs during development shows increased protein levels during early stages of postnatal development as compared to later stages in the hippocampus (H) and cortex (CX). Images are representative of 2-4 mice. (**B**) Left, Western blot showing the transient increase in A_{2A}R protein levels in the hippocampus during the first two postnatal weeks (values normalized to P60). Right, binding assays with the selective A_{2A}R antagonist ^{3}H-SCH58261 (2 nM) showing that A_{2A}Rs are more abundant in purified synapses (synaptosomal

membranes) than in total membranes of the hippocampus of P7 pups. N= 6-8 mice. (**C**) Subcellular localization of A_{2A}Rs in the hippocampus. Electron micrographs of the *stratum radiatum* of the hippocampal CA1 region showing immunoparticles for A_{2A}Rs. (*A,B*): at P7, immunoparticles for A_{2A}Rs were observed on the postsynaptic plasma membrane (arrows) of dendritic shafts of presumed pyramidal cells (Den) contacted by presumed GABAergic axon terminals (iax) establishing symmetric synapse, as well as in the intracellular compartment. (*C,D*): at P30, immunoparticles for A_{2A}Rs were found on the postsynaptic plasma membrane (arrows) of dendritic shafts of presumed pyramidal cells (Den), but they were more frequently observed at the edge of postsynaptic densities (double arrowhead). Scale bars: Top left panel, 500 nm; other panels, 1000 nm. (**D**) Double-detection of A_{2A}Rs and GAD67 in DIV 14 hippocampal cultures. Some (large arrows) but not all (thin arrows) A_{2A}R clusters were detected at GABAergic synapses. Some GABAergic synapses are devoid of A_{2A}Rs (crossed arrows). The graph shows that the clustering of A_{2A}Rs at GABAergic synapses increased during the peak of synaptogenesis *in vitro* (between DIV 5 and 14). Values were normalized to control. N= 12-46 cells, 2-3 cultures. (**E**) Hippocampal neurons stained for A_{2A}Rs (magenta) and gephyrin (green) imaged by DNA-PAINT. Images show a portion of dendrite with 5 zoomed synapses below from a DIV 10 (top) and DIV 24 (bottom) neuron, respectively. Scale bars, 2 µm (images) and 250 nm (zooms). (**F**) Quantifications of DNA-PAINT images shown in panel E indicating that A_{2A}Rs are more enriched at perisynaptic sites in DIV 10 neurons as compared to DIV 24 neurons. N = 55 synapses at DIV 10, 170 synapses at DIV 24. In all graphs, values and histograms represent means and s.e.m.; unpaired Student's t-test (B, left) or Dunnett's test (B, right): *P<0.05; Mann-Whitney test (D, F): ns - not significant; *p≤0.05; **p<0.01; ***p<0.001.

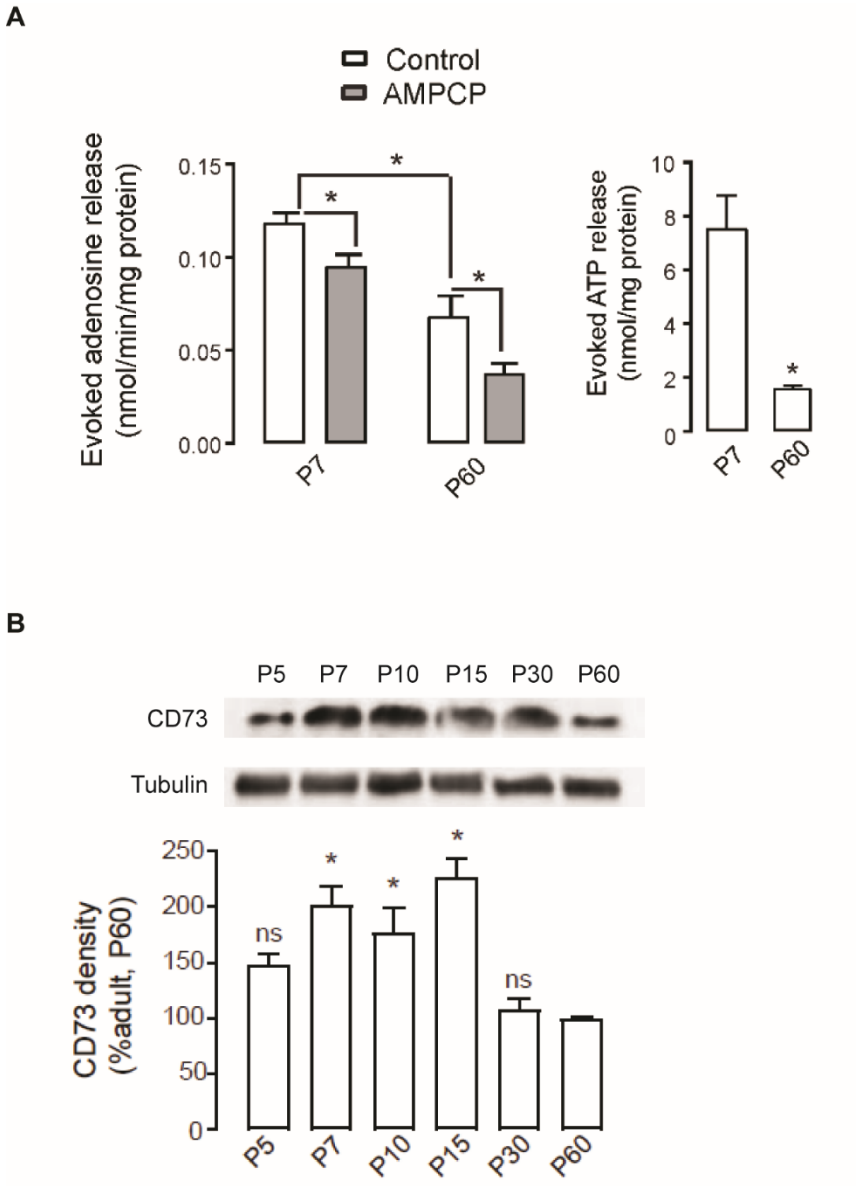

Fig. S2. Increased activity-dependent release of ATP and adenosine during the period of synaptogenesis.

(**A**) **Left:** Challenging synaptosomes with high K^+-evoked a larger release of adenosine at P7 than at P60. Note that AMPCP (100 μM) decreased adenosine levels at both ages. N= 6-8 P7 or P60 mice. **Right:** Larger K^+-evoked release of ATP at P7 than at P60. N=6-8 mice. (**B**) **CD73 density peaks during the period of synaptogenesis.** Western Blot on hippocampal synaptosomal membranes. N= 6-8 mice. One Way ANOVA followed by Dunnett's post hoc test: ns - not significant; *$p<0.05$.

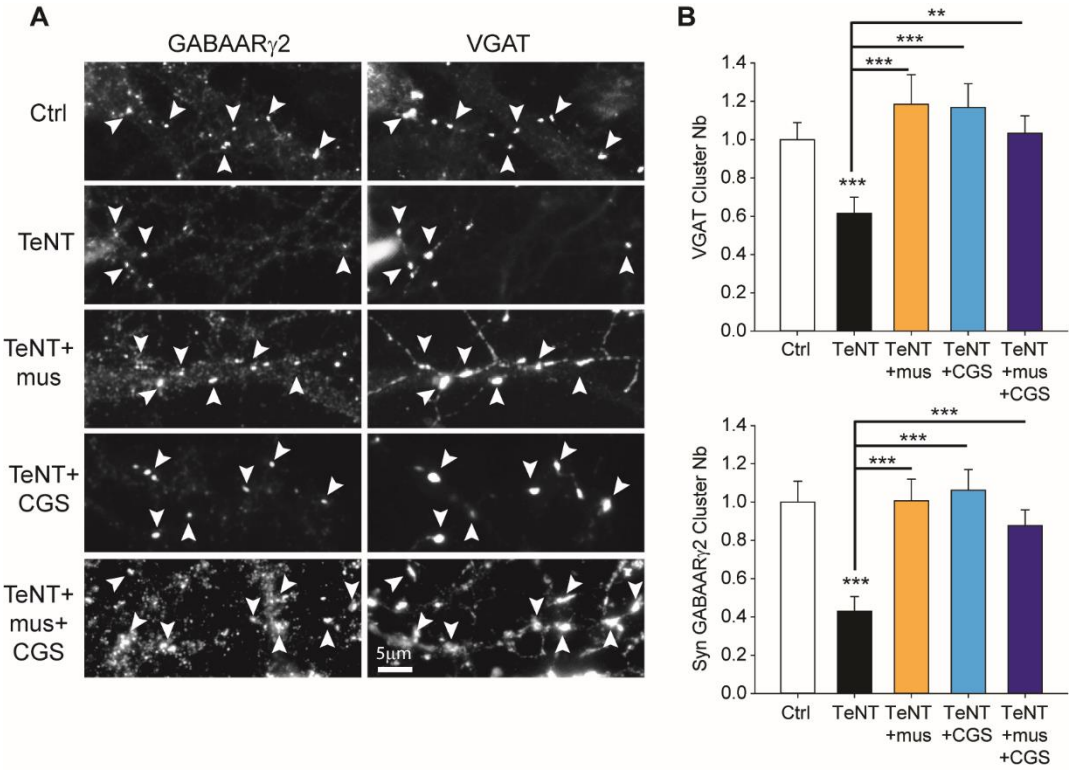

Fig. S3. Activity-dependent control of GABAergic synapse density requires the activation of A_{2A}Rs or $GABA_A$Rs.

(**A**) Representative images of VGAT and $GABA_A$Rγ2 immunostaining in DIV9 neurons pretreated with tetanus toxin (TeNT, 1-40 nM) for 48 hours before exposure to muscimol (10 µM), CGS21680 (30 nM) or muscimol + CGS21680 for 30 min. Scale bar, 5 µm. Arrowheads show examples of inhibitory synapses double-stained for VGAT and $GABA_A$Rγ2. (**B**) Quantification of VGAT (top) and synaptic $GABA_A$Rγ2 (bottom) cluster number (Nb) per dendrite length showing the loss of GABAergic synapses upon neuronal activity blockade and its rescue upon selective activation of A_{2A}Rs or $GABA_A$Rs. Note that the effects of A_{2A}Rs and $GABA_A$Rs on the stabilization of GABAergic synapses is not additive. Ctrl n=44, TeNT n=26, TeNT + muscimol n=29, TeNT + CGS21680 n=37, TeNT + CGS21680 + muscimol n=22, 3 cultures. In all graphs, values were normalized to the control; histograms represent means and s.e.m.; Mann-Whitney test: **p<0.01; ***p<0.001.

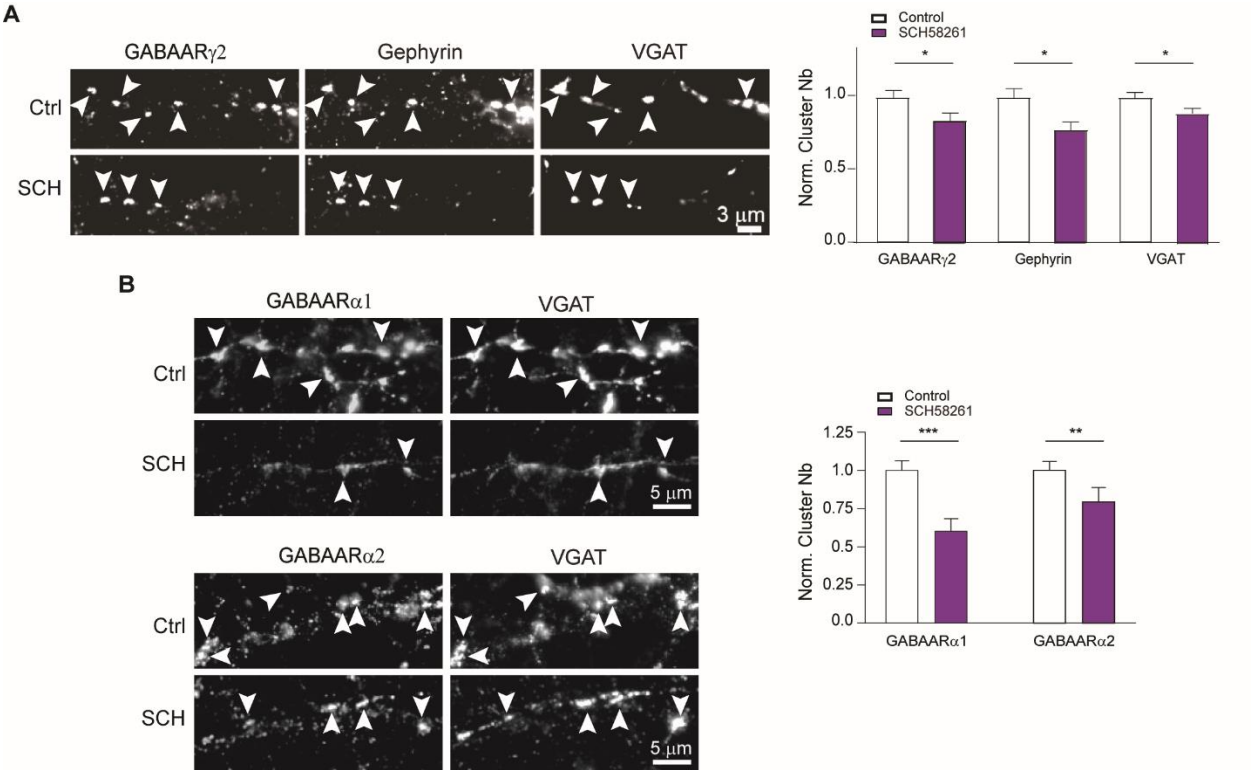

Fig. S4. Acute $A_{2A}R$ blockade leads to the loss of pre- and post- synaptic markers of GABAergic synapses.

(**A**) $GABA_AR\gamma2$, gephyrin and VGAT staining (left) and quantification (right) of DIV 10 neurons exposed or not for 30 min to SCH58261 (SCH, 100 nM). Scale bar, 3 µm. One fourth of GABAergic synapses were destabilized following $A_{2A}R$ blockade. N= 30-111 cells, 3-7 cultures. Arrowheads show examples of inhibitory synapses triple-stained for VGAT, $GABA_AR\gamma2$ and gephyrin. (**B**) $GABA_AR\alpha2$ or $GABA_AR\alpha1$ and VGAT staining (left) and quantification (right) of DIV 8-9 neurons maintained 30 min in absence or presence of SCH58261 (SCH, 100 nM). Scale bar, 5 µm. SCH58261 destabilizes GABAergic synapses containing either $GABA_AR$ α2 or α1 subunits. However, the effect of SCH58261 was more pronounced at synapses containing the α1 than the α2 subunit. N= 29-34 cells, 2 cultures. Arrowheads show examples of inhibitory synapses double-stained for VGAT and $GABA_AR\alpha2$ or $GABA_AR\alpha1$. In all graphs, values were normalized to the control values; histograms represent means and s.e.m.; Mann-Whitney test: **p<0.01; **p<0.001.

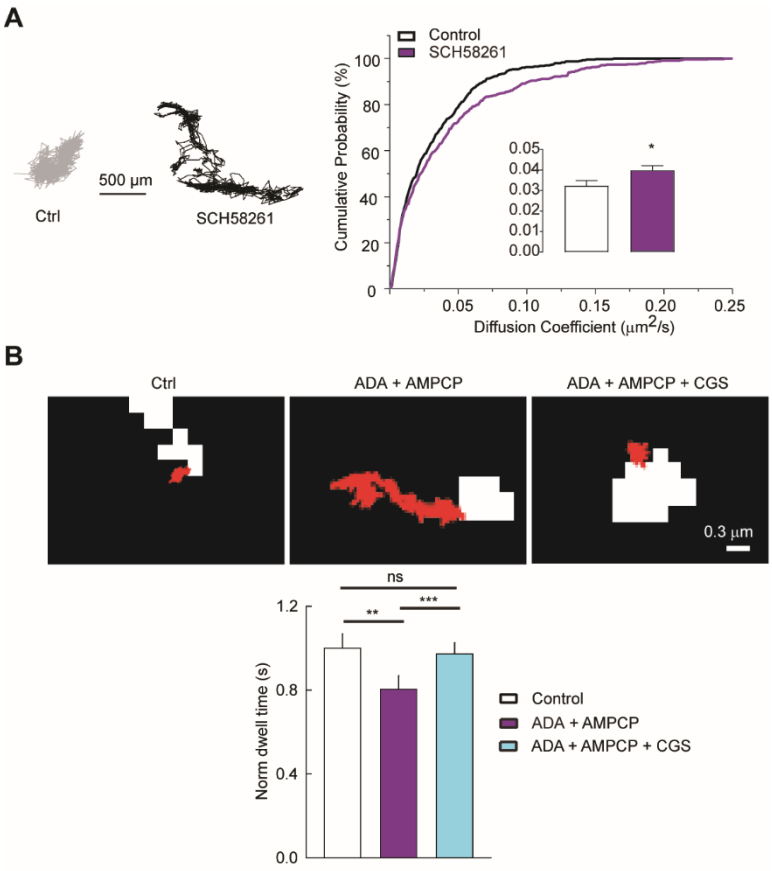

Fig. S5. A_{2A}Rs rapidly modulate the membrane dynamics of $GABA_AR\gamma2$.

(**A**) $GABA_AR\gamma2$ trajectories (left) and cumulative probabilities of diffusion coefficient (right) in the absence or presence of SCH58261 (100 nM) in DIV 8 hippocampal neurons. N≥ 400 trajectories, 3 cultures. Insert: histograms represent the mean value of diffusion coefficients and s.e.m. (**B**) Examples of $GABA_AR\gamma2$ synaptic trajectories (top) and quantifications (bottom) showing reduced receptor dwell time at synapses upon ADA+AMPCP exposure and recovery upon $A_{2A}R$ activation with CGS21680 (30 nM). Scale bar, 0.3 µm. N= 63-88 quantum dots, 2 cultures. Values were normalized to the control values; histograms represent means and s.e.m.; Kolmogorov-Smirnov test (A); Mann-Whitney test (B): ns - not significant; *p≤0.05; **p<0.01; ***p<0.001.

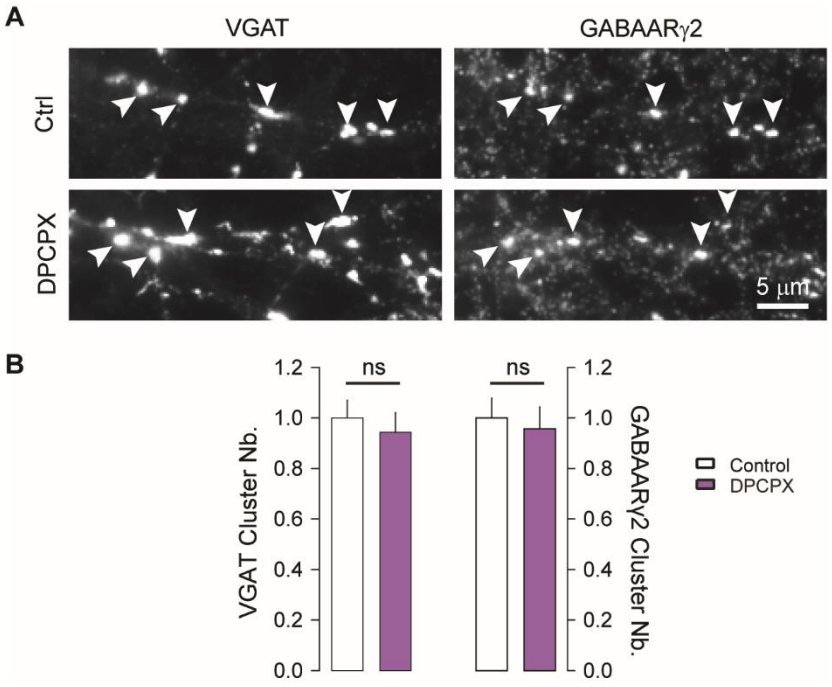

Fig. S6. No effect of a selective A_1R antagonist on GABAergic synapses.

(**A**) Representative images of VGAT and $GABA_AR\gamma2$ immunostaining in DIV9 neurons in the absence or presence of DPCPX (100 nM) in DIV 8-9 neurons. Scale bar, 5 µm. Arrowheads show examples of inhibitory synapses double-stained for VGAT and $GABA_AR\gamma2$. (**B**) Quantification of VGAT and synaptic $GABA_AR\gamma2$ cluster number (Nb) per dendrite length showing no loss of GABAergic synapses upon A_1R blockade. Ctrl n=34 cells, DPCPX n=32 cells, 3 cultures. Histograms represent means and s.e.m.; Mann-Whitney test: ns - not significant.

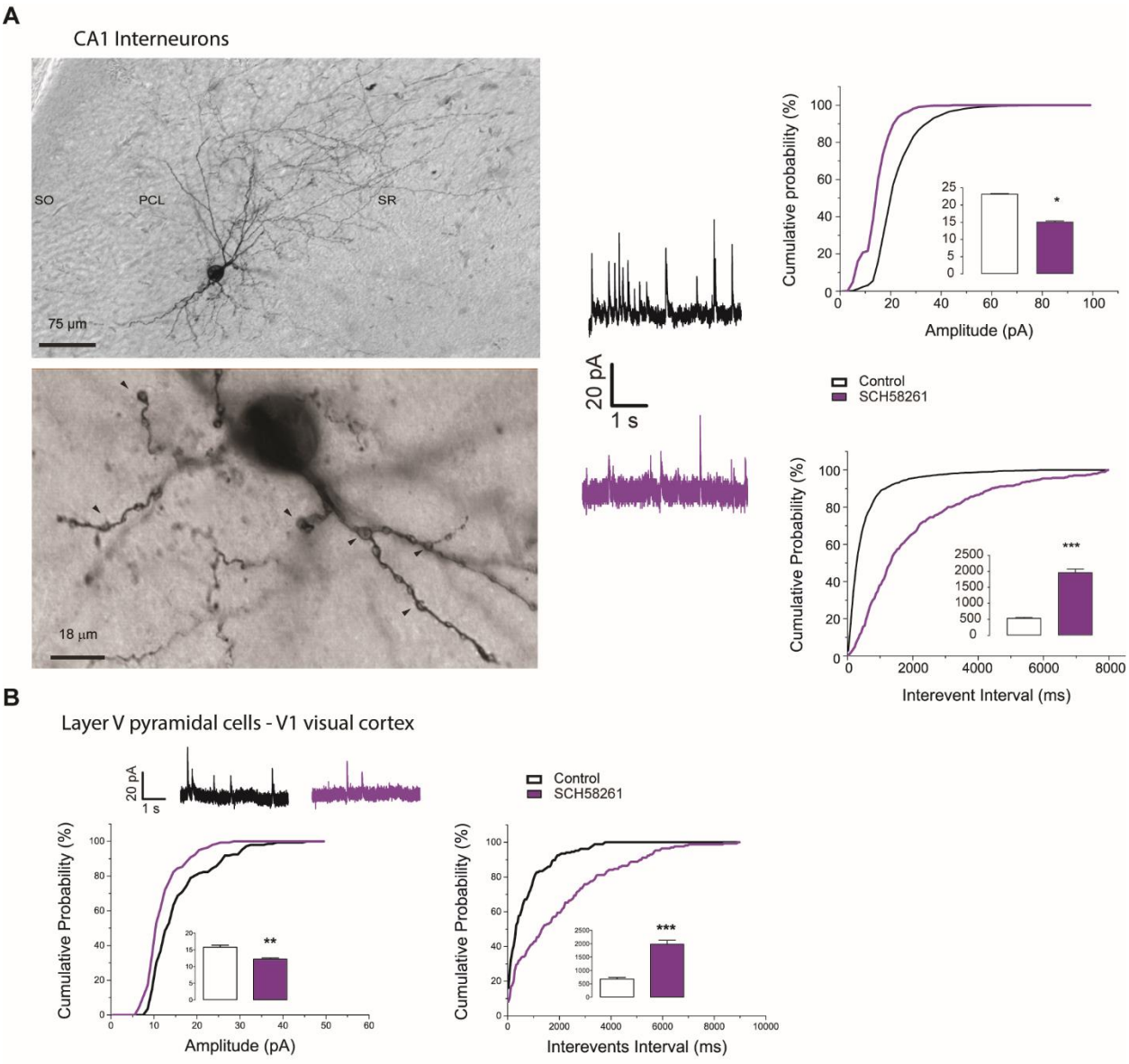

Fig. S7. Acute $A_{2A}R$ blockade decreases miniature GABAergic currents in different cell types.

(**A**) **Acute $A_{2A}R$ blockade decreases miniature GABAergic currents in CA1 hippocampal interneurons. Left:** mIPSC traces before (black) and 30 minutes after (red) application of 100 nM SCH58261 in a representative CA1 interneuron filled with biocytin (images at two different magnifications) in slices of P6 mice. **Right:** Application of SCH58261 during 30 min reduced the amplitude and frequency of $GABA_AR$-mediated mIPSCs in CA1 interneurons (8 cells, 8 slices, 6 P6 pups). (**B**) **Acute $A_{2A}R$ blockade decreases miniature GABAergic currents in layer V pyramidal cells in V1.** Application of SCH58261 during 30 min reduced the amplitude and frequency of $GABA_AR$-mediated mIPSCs in V1 pyramidal cells (5 cells, 5 slices, 3 P6 pups). In all graphs, histograms represent means and s.e.m. of the corresponding measured variables (IPSC amplitude or interevent interval); Kolmogorov-Smirnov test: *p≤0.05; **p<0.01; ***p<0.001.

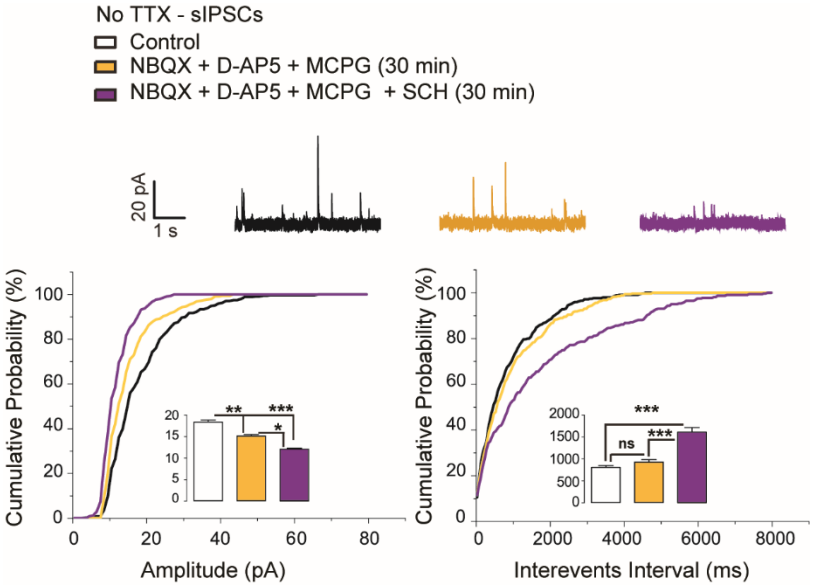

Fig. S8. Acute $A_{2A}R$ blockade decreases miniature GABAergic currents in CA1 pyramidal cells in conditions of glutamate ionotropic and metabotropic receptor blockade.

Application of glutamate receptor antagonists (1 μM NBQX, 50 μM D-AP5, 100 μM MCPG) during 30 min in slices of P6 mice reduced the frequency of $GABA_AR$-mediated spontaneous IPSCs in CA1 pyramidal cells. Subsequent application of SCH58261 (100 nM) during 30 min reduced the amplitude and frequency of spontaneous IPSCs (7 cells, 7 slices, 3 P6 pups). In all graphs, histograms represent means and s.e.m. of the measured variable (IPSC amplitude or interevent interval); Kolmogorov-Smirnov test: ns - not significant; *$p \leq 0.05$; **$p < 0.01$; ***$p < 0.001$.

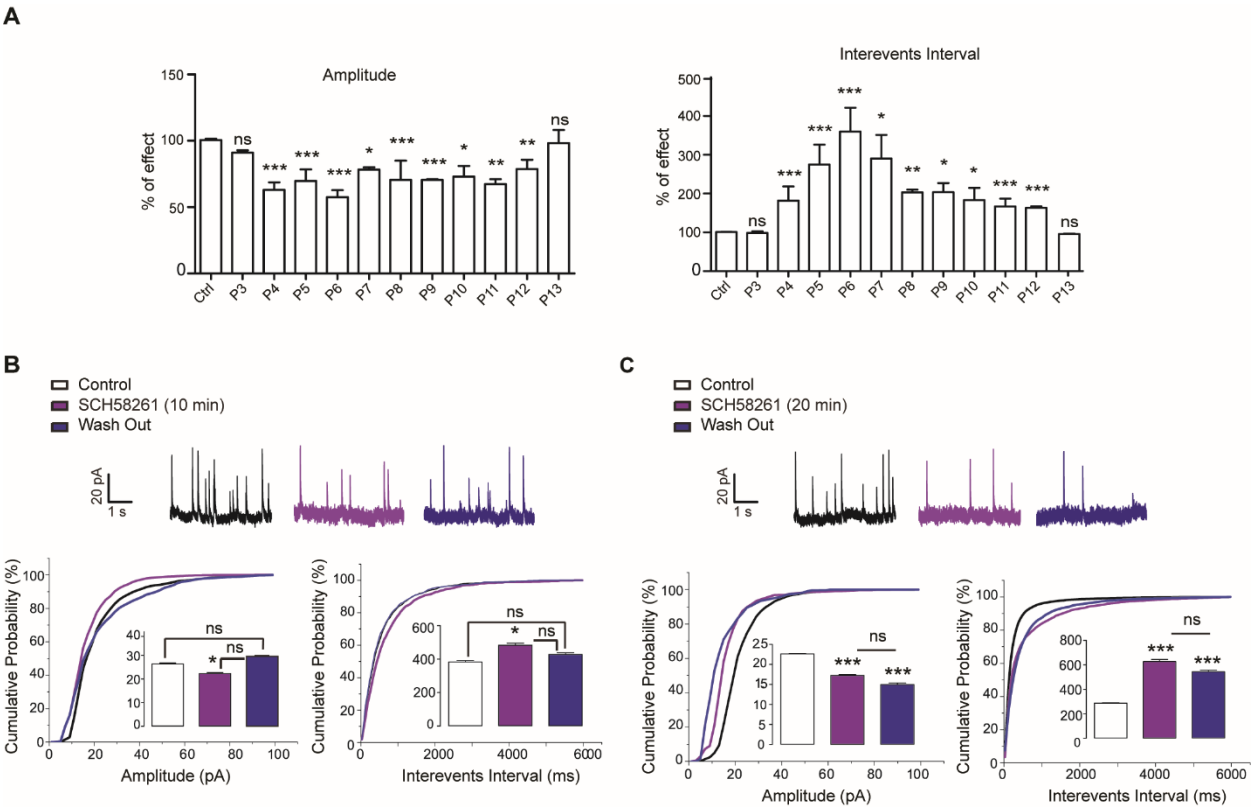

Fig. S9. A_{2A}R-mediated stabilization of GABAergic synapses is time-dependent.

(**A**) The effect of SCH58261 (100 nM) on mIPSCs was found between P4 and P12. Per time point: N= 4-5 pups, 5-10 slices, 4-11 cells. (**B**) The effect of A_{2A}R blockade on GABAergic currents was reversible within 10 min. Ten min application of SCH58261 (100 nM) resulted in a decrease of mIPSC amplitude and frequency. Following 30 min of wash out, mIPSCs were back to control values. N= 6 cells, 6 slices, 5 P6 pups. (**C**) The effect of A_{2A}R blockade on GABAergic currents was irreversible with 20 min application of SCH58261. N= 10 cells, 10 slices, 6 P6 pups. In all graphs, histograms represent means and s.e.m. of the measured variable (IPSC amplitude or interevent interval); Kolmogorov-Smirnov test: ns - not significant; *$p \leq 0.05$; **$p < 0.01$; ***$p < 0.001$.

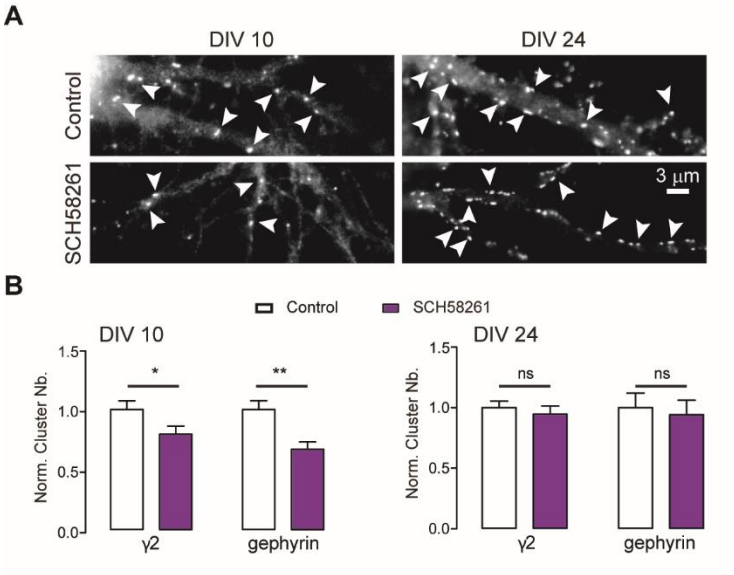

Fig. S10. $A_{2A}R$-mediated regulation of synapse density is restricted to the period of synaptogenesis.

(**A**) Detection of $GABA_AR\gamma2$ in DIV 10 or DIV 24 neurons in the absence or presence of 100 nM SCH58261. Arrowheads show examples of inhibitory synapses labeled for $GABA_AR\gamma2$. Scale bar, 3 µm. (**B**) Quantifications of the mean number of $GABA_AR\gamma2$ and gephyrin clusters in DIV 10 vs. DIV 24 neurons in control or SCH58261 conditions. Note the loss of clusters in DIV 10 but not in DIV 24 neurons upon SCH58261 treatment. $GABA_AR\gamma2$ at DIV 10: Ctrl n= 68 cells, SCH n= 52 cells, 4 cultures. Gephyrin at DIV10: Ctrl n= 18 cells, SCH n= 17 cells, 2 cultures. $GABA_AR\gamma2$ at DIV24: Ctrl n= 47 cells, SCH n= 46 cells, 2 cultures. Gephyrin at DIV24: Ctrl n= 8 cells, SCH n= 9 cells, 2 cultures. In all graphs, values were normalized to the corresponding control values; histograms represent means and s.e.m.; Mann-Whitney test: ns - not significant; *$p<0.05$; **$p<0.01$.

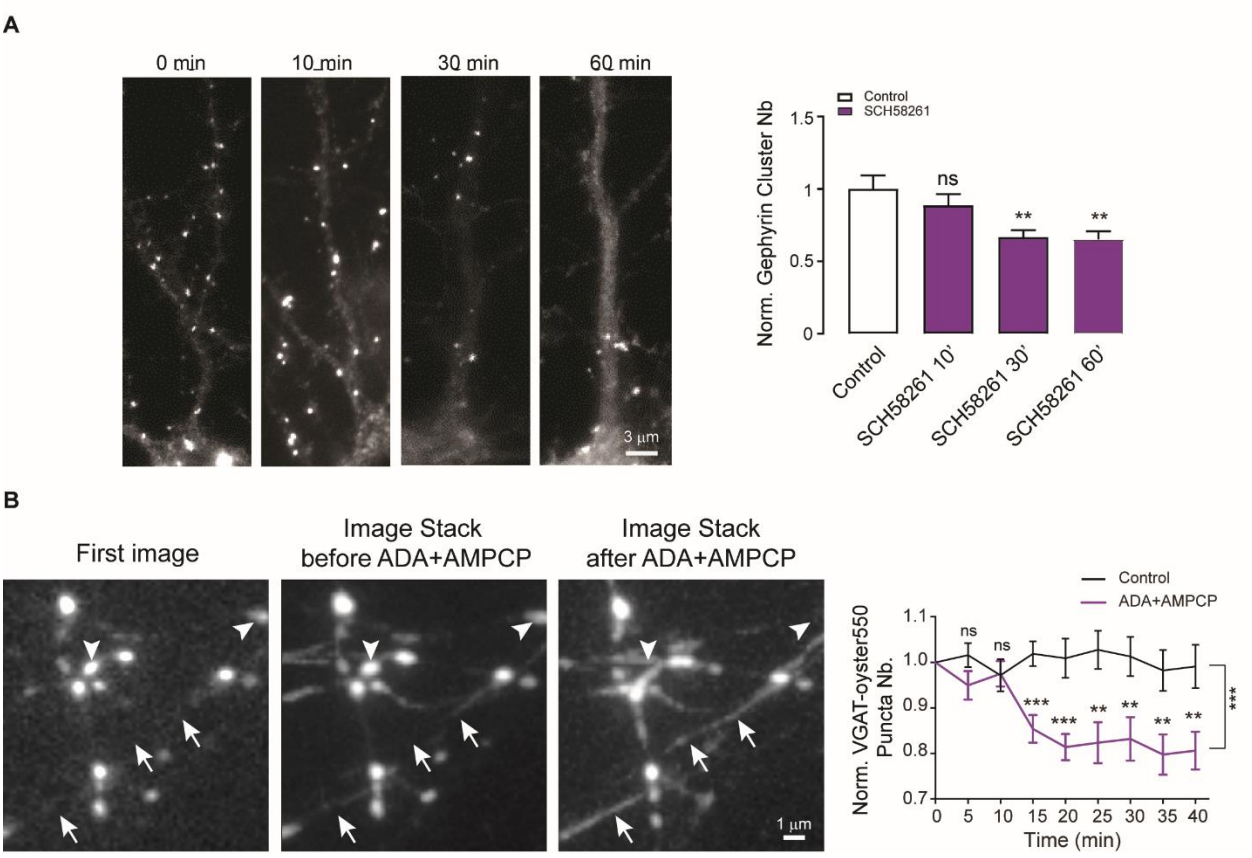

Fig. S11. Time-course of synapse destabilization following $A_{2A}R$ blockade.

(**A**) **Time-course of gephyrin cluster dispersion following $A_{2A}R$ blockade.** Quantification of gephyrin-monomeric Red fluorescent protein clusters in DIV 10 neurons after application of 100 nM SCH58261 (10', 30', 60'). N= 30-47 cells, 2-3 cultures. (**B**) **Removal of ambient adenosine destabilizes active GABAergic terminals within 15 minutes.** Live cell imaging of active GABA synaptic terminals visualized by the incorporation of VGAT-Oyster550 antibodies in recycling vesicles, in the absence or presence of ADA (4-20 U/mL) and AMPCP (100 µM) in DIV10 neurons. Left, Images showing a single recording frame of the neuron before drug application (first image) and maximum intensity projections of time lapses (1000 frames at intervals of 100 ms) before and after 15 min of ADA+AMPCP application. Note the loss (arrowheads) of some active inhibitory boutons (white dots) upon 15 min bath application of ADA+AMPCP and the high mobility of VGAT packets (seen as white lines on the projection) along the axonal processes (arrows). Right, quantifications of the mean number of VGAT puncta in the absence or presence of ADA+AMPCP over a 40-min recording. N= 10 cells, 30-39 regions of interest analysed. Histograms in A represent means and s.e.m.; Mann-Whitney test (A); Unpaired t-test (B) was used to compare time points between them; Paired t-test (B) was used to compare the whole curves. ns - not significant; **p<0.01; ***p<0.001.

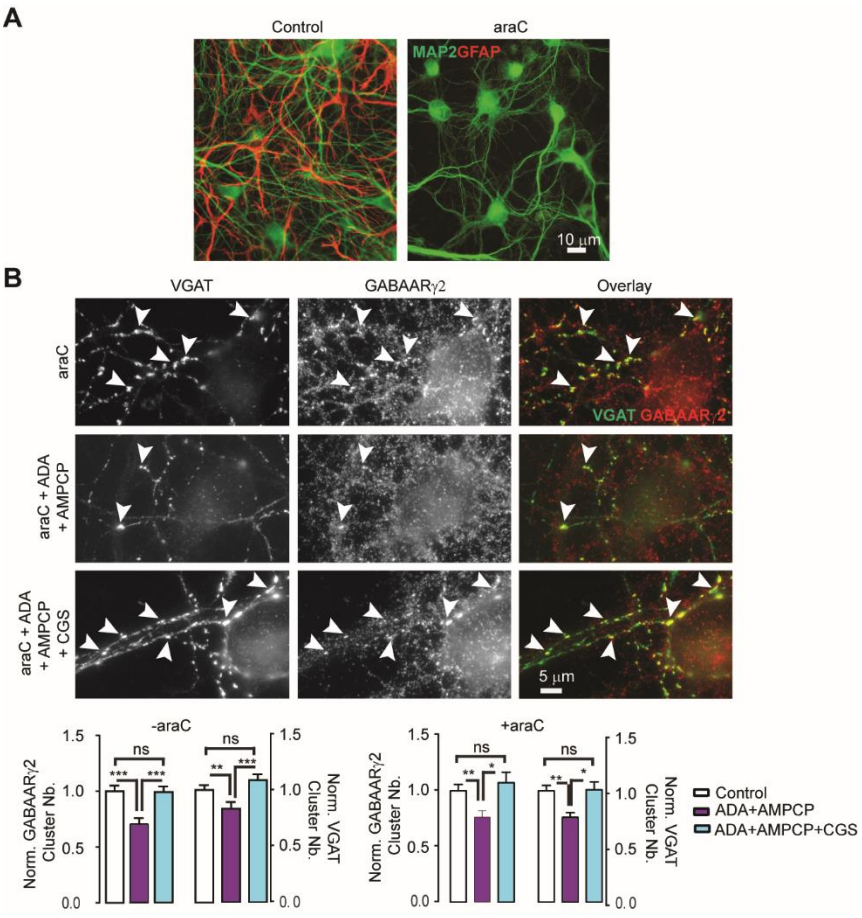

Fig. S12. Glial cells are not necessary for $A_{2A}R$-mediated stabilization of GABAergic synapses.

(**A**) Representative images of GFAP and MAP2 immunostaining in DIV9 neurons treated at DIV 1 with arabinosylcytosine C (AraC, 5 µM) showing the complete loss of GFAP-stained glial cells upon araC treatment. Scale bar, 10 µm. (**B**) Representative images of VGAT and $GABA_AR\gamma2$ immunostaining (top) and quantification (bottom) in DIV9 neurons pretreated with araC (5 µM) before exposure to the indicated drugs for 30 min. Scale bar, 5 µm. Arrowheads show examples of inhibitory synapses double-stained for VGAT and $GABA_AR\gamma2$. Decreasing extracellular adenosine levels led to synapse destabilization, an effect that could be prevented by the direct activation of $A_{2A}Rs$ with CGS21680. N= 53-56 cells, 3 cultures. Values were normalized to the control. Histograms represent means and s.e.m.; Mann-Whitney test (B): ns - not significant; *p≤0.05; **p<0.01; ***p<0.001.

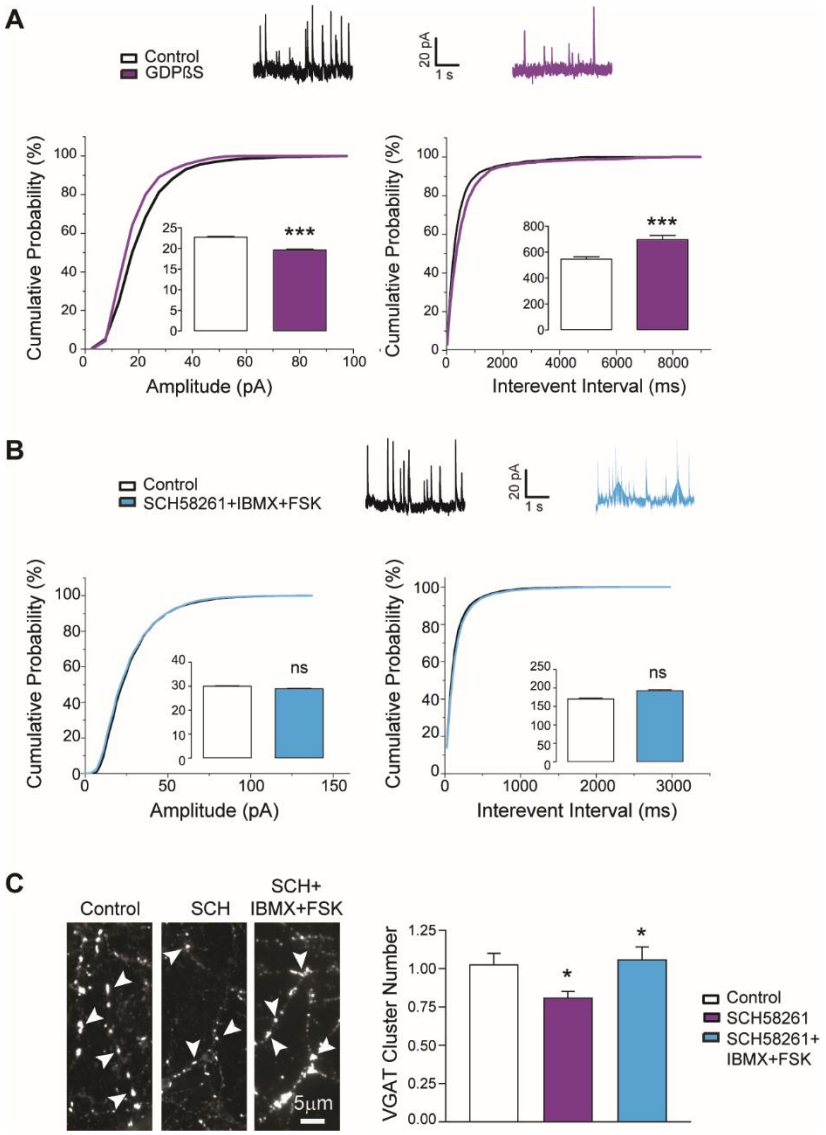

Fig. S13. Mechanism of synapse stabilization downstream of A_{2A}Rs involves G proteins and adenylyl cyclase.

(**A**) Blocking G protein activity within neurons reproduces the effects of A_{2A}R blockade. Top: mIPSC traces recorded 5 min (control) and 30 min after break-in using internal solutions containing GDPβS in CA1 hippocampal pyramidal cells from P6 hippocampal slices. GDPβS reduced mIPSCs amplitude and frequency. N= 7 cells, 7 slices, 6 P6 pups. (**B**) Using IBMX and forskolin (FSK) to activate the AC/cAMP signalling cascade, which is downstream of A_{2A}R activation, prevented the loss of mIPSCs induced by A_{2A}R blockade. N= 7 cells, 7 slices, 6 P6 pups. N= 7 cells, 7 slices, 6 P6 pups. (**C**) Immunostaining and quantification of VGAT in DIV 10 neurons in absence or presence of the indicated drugs for 30 min. Using IBMX and forskolin (FSK) to activate the AC/cAMP signalling cascade prevented the loss of GABAergic boutons induced by A_{2A}R blockade. Scale bar, 5 µm. Arrowheads show examples of inhibitory synapses labeled for VGAT. N= 45-50 cells, 3 cultures. Values were normalized to the control values. In all graphs, histograms represent means and s.e.m. of the measured variable (Insets in A, B: IPSC amplitude or interevent interval; C: VGAT cluster number); Kolmogorov-Smirnov test (A, B), Mann-Whitney test (C): ns - not significant; *p≤0.05; ***p<0.001.

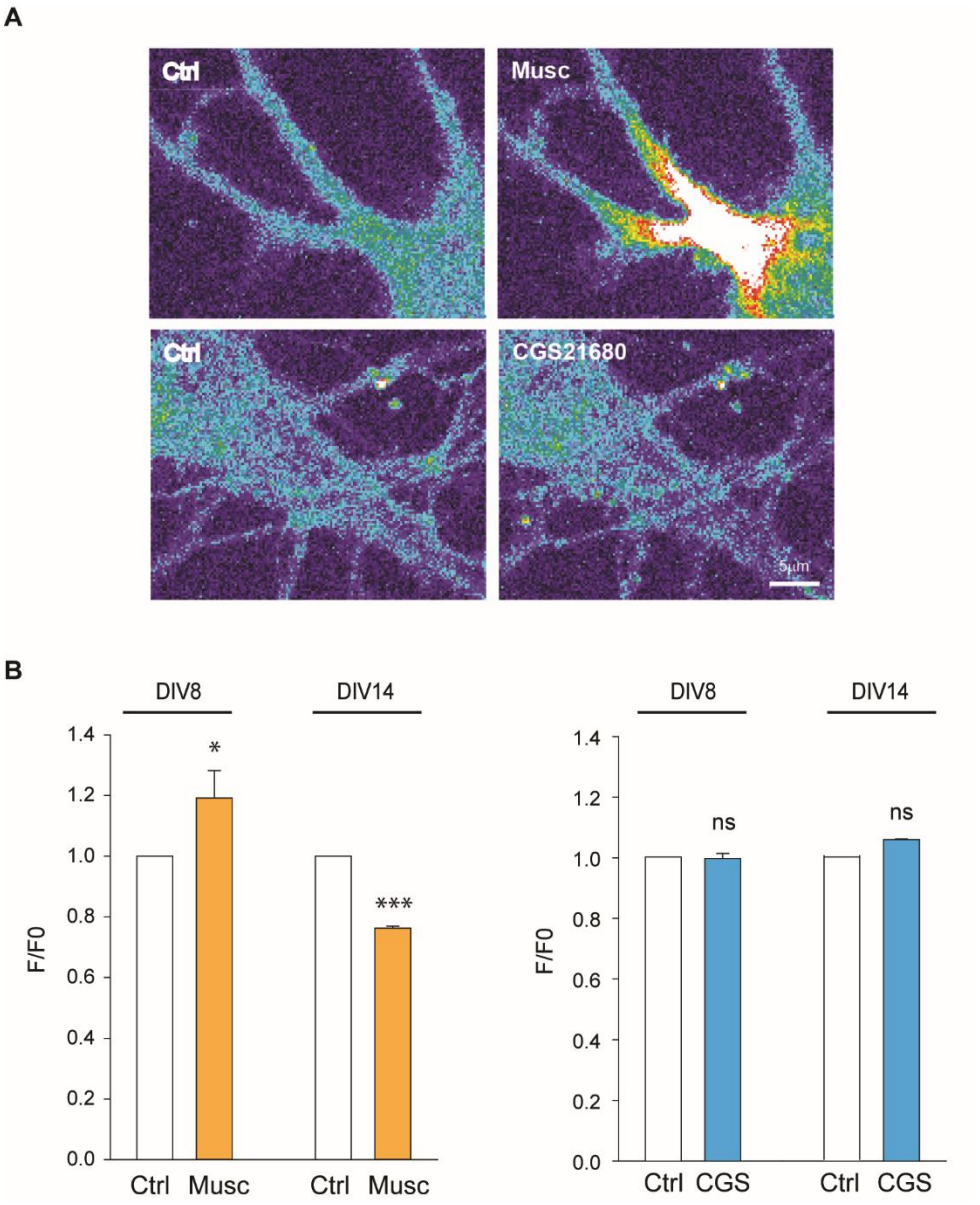

Fig. S14. GABA$_A$R but not A$_{2A}$R activation elevates intra-neuronal calcium levels in DIV8 neurons.

(**A**) Pseudocolor images of DIV8 neurons infected with GCaMP6-rubi AAVs, before (left) and after (right) 10 µM muscimol (mus), or 30 nM CGS21680 (CGS) application, as indicated. Warmer colors mean higher GCaMP fluorescence intensities. Scale bar, 5 µm. (**B**) Calcium levels in proximal dendrites shown as F/F0 ratio (mean ± s.e.m.) before and after muscimol or CGS21680 treatment. Note an increase and decrease in intracellular calcium levels after muscimol treatment in DIV8 and DIV14 neurons, respectively. In contrast, CGS21680 did not significantly alter intracellular calcium levels regardless of the age of the neurons. Muscimol: DIV8 21 cells, DIV14 10 cells; CGS21680: DIV8 13 cells, DIV14 10 cells; 3 cultures. paired t test: ns - not significant; *p≤0.05; ***p<0.001.

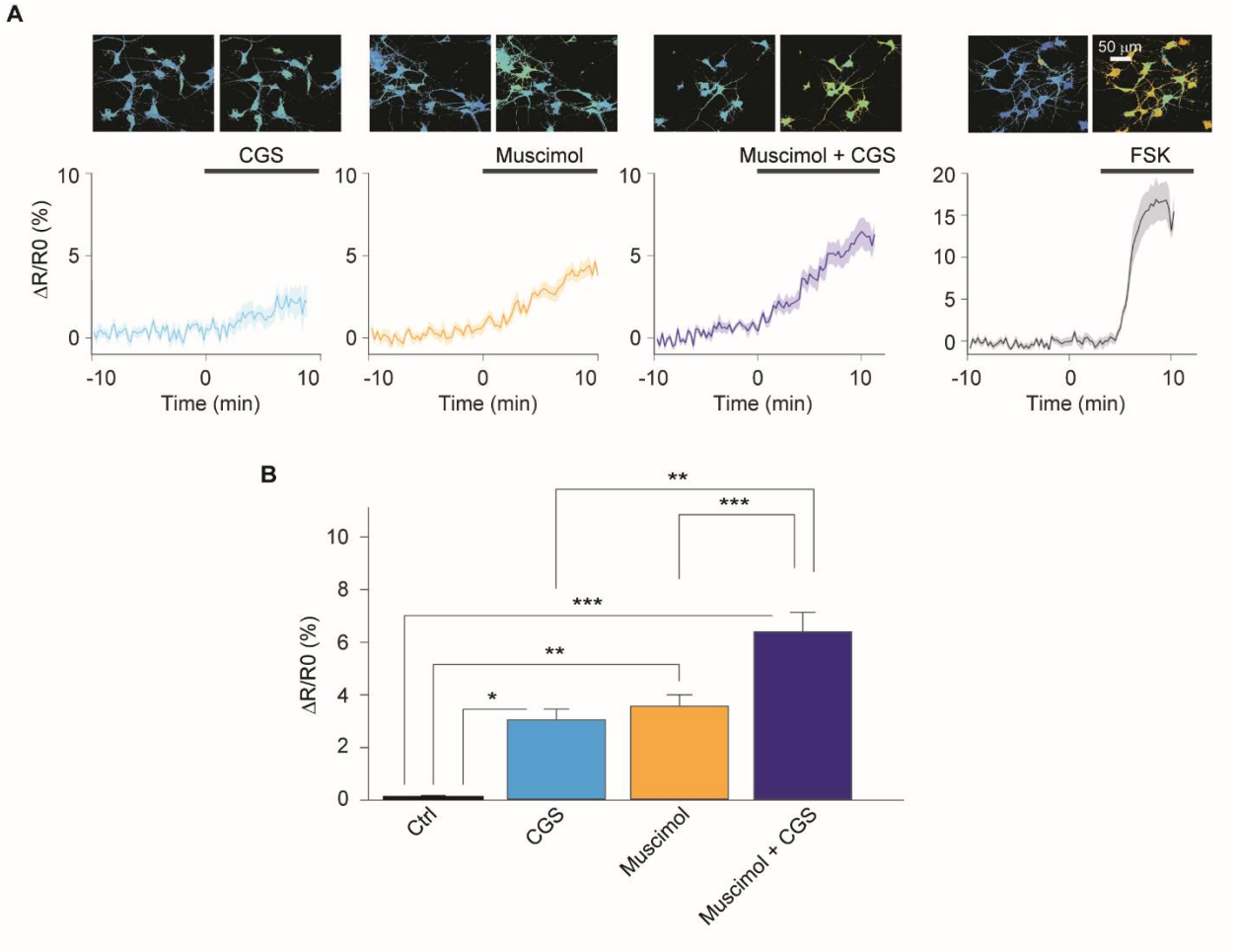

Fig. S15. GABA$_A$R activation potentiates A$_{2A}$R-mediated increase in cAMP intracellular levels.

(**A**) cAMP levels in proximal dendrites of DIV9 neurons infected with recombinant Sindbis virus encoding EPAC-sh150 cAMP sensor. Variation of FRET ratio was calculated as ΔR/R0. R0 was calculated as the ratio between the emission at CFP channel divided by the emission at YFP channel at baseline. R is the value of the FRET ratio recorded at each time point. Data are shown as ΔR/R0 ratio measured as a function of time following CGS21680 (CGS, 30 nM), muscimol (10 µM), muscimol + CGS, or forskolin (FSK, 10 µM) application, as indicated (black bars). (**B**) Quantitative analysis of cAMP levels as ΔR/R0 ratio in neurons in control conditions or after drug application. Muscimol and CGS21680 applied separately increased cAMP levels but note that cAMP level further increased when both drugs were applied simultaneously. N cells = 47-99, 3 cultures. Histograms represent means and s.e.m. One way ANOVA $F(3,333) = 61.78$, $p<0.0001$; Tukey's test: *$p<0.05$; **$p<0.01$; ***$p<0.001$.

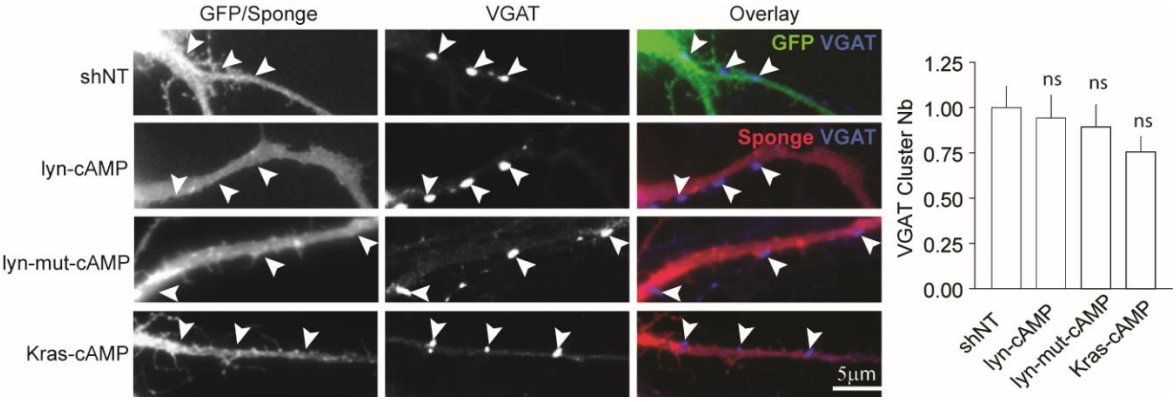

Fig. S16. Absence of effect of cAMP sponges on the density of VGAT inhibitory synapses in basal activity conditions.

VGAT staining (left) and quantification (right) of DIV 10-11 neurons transfected with non-target (shNT) or the different sponges constructs (lyn-cAMP, lyn-mutated cAMP, K-Ras cAMP). Scale bar, 5 µm. shNT n=57, lyn-cAMP n=37, lyn-mutated n=44, K-Ras n=41, 5 cultures. Arrowheads show examples of inhibitory synapses labeled for VGAT. Histograms represent means and s.e.m. Values normalized to their respective controls; Mann-Whitney test: ns - not significant.

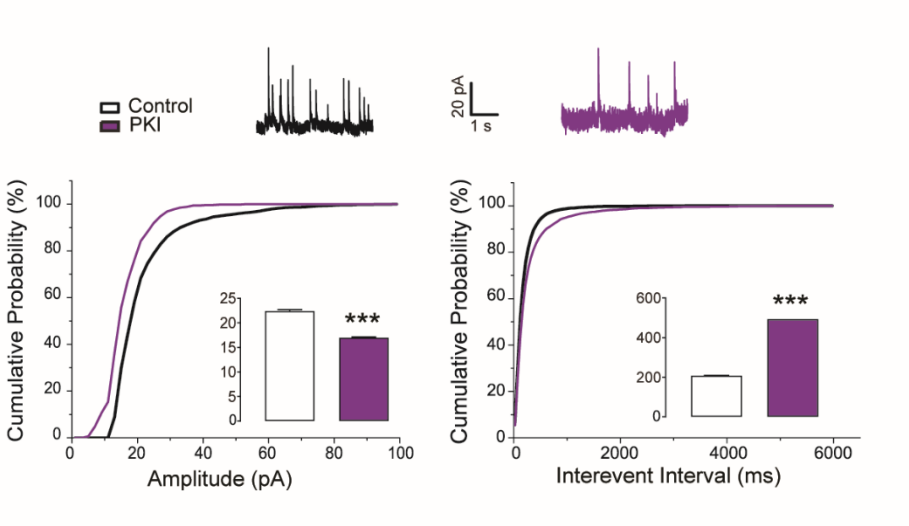

Fig. S17. A_{2A}R-mediated synapse stabilization requires PKA activation.

Intracellular blockade of PKA mimics the effects of A_{2A}R blockade. Top: mIPSC traces recorded 5 min (control) and 30 min after break-in using internal solutions containing PKI (10 µM) in CA1 hippocampal pyramidal cells from P6 hippocampal slices. PKI reduced mIPSC amplitude and frequency. N= 7 cells, 7 slices, 6 P6 pups. Insets, Histograms represent means and s.e.m. of the measured variables (IPSC amplitude and interevent interval); Kolmogorov-Smirnov test; ***p<0.001.

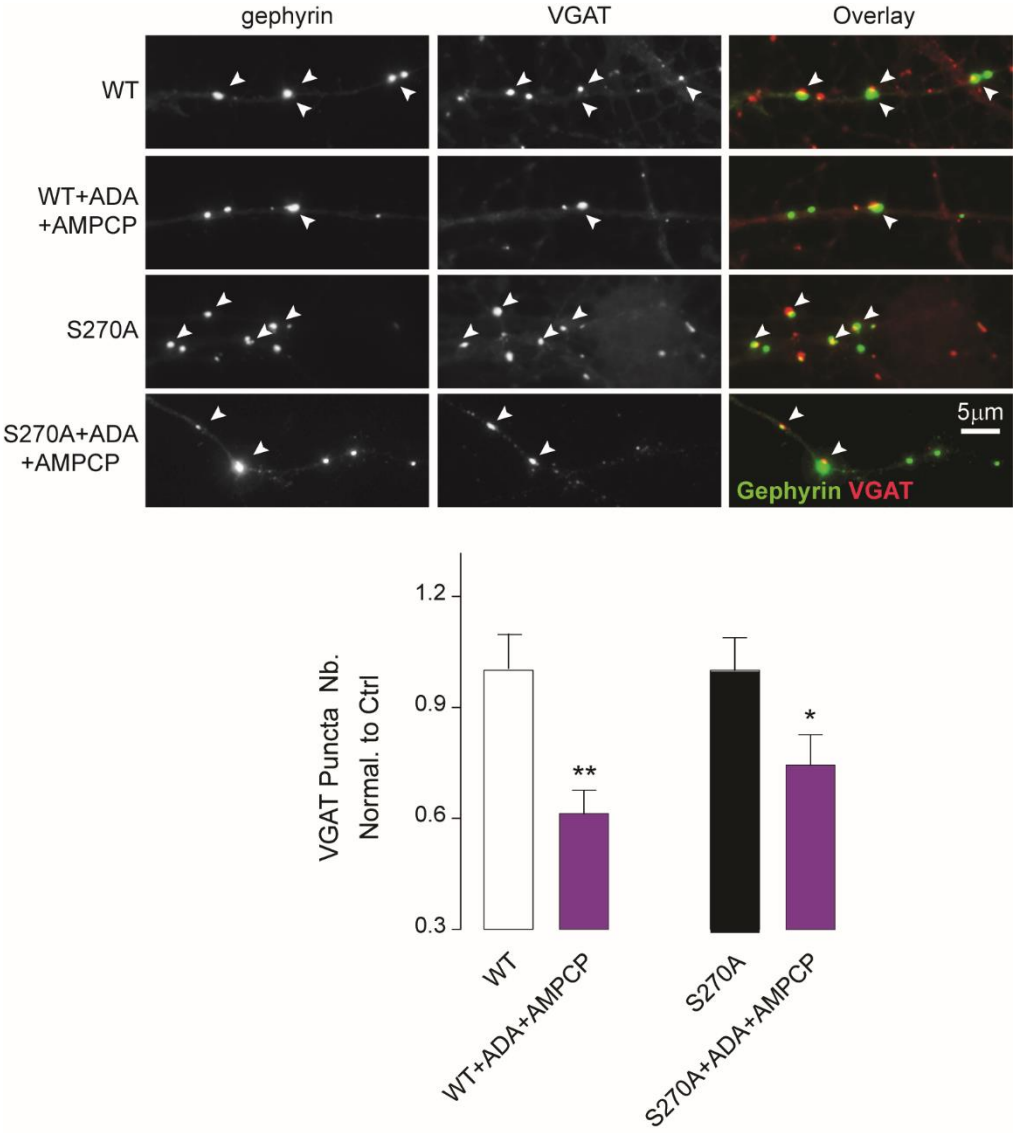

Fig. S18. Adenosine-mediated stabilisation of GABAergic synapses does not require gephyrin phosphorylation by glycogen synthase kinase 3β (GSK3β).

Gephyrin and VGAT staining in the absence or presence of ADA (4-20 U/mL) and AMPCP (100 µM) (top) and quantification (bottom) in DIV 10 neurons expressing the gephyrin-WT or the glycogen synthase kinase 3β (GSK3β) phospho-null mutant (S270A). One fourth of GABAergic synapses were destabilized following extracellular adenosine removal in neurons expressing the gephyrin WT or S270A construct. N= 63-68 cells, 5 cultures. Arrowheads show examples of inhibitory synapses labeled for VGAT. Histograms represent means and s.e.m.; Mann-Whitney test: *$p \leq 0.05$; **$p < 0.001$.

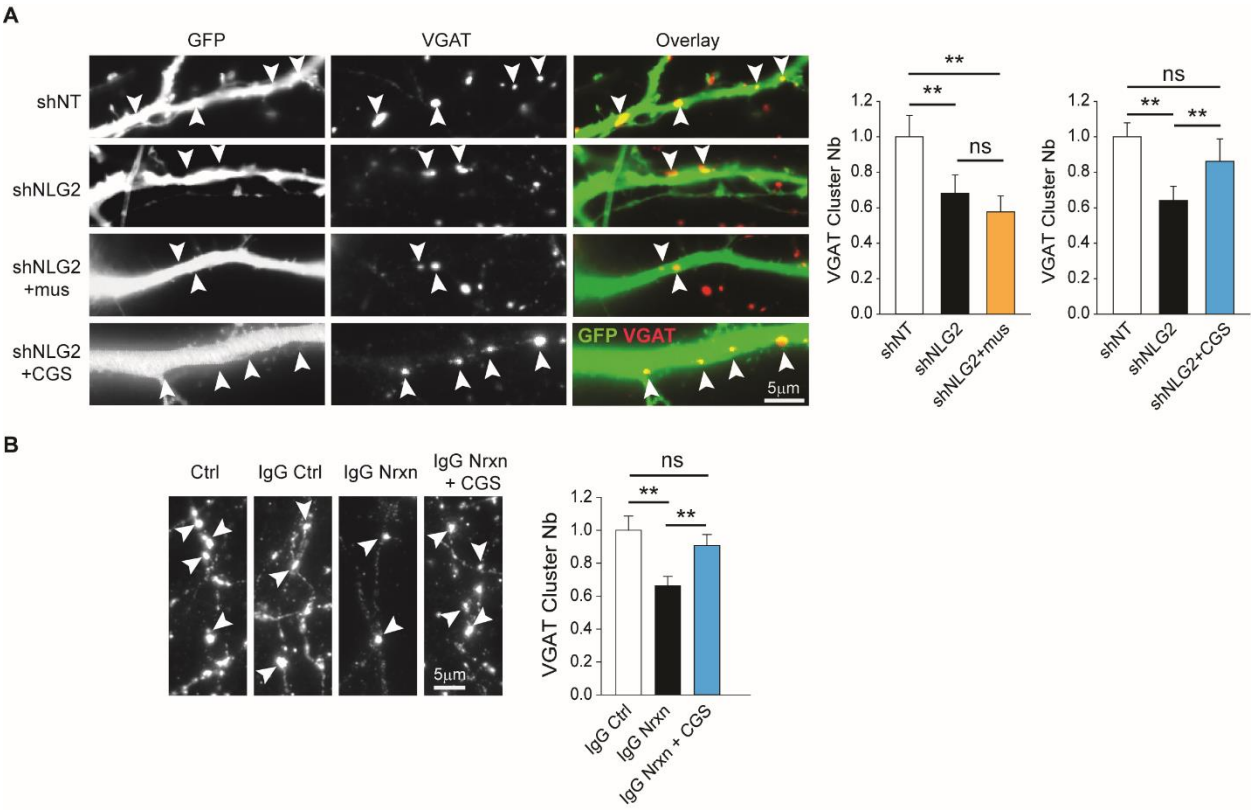

Fig. S19. Synapse stabilization downstream of $A_{2A}R$ does not involve the synaptogenic organizer neuroligin-2.

(**A**) The loss of GABAergic synapses upon suppression of neuroligin-2 (NLG2) can be rescued by the activation of $A_{2A}Rs$ but not of $GABA_ARs$. VGAT staining (left) and quantification (right) of DIV 10-11 neurons transfected with shNT or shNLG2 exposed or not to muscimol (Mus, 10 µM) or CGS21680 (CGS, 30 nM) for 30 minutes. Scale bar, 5 µm. (Muscimol) shNT n=39, shNLG2 n=36, shNLG2 + muscimol n=33, 3 cultures. (CGS) shNT n=39, shNLG2 n=36, shNLG2 + CGS n=33, 3 cultures. (**B**) The loss of GABAergic synapses induced by blockade of neurexin activity could be rescued upon $A_{2A}R$ activation. VGAT staining (left) and quantification (right) of DIV 10-11 neurons incubated with IgG control or IgG Neurexin blocking antibody for 30 min and exposed or not to CGS21680 for another 30 minutes. Scale bar, 5 µm. IgG Ctrl n=44, IgG Nrxn n=50, IgG Nrxn + CGS n=48, 3 cultures. In all images, arrowheads show examples of inhibitory synapses labeled for VGAT. In all graphs, histograms represent means and s.e.m.; values were normalized to corresponding controls; Mann-Whitney test (A, B): *p<0.05; **p<0.01; ***p<0.001.

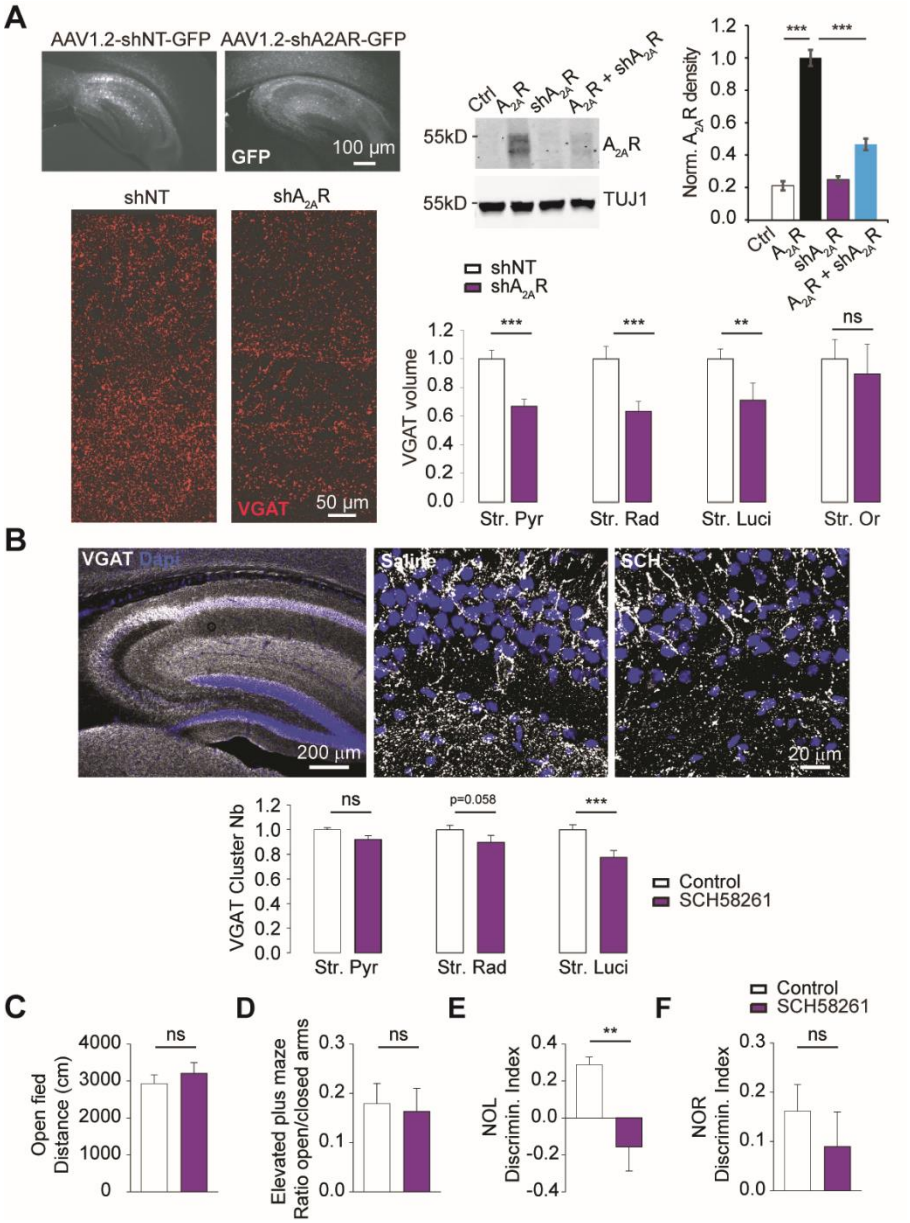

Fig. S20. Chronic $A_{2A}R$ blockade or suppression during synaptogenesis *in vivo* induces GABAergic synapse loss and cognitive deficits.

(**A**) Chronic $A_{2A}R$ suppression with an AAV1.2-sh$A_{2A}R$-GFP in the hippocampus at P3 leads at P21 to the loss of GABAergic synapses. Up: Left, Confocal micrographs show shNT- and sh$A_{2A}R$-infected cells in a parasagittal hippocampal slice 18 days post-infection. Scale bar, 100 µm. Middle, Characteristic Western blot from 3 cultures infected with the same adenoviruses (AAVs), expressing either shNT or sh$A_{2A}R$. Right, summary graph shows $A_{2A}R$ density normalized to Control. Results are from 3 independent N2A cultures. Bottom: Left, Characteristic immunofluorescence of VGAT in the CA3 hippocampal region of shNT- and sh$A_{2A}R$-infected animals. Scale bar, 50 µm. Right, the total number of VGAT synapses per area was decreased in the *stratum radiatum* (str rad), *stratum pyramidale* (str pyr), *stratum lucidum* (str luci) and *stratum oriens* (str or) of sh$A_{2A}R$-infected animals. N=14-16 images from 4 mice per group. (**B**) Representative confocal images (top) and quantification (bottom) of DAPI and VGAT

immunohistochemical staining of the whole hippocampus (left) or CA3 region (right) from P16 animals chronically treated with either saline or SCH58261 (0.1 mg/kg) from P3-P16. Scale bars: low magnification, 200 μm; high magnification, 20 μm. N = 9 animals per condition, 2 regions of interest from 3-4 slices per animal were used for quantification. (**C-F**) Effect of chronic $A_{2A}R$ blockade *in vivo* on mice behavior. Animals chronically treated with saline or SCH58261 (0.1 mg/kg) from P3-P16 were allowed to habituate on days 1-3 prior to behavioral testing at adult stage (P70). Note that chronic treatment with SCH58261 did not increase locomotion or induce anxiety in adult animals, as measured using the open-field (C) and elevated plus maze (D), respectively. Open-field: No significant differences between saline and SCH58261 animals in total distance travelled. Saline N = 16 mice, SCH58261 N = 14 mice. Elevated plus maze: Graph shows the ratio of time spent in the open vs. closed arms. Saline N = 13 mice, SCH58261 N = 9 mice. E-F: Chronic treatment with SCH58261 induces deficits in hippocampal- but not non-hippocampal dependent memory as checked using the novel object location (NOL, E) and novel object recognition (NOR, F) tasks at P70. The NOL discrimination index was calculated as (time new location – time old location)/(time new location), while the NOR discrimination index was calculated as (time new object – time old object) / time new object. Saline N = 18 mice, SCH58261 N = 16 mice. Histograms represent means and s.e.m.; Values were normalized to their respective controls (A, B). Mann-Whitney test: ns - not significant; **$p<0.01$; ***$p<0.001$.

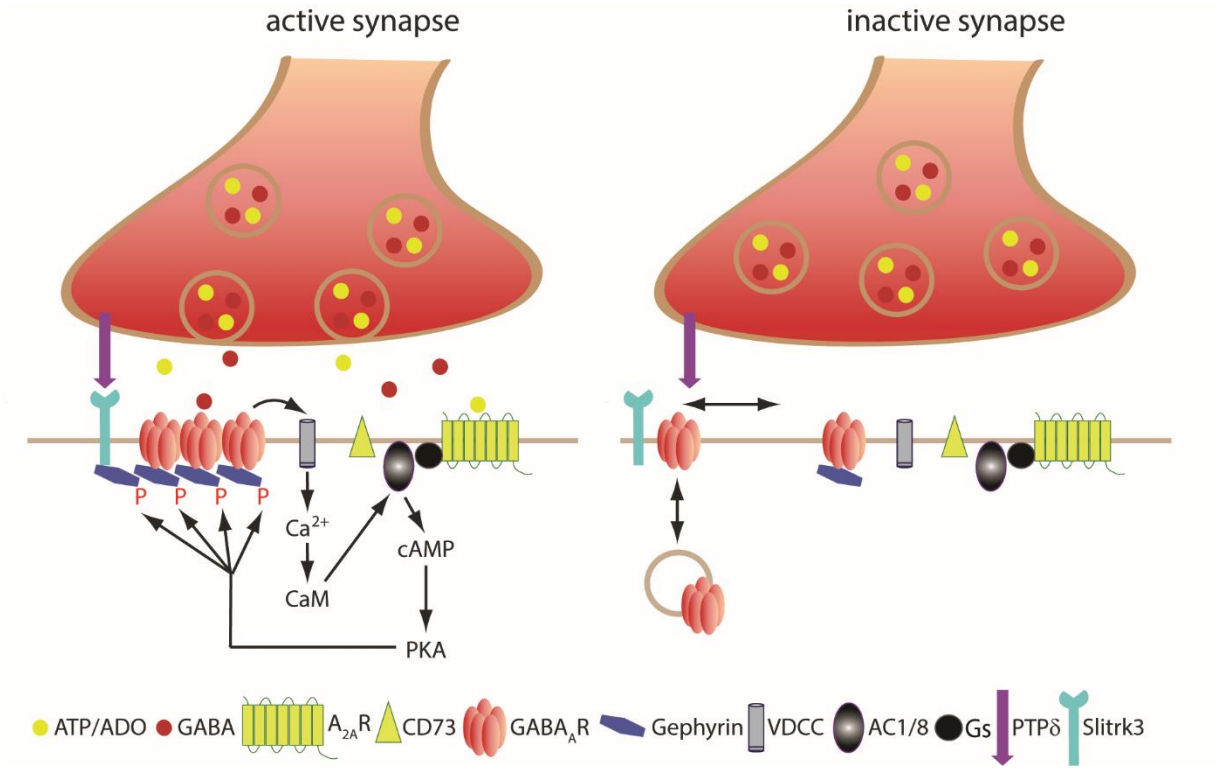

Fig. S21. Scheme showing how GABA and adenosine signaling converge onto cAMP production to stabilize/validate nascent GABAergic synapses.

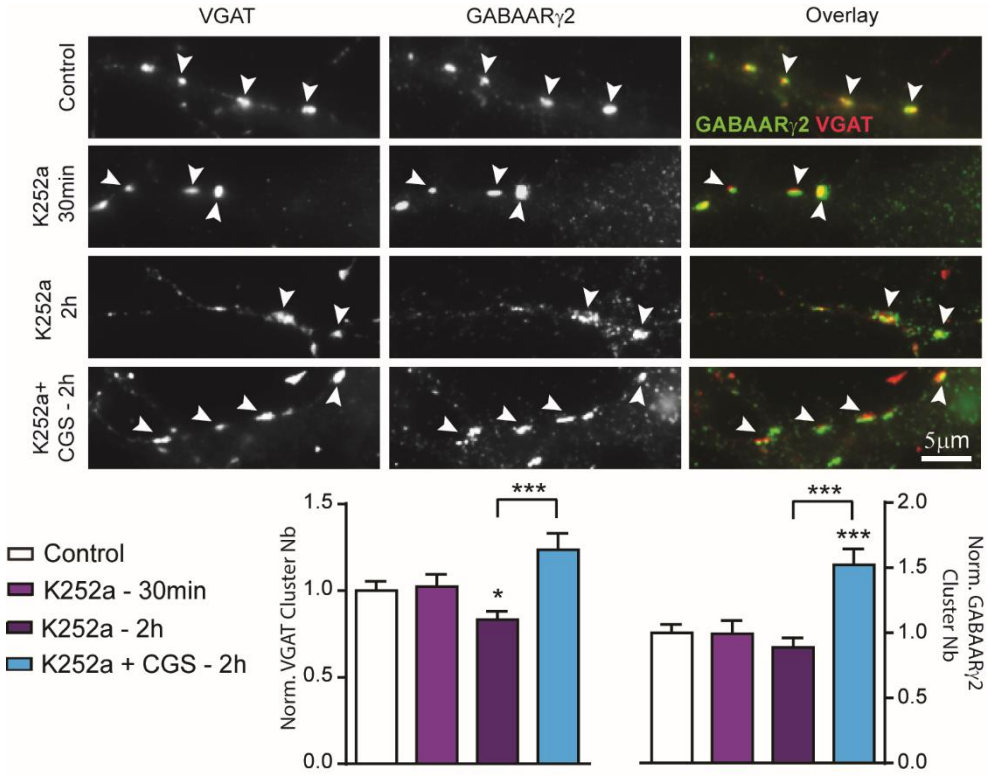

Fig. S22. $A_{2A}R$ signalling rescues synapse loss induced upon blockade of TrkB receptor activity.

Top: Immunostaining and quantification of VGAT and $GABA_AR\gamma2$ in DIV 10 neurons in absence or presence of the indicated drugs for 30 minutes or 2 hours. Scale bar, 5 µm. In all images, arrowheads show examples of inhibitory synapses double-labeled for VGAT and $GABA_AR$ γ2 subunit. **Bottom:** Quantification of the mean number of VGAT and $GABA_AR\gamma2$ clusters in neurons maintained in control condition or exposed to K252a (200 nM) for 30 minutes or 2 hours in absence or presence of CGS21680 (CGS, 30 nM). Values were normalized to the corresponding control values. Histograms represent means and s.e.m. N= 28-44 cells, 2-3 cultures. In all graphs, Mann-Whitney test: *p<0.05; ***p<0.001.